Condition Monitoring of Gearboxes Operating Under Fluctuating Load Conditions

by

Cornelius Johannes Stander

A thesis submitted in partial fulfilment of

the requirements for the degree

Philosophiae Doctor

in the Department of Mechanical and Aeronautical Engineering

of the Faculty of Engineering, Build Environment and Information Technology

of the

University of Pretoria

March 2005

Condition Monitoring of Gearboxes Operating Under Fluctuating Load Conditions

by

Cornelius Johannes Stander

Supervisor : Prof. P.S. Heyns
Department : Mechanical and Aeronautical Engineering
Degree : PhD. Eng.

Summary

Conventional gearbox vibration monitoring techniques are based on the assumption that changes in the measured structural response are caused by deterioration in the condition of the gears in the gearbox. However, this assumption is not valid under fluctuating load conditions, since the fluctuating load will amplitude modulate the measured vibration signal and cause the rotational speed of the system to change. In general monitoring of machines subject to fluctuating load conditions is dealt with by considering the constant load conditions on gearboxes or during free rotational tests.

The need to monitor the condition of large gearboxes in mineral mining equipment has attracted greater interest in order to improve asset management. An inherent need for signal processing techniques, with the ability to indicate degradation in gear condition, under fluctuating load conditions exist. Such techniques should enable the online monitoring of gearboxes that operate under fluctuating load conditions. A continued flow of up to date information should consequently be available for asset and production management.

With this research, a load demodulation normalisation procedure was developed to remove the modulation caused by fluctuating load conditions, which obscures the detection of an incipient gear fault conditions.

A rotation domain averaging technique is implemented which combines the ability of computer order tracking and time domain averaging to suppress the spectral smearing effect caused by the fluctuation in speed, as well as to suppress the amplitude of the vibration which is not synchronous with the rotation of the gear shaft.

It is demonstrated that the instantaneous angular speed of a gearbox shaft can be utilised to monitor the condition of the gear on the shaft. The instantaneous angular speed response measurement is less susceptible to phase distortion introduced by the transmission path when compared to conventional gearbox casing vibration measurements.

A phase domain averaging approach was developed to overcome the phase distortion effect of the transmission path under fluctuating load conditions. The load demodulation normalisation and rotation domain averaging signal processing procedures were applied to both the conventional gearbox casing vibration and instantaneous angular speed measurements prior to the calculation of a smoothed pseudo Wigner-Ville distribution of the data. Statistical parameters such as the energy ratio were calculated from the distribution. These parameters could be monotonically trended under different load conditions to indicate the degradation of gear conditions.

Keywords: Gearbox, condition monitoring, vibration, fluctuating load, modulation, order tracking, rotation domain averaging and normalisation.

Acknowledgements

A word of gratitude to the following people and institutions that enabled me to conduct and complete the research:

- Professor Stephan Heyns my promoter for the opportunity and support in making the research possible.
- The Department of Mechanical and Aeronautical Engineering University of Pretoria.
- Mr Windell for his assistance during the experimental tests.
- Ms Calder for her assisting in the administrative tasks.
- Ms Steynberg, Ehlers and Boshoff at the academic information services.
- To the ESKOM TESP program and SASOL Mining for the financial support of the project.
- My parents for their endless support, love and encouragement during my studies.

Table of contents

1 Introduction and literature survey

1.1 Introduction 1
1.2 Literature survey 5
1.3 Research objectives 33
1.4 Document overview 36

2 A load demodulation normalisation approach for vibration monitoring of gears operating under fluctuating load conditions

2.1 Introduction 38
2.2 Experimental set-up 39
2.3 Order tracking and synchronous averaging 42
2.4 Load demodulation normalisation 43
2.5 Pseudo Wigner-Ville distribution 49
2.6 Statistical features of the PWV distribution 54
2.7 Divergence analysis 59
2.8 Neural networks 61

3 Instantaneous angular speed monitoring of gearboxes under non cyclic stationary and cyclic stationary load conditions

3.1 Introduction 65
3.2 Dynamic gear model 67
3.3 Cyclic stationary and non-cyclic stationary load conditions 73
3.4 Convergence of rotation domain averaging 76
3.5 Implementation of the techniques on the gear model 83
3.6 Experimental set-up 85
3.7 Experimental verification under non-cyclic stationary load conditions 87

4 Transmission path phase compensation for gear monitoring under fluctuating load conditions

4.1 Introduction 94

4.2 Transmission path phase distortion 95

4.3 Phase compensation methodology 99

4.4 Experimental investigation 101

5 Conclusion and recommendations for further research

5.1 Conclusion 106

5.2 Recommendations for further research 108

References 109

Appendix: Experimental test rigs and measurement instrumentation

A.1 Introduction 121

A.2 Load control 121

A.3 Measurement system and instrumentation 124

A.4 Low pass filter 126

A.5 Spur gear test rig 128

A.6 Helical gear test rig 132

Nomenclature

Symbols

$\overline{a}$	Output vector
$a(t)$	Real signal
$\overline{a}(t)$	Analytical signal
$\widetilde{a}(t)$	Hilbert transform of the real signal
$\overline{a}^*(t)$	Complex conjugate of the analytical signal
$\overline{b}$	Bias vector
C_1	Structural damping coefficient
C_2	Bearing damping coefficient
C_3	Gear mesh damping coefficient
c	Damping coefficient of a SDOF system
$d^2(\overline{x},\overline{y})$	Mahalanobis distance
E	Energy of the PWV distribution
E_D	Energy in the order band in which the amplitude of the distribution increases when gear damage is introduced
E_{ND}	Energy in the gear mesh order band, which is present when no gear fault condition is induced
ER	Energy ratio
e	Complex exponential
f	Low pass filter frequency or shaft order / frequency
GR	Gear ratio
H	Hilbert transform
h	Frequency smoothing window
K_1	Structural stiffness
K_2	Bearing stiffness

K_3	Gear mesh stiffness function
k	Stiffness of a SDOF system
L_I	Load intensity
L_O	Load order
M_1	Translating mass
M_2	Pinion mass
M_3	Gearwheel mass
$\overline{M}(\overline{y})$	Average mean value vector for the Mahalanobis distance
m	Mass of a SDOF system
$m(\overline{y})$	Mean scalar value for the Mahalanobis distance
$m_\beta(\theta)$	Rotation marginal of the PWV
$m_\theta(\beta)$	Order marginal of the PWV
N	Number of load conditions / Number of values in a vector / Number of gear teeth
N_S	Number of samples per shaft revolution
NSP	Normalised statistical parameter
$\overline{n}$	Input to the hard limit transfer function
$OFV(f)$	Objective function value
$PWV_a(t,f)$	Pseudo Wigner-Ville function
$\overline{p}$	Input vector
RP	Reference parameter
R_g	Gearwheel base circle radius
R_N	Rotation number
R_p	Pinion base circle radius
r	Frequency ratio
S	Number of statistical parameters
SP	Statistical parameter
T_I	Input torque

T_2	Torque load
t	Time
$\bar{t}$	Target vector
W	Weight matrix
X_1	Displacement of the translating mass
$\dot{X}_1$	Velocity of the translating mass
$\ddot{X}_1$	Acceleration of the translating mass
X_2	Displacement of the input pinion
$\dot{X}_2$	Velocity of the input pinion
$\ddot{X}_2$	Acceleration of the input pinion
X_3	Displacement of the gear wheel
$\dot{X}_3$	Velocity of the gear wheel
$\ddot{X}_3$	Acceleration of the gear wheel
x	Mass displacement of a SDOF system
$\bar{x}$	Vector to which the Mahalanobis distance is calculated
$\bar{y}$	Mean reference vector for the Mahalanobis distance
y	Base displacement of a SDOF system
α	Constant modulation phase shift
β	Order
$\Delta\theta$	Angular increment
μ	Mean value of the statistical parameter
ϕ	Modulation phase shift per revolution / Phase of a SDOF system
θ	Angle of shaft rotation
θ_1	Angular rotation of the input pinion
$\dot{\theta}_1$	Instantaneous angular speed of the input pinion
$\ddot{\theta}_1$	Angular acceleration of the input pinion
θ_2	Angular rotation of the gear wheel
$\dot{\theta}_2$	Instantaneous angular speed of the gear wheel

$\ddot{\theta}_2$	Angular acceleration of the gear wheel
τ	Time delay
ζ	Damping ratio

Abbreviations

ANN	Artificial Neural Network
COT	Computer Order Tracking
ER	Energy Ratio
FM	Frequency Modulation
FRF	Frequency Response Function
GMS	Gear Mesh Signal
IAS	Instantaneous Angular Speed
ICP	Integrated Circuit Piezoelectric
LDN	Load Demodulation Normalisation
LNA	Load Normalised Acceleration
MAS	Measured Acceleration Signal
NMGMS	Narrowband Modulated Gear Mesh Signal
NRDV	Normalised Relative Difference Value
NSP	Normalised Statistical Parameter
OFV	Objective Function Value
PDA	Phase Domain Averaging
PWV	Pseudo Wigner-Ville
RDA	Rotation Domain Averaging
RMS	Root Mean Square
RP	Reference Parameter
SDOF	Single Degree Of Freedom
SP	Statistical Parameter
SPWV	Smoothed pseudo Wigner-Ville
TDA	Time Domain Averaging

List of publications based on this research

1. Stander C.J., Heyns P.S. & Schoombie W. Local fault detection on gears operating under fluctuating load conditions through vibration monitoring. *Mechanical Systems and Signal Processing, November 2002 Volume 16 Issue 6*, pp 1005-1024.
2. Stander C.J. & Heyns P.S. Instantaneous angular speed monitoring of gearboxes under non-cyclic stationary load conditions. *Mechanical Systems and Signal Processing, July 2005 Volume 19 Issue 4*, pp 817-835.
3. Stander C.J. & Heyns P.S. Transmission path phase compensation for gear monitoring under fluctuating load conditions. (*Accepted for publication in the Mechanical Systems and Signal Processing journal in May 2005*)
4. Stander C.J. & Heyns P.S. Fault detection on gearboxes operating under varying speed and load. *Proceedings of the 13th International Congress on Condition Monitoring and Diagnostic Engineering Management, 2000*, pp 1011-1020, Houston Texas.
5. Stander C.J., Heyns P.S. & Schoombie W. Fault detection on gearboxes operating under fluctuating load conditions. *Proceedings of the 14th International Congress on Condition Monitoring and Diagnostic Engineering Management, 2001*, pp 457-464, Manchester UK.
6. Stander C.J. & Heyns P.S. Instantaneous shaft speed monitoring of gearboxes operating under fluctuating load conditions. *Proceedings of the 15th International Congress on Condition Monitoring and Diagnostic Engineering Management, 2002*, pp 220-230, Birmingham UK.

7. Stander C.J. & Heyns P.S. Condition monitoring of gears under cyclic stationary and non-cyclic stationary loading conditions. *Proceedings of the 16th International Congress on Condition Monitoring and Diagnostic Engineering Management, 2003*, pp 601 – 610, Växjö Sweden.
8. Stander C.J. and Heyns P.S. A review of signal processing techniques for condition monitoring. *Proceedings of the International Conference on Asset and Maintenance Management, 1-2 October 2003*, Pretoria South Africa.

Chapter 1

Introduction and literature survey

1.1 Introduction

The condition monitoring of large gearboxes during operation in industry has attracted greater interest in recent years, owing to the need to decrease the down time on production machinery and to reduce the extent of the secondary damage caused by failures. Effective condition monitoring systems and strategies will assist the scheduling of optimal maintenance intervals and therefore minimise unnecessary down time of production equipment.

The cutting head on a continuous mining machine consists of a rotating cylinder with cutting bits mounted around the circumference as shown in figure 1.1 The cutting head is driven through a gear transmission, which is subjected to variable loads as coal is sheared from the coalface in the mining operation. During this process shock loads are induced on to the transmission as the picks come into contact with the coalface.

The cutting head transmission is a critical component of the continuous coal miner and the coal mining process since the entire mining process in the section of the mine is aborted when it fails. Replacement costs range between R1100 000 and R1710 000, depending on the model. The mining process induces high levels of operational vibration onto the machine structure, which complicates the interpretation of the signals with commercially available vibration monitoring software and techniques.

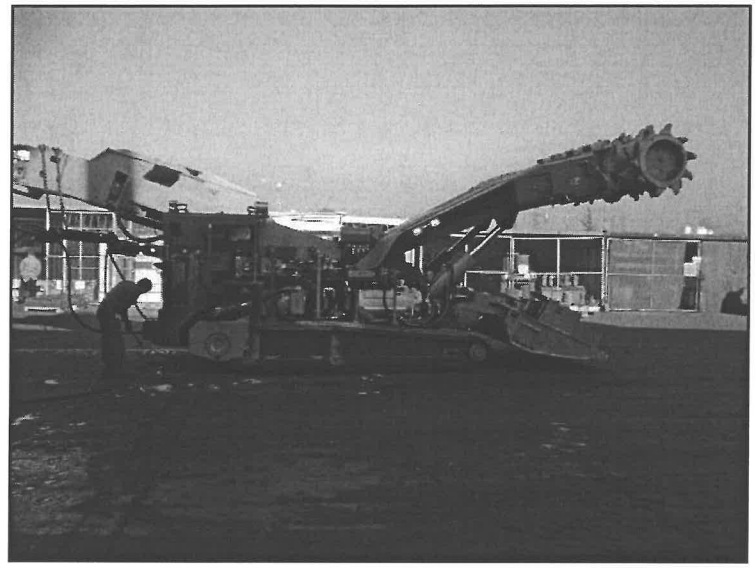

Figure 1.1 Continuous mining machine

Therefore, the vibration monitoring is normally conducted during a free rotational test with no load on the transmission. Figure 1.2 shows the acquisition of a typical vibration monitoring measurement with conventional strategies.

Figure 1.2 Conventional monitoring of the continuous mining machine gearbox

A dragline is used in opencast mining to move the overburden in order to expose the coal layer, which is being mined in the mining operation. The loading device is controlled and supported by cables which drags, hoists and tips its contents as shown in figures 1.3. A human operator controls the process with two joysticks from the control room of the dragline. The rate at which the cables are drawn in and out as well as the weight of the load changes randomly between certain limits during operation. A random variation in the tension of the cables is consequently obtained.

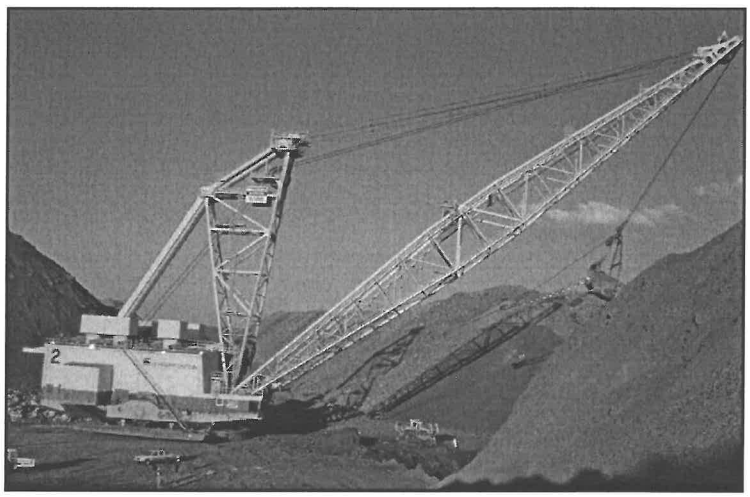

Figure 1.3 Marion 2 dragline Syferfontein mine SASOL Secunda

The cable length is controlled with cables drums, which in turn is rotated by so-called drag motors and gearboxes. Figure 1.4 shows the cable drums, drag gearboxes and direct current electric motors. The load on the gears fluctuates due to the fluctuation in the tension of the cables. The typical life span of the pinion gear is in the range of six to twelve months. Down time on the dragline is estimated at approximately R600 000.00 per hour. Early detection of incipient gear failure is therefore of paramount importance in order to enable maintenance personnel to minimise the down time for gear pinion replacement.

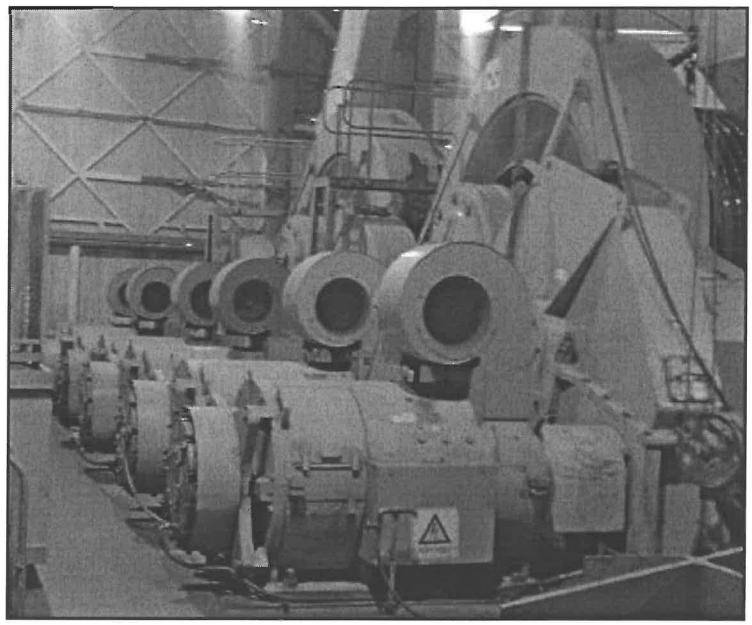

Figure 1.4 Dragline drag motors and gearboxes

Trends in the coal mining industry are towards a situation where the equipment manufacturers are introducing service contracts on their machinery. This implies that manufacturers provide and maintain the machines for production and are remunerated per tonnes of coal produced. Therefore, the optimal utilisation and management of the gear transmission life is becoming a point of increased concern for manufacturers. The smaller the number of replacement parts used by the manufacturers, the higher the profit margin. However, the mines manage the production process and the mine personnel operate the equipment. Therefore, the manufacturers have to monitor the integrity of their investment in terms of optimal life expectancy as well as mishandling by mine personnel and management.

An on-line integrity monitoring system could be implemented to indicate periods of equipment mishandling that accelerate degradation of equipment integrity. A real time or on-line monitoring system that includes measurements under loaded conditions may therefore render advantages in terms of normal predictive maintenance and the ability to detect mishandling.

Conventional vibration monitoring techniques are based on the assumption that changes in the measured structural response are caused by deterioration in the condition of the gearbox. However, this assumption is not valid under fluctuating load conditions, since the fluctuating load will amplitude modulate the measured vibration signal and cause the rotational speed of the system to change. The change in system speed results in a frequency modulation of the gear mesh signal.

The development of on-line gear vibration monitoring systems therefore require signal processing procedures that compensate for the fluctuation in the shaft speed as well as the amplitude modulation caused by the varying load. Note that oil sampling and analysis cannot detect certain failure modes in a gearbox such as a root crack at a gear tooth. Hence, it is necessary to develop vibration signal processing procedures to monitor these failure modes.

1.2 Literature survey

The literature survey was conducted over a variety of topic areas in order to assist the development of vibration monitoring signal-processing procedures that compensates for the effects of fluctuating load conditions on gears of which the condition is monitored through vibration measurements.

1.2.1 Order tracking

If conventional spectrum analysis is applied to data that is measured under changing shaft speed conditions, the harmonics of the shaft speed will smear the spectrum in the frequency domain. This complicates the analyses of the spectrum. According to Randall [1] order tracking is a process, which is utilised when applying spectral analysis to vibration measurements, which are taken on machines of which the rotational speed changes during measurements. A signal representing the rotational speed of the shaft is measured in order to enable the spectral smearing compensation process known as order tracking.

Conventional or traditional order tracking is implemented in the hardware of the vibration analysers which adapt the sampling frequency of the analogue to digital converter so that the vibration signal may be sampled at constant increments of the shaft being analysed. Due to processing time constraints, a time delay between the speed signal and sampling rate adaptation occurs. Hence, conventional order tracking cannot compensate for rapidly changing shaft speed situations.

Potter [2] as well as Potter and Gribler [3] presented the computed order tracking process in which the vibration and speed data is sampled at a constant sampling rate. The sampling is therefore conducted asynchronous to the rotation of the shaft being analysed. Once the data is captured, the vibration signal is re-sampled at constant increments of the shaft off-line. Due to the fact that the sampling is conducted off line with software much more flexibility is available to manipulate the signal. The approach does not require specialised hardware and results that are more accurate can be obtained when compared with conventional methods.

Fyfe and Munck [4] investigated the factors, which have an effect on computer order tracking. It was indicated that the method is extremely sensitive to the timing accuracy of the key-phasor pulses representing the shaft speed. Higher order interpolation functions were successfully utilized to estimate the rotational speed between key-phasor pulses in order to improve the accuracy of the order tracking process.

Bossley *et al.* [5] evaluated various interpolation algorithms such as linear interpolation, B-spline interpolation, Lagrange interpolation and Fourier series interpolation. A hybrid computed order-tracking approach was proposed to overcome the key-phasor arrival time sensitivity problem of conventional computer order tracking.

1.2.2 Synchronous time domain averaging

The averaging of power spectra amplitudes in the frequency domain is conducted in order to reduce variance in spectral analysis according to Randall [1]. Braun [6] states that time domain averaging is a well-known process, which can be utilised to extract a periodic signal from noise waveforms. The signal is averaged synchronously with a key-phasor signal in the time domain in order to attenuate the signal content that is not periodic with a key-phasor signal.

In simplistic terms, the signal is split up into intervals of the shaft rotation indicated by the key-phasor pulse. The amplitude values of the signal are added chronologically over time for each revolution of the shaft. Synchronous components in the signal will always have the same sign, which may be positive or negative at a particular point of shaft rotation. However, the non-synchronous components will not have the same sign at a particular point of shaft rotation. Consequently, the addition of the signal will strengthen the presence of the synchronous components in the signal and attenuate the non-synchronous components resulting in the synchronous time domain average of the signal.

Time domain averaging can be modelled as the convolution of a signal with a finite train of impulses of which the time duration between the impulses is equal to the period of the so-called desired signal. The convolution process is equivalent to the multiplication of the signal with a comb filter in the frequency domain. Only the fundamental and harmonic frequency components of the desired signal will remain in the signal once the frequency multiplication process or convolution has been completed. Braun [6] indicated that the process is less sensitive to triggering errors when compared to conventional time domain averaging. Braun and Seth [7] further investigated the extraction and filtering of signals acquired from rotating machines through multiplication with windows in the frequency domain. McFadden [8] revised the model of Braun [6], to only use a finite number of samples from the signal to produce a result, which is periodic. The methodology involves the application of a rectangular window to the signal in the time domain and sampling of the signals Fourier transform in the frequency domain.

In specialised gear monitoring applications, a rotating reference signal or key-phasor signal is only available on the input shaft of the gearbox. Therefore, phase locked frequency multipliers are used to calculate the time domain average signals for the gears on the remaining shafts in the gearbox. McFadden [9] proposed a methodology where the time domain average can be calculated off-line through interpolation on a digital computer. The methodology provides an alternative way to a phase-locked frequency multiplier, in order to calculate the time domain average when a rotational reference signal or key-phasor signal on the gear of interest is not available.

Forrester [10] states that a discrepancy or confusion exists regarding the methodology and terminology of time domain averaging. Braun [6] and McFadden [8] referred to the concept as time domain averaging, however Stewart [11] referred to the concept as time synchronous averaging. Furthermore Swanson *et al.* [12] referred to it as coherent rotational signal averaging and Succi [13] as synchronous averaging. Forrester [10] states that time domain averaging does include order tracking as a pre-processing technique before the averaging in the time domain is performed. Stander *et al.* [14] distinguished between time domain averaging where the signal is averaged without conducting any form of order tracking, and rotation domain averaging where order tracking is conducted before averaging the signal in the rotation domain which is expressed in degrees of shaft rotation. The term rotation domain averaging is more appropriate since the signal cannot be referred to in the time domain once order tracking is applied. The terms synchronous averaging and rotation domain averaging will henceforth be used.

McFadden [15] employed a matched difference technique in order to adjust the synchronous time domain average to minimise phase and amplitude differences between consecutive signals. The differences were caused by variation in shaft speed and load as well as alignment deviation due to the reassembling of the gearbox on which the measurements where taken. Gearbox reassembly between measurements was necessary since five different fault conditions were seeded for the investigation.

The matched difference technique entailed subtracting the consecutive time domain averages from one another and adjusting the amplitude and phase in order to reduce the difference between the signals.

1.2.3 Adaptive noise cancellation

Chaturvedi and Thomas [16] stated that the objective of adaptive noise cancellation is to reduce the signal to noise ratio of signals, which are measured for diagnostic purposes. Time domain synchronous averaging is used for the same purpose however, it cannot be applied in all situations since not all of the diagnostic signal content of interest is synchronous with the rotation of the shafts in a rotating machine. A typical example is a rolling element bearing where the rotation of the rolling elements is not synchronous with the rotation of the shaft.

Bremer [17] applied adaptive noise cancellation on a bearing test rig to determine which one of three bearings had a defect. Two transducers were used, one near the component being monitored and the other at the noise source. The one transducer will therefore measure the noise signal and the other the noise signal that is modified by the transmission path plus the signal content that is generated by the interacting of the defect with the other components in the machine. The signal of the noise source is filtered in order to impose the transmission path effects on the signal, which is measured to represent the noise content in the diagnostic signal. The filtered signal is subtracted from the diagnostic signal in order to attenuate the noise content. The filter coefficients are calculated through an optimisation process.

Blind source separation is a variation on the theme of adaptive noise cancellation. The aim of blind source separation is to measure multiple signals and filter the influence of the various signals from one another. Gelle *et al.* [18] applied blind source separation to vibration signals measured on a test bench, which consisted of two direct current electric machines running at different speeds.

The authors where able to remove the running speed harmonics of the apposing machines from the vibration spectra measured to a certain extent.

1.2.4 Amplitude and phase demodulation

Smith [19] states that the gear mesh vibration measured on the casing of a gearbox descends from the fluctuation in gear meshing stiffness as the gears rotate in and out of the gear mesh. If a time domain average or synchronous average of the vibration on the gearbox casing is calculated and band pass filtered around the fundamental gear mesh harmonic, the resulting signal will approximate a sinusoid where each peak in the sinusoid represents the structural response due to a gear tooth entering the gear mesh. According to Randall [1] the amplitude modulation of the time domain average signal can be calculated by taking the absolute value of the signal's analytical signal. The analytical signal is a complex time signal of which the imaginary part is the Hilbert transform of the real part. Note that the phase modulation can be calculated by calculating the phase of the analytical signal.

McFadden and Smith [20] band pass filtered the time domain averaged signal around the prominent gear-meshing harmonic and removed the gear mesh harmonic itself in order to obtain what they referred to as a residual signal. The amplitude modulation of the residual signal was analysed and statistical parameters of the residual signal modulations were calculated. The methodology proved to be an effective way to detect local defects on gears.

McFadden [21, 22 and 23] utilised the amplitude and phase modulation of the time domain average which is band passed filtered around the prominent gear mesh harmonic to detect fatigue cracks in the gears of a helicopter's main rotor gearbox. Ma and Li [24] extended the technique to incorporate all of the gear meshing harmonics and applied the technique to torsional vibration measurements measured on an experimental test rig with artificially seeded defects. They concluded that the technique is more sensitive in detecting gear defects when compared to a narrow band-filtered approach.

Brie *et al.* [25] developed an adaptive amplitude and phase demodulation approach, which has lower numerical complexity when compared to the conventional route of calculating the modulation using the Hilbert transform. The algorithm is sequential which allows it to be implemented in real time.

Wang [26] applied a resonance demodulation technique common to rolling element bearing defect detection and monitoring to detect incipient gear tooth cracks. The methodology is based on the fact that a root crack will lower gear tooth stiffness in the gear mesh resulting in impacts as the gear tooth after the damaged gear tooth enters the gear mesh. This impacting will excite the structural resonance. A residual signal is calculated from the time domain average and band pass filtered around the structural resonance. The band passed filtered residual signal is then demodulated to detect sudden changes in the modulation, which are related to the presence of fatigue cracks in the gears.

1.2.5 Time domain analysis

The application of statistical analysis to measured diagnostic signals is as old as the science of measuring the signals. A review of time domain analysis using statistical methods forms part of virtually every PhD thesis and Masters dissertation conducted in the field of vibration monitoring. Authors such as Forrester [10], Al-Balushi [27], Birch [28], Engin [29] and Andrade [30] have compiled such literature surveys and reviews.

In general, time domain analysis entails calculating the root mean square, peak value, crest factor and kurtosis values of a signal. The root mean square value gives an indication of the continuous or steady state amplitude in a time varying signal. Peak level or value is defined as half of the difference between the maximum and minimum values in the signal. This is not a statistical value and it is known not to be a reliable indicator of damage. The crest factor is defined as the ratio of the peak value divided by the root mean square value of the signal. It gives an indication of impulsiveness in the signal.

The kurtosis is the normalised fourth statistical moment of a signal. It also used to indicate impulsiveness in the signal. The parameters defined above are also referred to as overall vibration parameters. In general, they are calculated for each measurement and trended over time to give an indication of machine condition, rather than the condition of specific components in the machine. The parameter does not provide any diagnostic information. However, the parameters are easy to implement in low cost online monitoring equipment.

Komura *et al.* [31] developed a hand held vibration monitoring sensor which utilises the root mean square, kurtosis and mutations thereof to classify a machines condition according to three categories namely *normal, warning* and *alert*.

Martin *et al.* [32], Ismall *et al.* [33] and Oguamanam *et al.* [34] applied statistical distributions to experimental data measured on gear and gear pump test rigs. A synchronous or time domain average of the vibration signal was calculated before applying the statistical distribution to segments of the time domain averaged signal. The segmentation of the signal enables local fault detection on the gear teeth of the gears. A beta distribution was fitted since the kurtosis of a normal distribution was to sensitive to noise in the vibration data. It was indicated that the reciprocal of the beta kurtosis value could indicate the presence of a local defect on a gear.

Howard [35] developed a composite signal averaging technique to overcome the monitoring problems encountered when monitoring gears in an epicyclic gearbox. Typical problems were the varying transmission path to the transducer and the fact that multiple components mesh at the same frequency. Experimental tests where done with progression in induced gear damage and vibration measurements where taken for the various fault conditions in order to validate the technique. The composite signal averaging technique was applied to the experimental data and the modulation of the averaged signals was calculated.

Kurtosis values for the modulation were estimated and it was shown that the kurtosis increased as the extent of gear damage increased. The kurtosis value of the modulation therefore proved to be an effective indication of gear condition once composite signal averaging had been done.

The Kolmogorov-Smirmov test was applied by Andrade *et al.* [36] to detect early fatigue cracks in gears. The test is a time domain signal processing technique that compares two signals to indicate the likelihood that the two signals have the same probability density function. In essence, the test determines whether two signals are similar or not. Therefore, a fault condition can be indicated by comparing a signal with a number of signal templates of known fault conditions. The technique was applied to experimental data and it was indicated that the technique could successfully detect the presence of a fatigue crack.

Baydar *et al.* [37] utilised multivariate statistics in combination with principal component analysis to detect localised faults in a two stage helical gearbox. Principal component analysis is utilised to reduce the dimension of a data set to fewer samples. In essence, it is utilised for data compression. Vibration signals under different fault conditions where measured. Principal components were calculated for the *normal* or *no fault* present condition. These components where statistically represented and statistical techniques such as square predictor error and T^2 statistics were calculated for the new measurements to observe any deviations form the normal condition. The square predictor error is the sum of the squared difference between the data indicating the normal condition and the measured data. The T^2 value is merely the sum of the squared principal component values. A deviation in the value will indicate a deviation in the condition of the machine.

1.2.6 Spectrum analysis

Spectrum analysis entails the conversion of a time signal in to a frequency domain representation through a discrete Fourier transform. The term spectrum is used for the amplitude representation versus the positive frequency range of the time signal's Fourier transform.

The advantage in using spectrum analysis lies in the fact that the amplitude at each discrete frequency can be monitored in contrast to the overall amplitude monitoring approach of time domain analysis. A log scale for the amplitude axes can be chosen to improve the dynamic range of the representation. Defects that will cause a small change in amplitude at a certain frequency with low amplitude will therefore be detected much easier in comparison with time domain analysis.

The frequencies at which a certain defect on a particular component will cause an increase in the amplitude of the spectrum are referred to as defect frequencies. Hence, diagnostic capability can be obtained by relating amplitude growth at a certain frequency to a particular component in the machine based on its physical parameters. This type of analysis is conventionally used in practice to monitor plant equipment. Goldman [38], Hunt [39], Rao [40] and Davis [41] have described spectral analysis in detail.

1.2.7 Cepstrum analysis

The term cepstrum analysis is used for a range of techniques in which the spectrum of a logarithmic spectrum is calculated. In general terms, it is a frequency analysis of a frequency analysis. It is utilised to detect a series of harmonics or sidebands and to estimate their strength. The various harmonics in a conventional spectrum is reduced to predominantly one peak in what is referred to as the quefrequency domain. Periodicity in the conventional spectrum is therefore detected.

Only a single peak needs to be detected to diagnose a fault condition. Logarithmic values of the spectrum is utilised in the calculation of the cepstrum in order to improve the dynamic range of the analysis.

The vibration spawning from the meshing of a gear pair in a gearbox has to be transmitted through the shaft, roller element bearings and casing before being measured. It is common knowledge that this transmission path has structural impedance characteristics in terms of amplitude and phase. If the gears rotate at a certain frequency, the forces being transmitting from the meshing gears will be subject to amplitude and phase changes induced by the structural impedance at the particular frequencies. However, if the rotational speed changes the forces being transmitted from the meshing gears are subject to different amplitude and phase changes induced by the transmission path impedance at the alternative frequencies. As a result, the amplitude and relative phase of the measured structural response will be different depending on the structural dynamic characteristics.

Randall [1, 43] and Angelo [42] stated that cepstrum analysis is insensitive to the phase variations in the transmission path. The power spectrum of a signal measured at an external point on the casing of a rotating machine such as a gearbox can be expressed as the product of the power spectrum of the source function with the squared amplitude of the frequency response of the transmission path. By taking the log of the transforms, the multiplication turns into an addition of the logarithmic source function power spectrum and the logarithmic frequency response function, to obtain the logarithmic spectrum of the response. This implies that the source and transmission path effects are additive in the cepstrum. The transmission path transfer function has low quefrequency components, which will be well separated from the high quefrequency components representing the source function. Randall [43] applied the cepstrum analysis to the vibration measured on a gearbox at two different positions on the casing. He concluded that the spectra of the two signals were different but the cepstra were almost identical.

Forrester [10] however stated that cepstral analysis is not very useful in the analysis of synchronously averaged signals, since the signal is not periodic in the so-called angle domain and periodicity is lost when translated to the quefrequency domain.

A variety of expressions and forms of the cepstrum has been developed. Childers *et al.* [44] described the relationships between the various forms. Wu and Crocker [45] developed a modified cepstrum technique to determine the magnitude of a structure's frequency response function. The novelty of the technique is based on the fact that no prior knowledge of the input force is required to calculate the magnitude of the structural transfer function. Debao *et al.* [46] applied cepstrum analysis to detect misalignment, unbalance and bearing damage in generators. Van Dyke and Watts [47] utilised the cepstrum analyses as a data pre-processor for an expert system, which can detect rolling element bearing deterioration and predict fault severity.

Badaoui *et al.* [48] proposed a moving cepstrum integral to detect and localise tooth spalls in gears. The technique applies a moving window in order to isolate the gear tooth faults. This enables the detection and localisation of local tooth spalls on gear teeth. The technique was applied to numerical and experimental data and the authors where able to detect light spalls on gear teeth.

1.2.8 Higher order spectral analysis

A spectrum is conventionally utilised to indicate the energy distribution of a signal in the frequency domain. Note that a spectrum analysis is a linear analysis and it assumes that all of the frequency components in a signal are uncorrelated which means that the phase relationship between the frequency components is ignored. Higher order spectral analysis is utilised to detect phase coupling due to non-linear interaction between the frequency components.

The most commonly used higher order spectral analysis technique is bispectral analysis, which is utilised to detect quadratic phase coupling. Quadratic phase coupling is a physical phenomenon, which occurs when two waves interact to generate a third wave which has frequency and phase equal to the sum of the two source waves. Hence, all of the signals are phase related. A bispectrum is calculated for a two-dimensional frequency plane. The normalised bispectrum with amplitude values ranging between one and zero is referred to as bicoherence. Amplitudes approximating the value of one will indicate that the phase of the frequency components are correlated. A region in the bicoherence where the amplitude approximates zero, indicates that the frequencies are uncorrelated and that phase coupling between the frequencies do not exist. The concept is applied in gear damage detection in order to detect the frequencies, which are modulated with a certain frequency component.

Li *et al.* [49] utilised bispectrum analysis to diagnose localised defects in rolling element bearings from experimental measurements. Ning *et al.* [50] proposed a modified bispectral analysis approach in order to detect distributed gear faults such as eccentricity and shaft imbalance. Howard [51] determined that bispectral and trispectral analyses techniques could detect amplitude and phase modulation in gear vibration signals. Parker *et al.* [52] applied bispectrum analysis to synchronously sampled helicopter transmission data. Statistical change detection was applied to the bispectrum in order to detect the appearance of energy at known frequency pairs in the bispectral domain. Kocur and Stanko [53] proposed the order bispectrum to analyse the sound radiation from rotating machines with non-stationary shaft speed such as a motorcar engine. A computer order tracking approach is presented as a pre-processor prior to the calculation of the bispectrum. Experimental results are shown with and without the computer order tracking pre-processing which indicated an improvement in terms of the reduction in bispectral smearing.

1.2.9 Time frequency analysis

Conventional spectrum analysis assumes that the signals, which are analysed, are stationary. It is therefore unsuitable for the analysis of non-stationary signals. Non-stationary components in a vibration signal measured on a rotating machine may be caused by defects. Time frequency analysis techniques can be utilised to conduct non-stationary signal analysis on vibration measurements to detect defects. Time frequency analysis is the three-dimensional time, frequency and amplitude representation of a signal, which is inherently suited to indicating transient events in a signal.

The Fourier transform can be adapted to analyse only small sections of the vibration signals in order to reduce the loss of transient or non-stationary time information. A sequence of overlapped transforms is performed, by shifting a window function in time over the whole signal. Transforms are arranged chronologically to construct the time-frequency distribution of the signal. The approach is referred to as the short time Fourier transform and provides information on the time and frequency at which events occur.

Information can however only be obtained with limited precision, which is determined by the length and shape of the time window. A short time window will result in good time resolution but poor frequency resolution and vice versa. Hence, either good time resolution can be obtained or good frequency resolution. Consequently, additional transforms were developed in order to improve the time frequency resolution.

The Wigner distribution and its various permutations is a time frequency technique, which was developed to improve on the resolution constraints of the short time Fourier transform. The Wigner distribution is derived through the generalization of the relationship between the power spectrum and the autocorrelation function for non-stationary time-variant processes. The amplitude of the negative frequencies in the frequency domain is zero for an analytical signal. Therefore, the application of the Wigner distribution to the analytical signal will account for all frequencies.

The application is referred to as the Wigner-Ville distribution. However, the distribution is influenced by what is referred to as cross-terms or interference terms. A frequency-smoothing window is applied to the Wigner-Ville distribution in order to attenuate these interference and cross-terms that are inherent to the distribution. The application of the frequency-smoothing window results in a pseudo-Wigner-Ville distribution.

Cohen [54] as well as Qian and Chen [55] have documented various time frequency analysis techniques. Forrester [10, 56, 57] applied the Wigner-Ville distribution to synchronously averaged vibration measurement data from a Wessex helicopter main rotor gearbox and an epicyclic gearbox test rig. He concluded that it was possible to detect, classify and determine the extent of the damage by the patterns produced by the Wigner-Ville distribution.

Staszewski [58, 59] and Tomlinson [59] applied a variation of the short time Fourier transform referred to as the moving window approach to detect local defects in the vibration measured on an experimental spur gear test rig. Fault conditions in the form of tooth breakage and root cracks were seeded for their investigation. They concluded that the success rate of the approach depends on the proper selection of the window parameters. Staszewski [58, 60], Worden and Tomlinson [60] detected fault conditions on a spur gear test rig by applying the Wigner-Ville distribution to vibration measurements taken on the test rig. They concluded that the defect manifests as wideband amplitude dispersion in the contour plot of the distribution. Hence, fault localisation in the time domain is possible with the approach. Progression in the fault condition could be observed by changes in the contour plot of the distribution. Statistical and neural network pattern recognition techniques were applied to classify fault condition advancement.

McFadden [61] investigated the failure of a military aircraft starter gearbox using cascade plots of vibration measured on the power take off gearbox of the turbines. Measurements were taken on more than 200 gearboxes. Discs were machined and fitted on the flange of the power take off drive shaft in order to construct a shaft encoder to indicate the rotational speed of the shaft. With this work, McFadden illustrated that both order tracking and time frequency representation is required to conduct a comprehensive investigation on gearboxes.

Wang [62] as well as Wang and McFadden [63, 64, 65, 66] applied the spectrogram for early gear failure detection. They concluded that the Wigner-Ville distribution causes too many cross in the time frequency distribution, which make the images difficult to interpret. They applied the spectrogram to the vibration measured on an industrial gearbox. However, the fundamental gear mesh frequency was removed before calculating the spectrogram of the data in order to improve the sensitivity in the distribution. An image processing technique was used to detect gear faults by extracting, comparing and analysing patterns in the distribution.

Zheng and McFadden [67] introduced an alias-free exponential time-frequency distribution referred to as the modified exponential distribution. They indicated numerically and experimentally that the distribution is well suited to detect transient signal components in the presence of steady components.

Yesilyurt *et al.* [68] compared the efficiency of the pseudo-Wigner-Ville, Choi-Williams and the instantaneous power spectrum distributions to detect local incipient tooth damage on helical gears. Measurements were taken on a test rig with induced damage. It was concluded that the pseudo Wigner-Ville distribution gave improved frequency resolution in comparison with the instantaneous power spectrum. However, the interference terms in the pseudo Wigner-Ville distribution made it difficult to detect incipient damage. Results obtained from the application indicated that the Choi-Williams distribution was not suited for incipient damage detection. The instantaneous power spectrum proved to be the most sensitive to detect incipient gear damage.

In the smoothed pseudo Wigner-Ville distribution, both time and frequency smoothing is applied to attenuate interference terms, in contrast to the pseudo Wigner-Ville distribution in which only frequency smoothing is applied. Thus, greater attenuation of the interference terms is obtained by applying the smoothed pseudo Wigner-Ville distribution. Baydar and Ball [69, 70] as well as Baydar [71] applied the smoothed pseudo Wigner-Ville distribution to vibration and acoustic signals measured from a helical gearbox test rig. It was concluded that the acoustic signals were influenced by background noise. However, gear defects could be detected with both signals, by monitoring the broadening of the frequency band outside the meshing frequency band in the smoothed pseudo Wigner-Ville distribution. The sensitivity of the instantaneous power spectrum was compared to the smoothed pseudo-Wigner-Ville distribution. In terms of early fault detection capability, the performance of the instantaneous power spectrum and the smoothed pseudo Wigner-Ville distribution were found to be similar.

Han and Lee [72] proposed a transient signal processing technique utilising the directional Wigner distribution for accurate tracking. The technique reduces interference terms by converting the original time signal sampled at uniform time intervals to a regenerated signal sampled at uniform angular distances. The technique does not require the measurement of a tacho pulse signal as long as the rotational speed can be well estimated from the directional Wigner distribution itself.

Lee and White [73] investigated the use of the third and fourth order Wigner bi- and tri-spectra to detect fault conditions on industrial gearboxes and internal combustion engines. It was concluded that the Wigner tri-spectrum is more suitable to detected impulses in signals compared to the conventional Wigner-Ville distribution.

Various other authors have implemented time frequency techniques to detect defects in rotating machinery, such as Oehlmann *et al.* [74] who detected gear and rolling element bearing defects in motor vehicle gearboxes, Meng and Qu [75] who detected faults in compressors and turbines, Rossano *et al.* [76] detected pump speed variation, Chiollaz and Favre [77] who characterized engine noise, Choy *et al.* [78] detected gear defects in helicopter gear transmissions and Kim et al. [79] who also detected roller element bearing defects. Auger *et al.* [80] developed a shareware Matlab toolbox in which a variety of time frequency algorithms have been implemented. A comprehensive users guide and tutorial manual is included in the share ware package.

1.2.10 Wavelet analysis

The drawback of the short time Fourier transform is the fact that the time frequency resolution remains constant once the window length and shape has been chosen. A more flexible approach is required where the window size can be varied in order to enhance the accuracy of either the time or the frequency resolution. A wavelet is a waveform of limited duration with an average value of zero. It is used to decompose a signal into windowed basis functions with variable size regions. Wavelet analysis performs a decomposition of the measured vibration signal into a weighted set of scaled wavelet functions. The frequency variable is replaced by a scale variable. The wavelet transform does not overcome the uncertainty principle but since the window lengths are variable, there is variable resolution that can increase performance. Wavelet analysis allows long time intervals where more precision is required for low frequency information and shorter time intervals where high frequency information is required. The flexible scheme of time and frequency localisation makes the wavelet transform attractive for the analysis of signals involving discontinuities and transients.

Wang and McFadden [81, 82, 83] applied the wavelet transform to analyse gear vibration signals in order to detect early signs of incipient mechanical failure. In theory, the wavelet transform can simultaneously display both the large and small-scale features present in the signal. This enables the detection of localised as well as distributed fault conditions. Orthogonal wavelets such as Daubechies 4 and harmonic wavelets were used to transform the time synchronous gearbox vibration signal into the time-scale domain. However, it was concluded that due to the limited number of scales, a single wavelet amplitude map does not have enough scales to describe all details both large and small, of the signal. Hence, small changes in the vibration signal could not be detected. This problem can be overcome through the utilisation of non-orthogonal wavelets, which are able to give finer steps of dilation and translation. It was found that a Gaussian-enveloped oscillating wavelet is well suited to detect various sizes of gear faults.

Lin and McFadden [84] investigated the use of a linear wavelet transform to obtain the time frequency spectrogram of a vibration signal. The linear wavelet transform is calculated in the frequency domain by filtering the signal spectrum with wavelet filters, and can be computed easily and efficiently by the fast Fourier transform. It is shown that the linear wavelet transform can be used to detect a localized fatigue crack in a gear. Wang [85] developed a joint time-frequency-scale distribution. The three variables, time, frequency and scale increase the possibility of detecting fault conditions in a system under inspection.

Staszewski and Tomlinson [86] applied the wavelet transform to detect damage on spur gears. A fault detection algorithm was presented, based on similarity analysis of patterns obtained from the modulus of the wavelet transform. Staszewski [87] reviewed wavelet based compression methods for application in vibration analysis. It was concluded that wavelet based compression is effective in compressing non-stationary data. The compressed data can be used for feature selection and coefficient selection procedures are proposed.

Yesilyurt and Ball [88] applied the continuous wavelet transform to detect and locate defects in gear teeth caused by bending fatigue. Experiments were conducted on a spur gear test rig. Measurements were taken with accelerometers at the bearing housing closest to the gear with the defect. The Morlet wavelet was used as the analysing wavelet. It was concluded that for low levels of bending fatigue damage the presence of a weakened gear tooth is not clearly revealed in the wavelet amplitude plot.

Boulahbal *et al.* [89] investigated the utilisation of amplitude and phase maps of the wavelet transform to detect localised gear defects in gear trains. It was found that the phase map displays distinctive features for data measured on a test rig with a cracked gear tooth present. The amplitude wavelet map of the residual signal was found to be more sensitive to detect gear damage in comparison to the amplitude map of the actual signal. The work of Wang *et al.* [90] confirmed the findings of Boulahbal *et al.* [89].

Dalpiaz *et al.* [91] compared the effectiveness of different diagnostic methods to detect gear teeth cracks from experimentally measured data. It was concluded that the application of the wavelet transform to the raw measured signals is insensitive to the presence of gear tooth cracks. However, the application of the wavelet transform to the synchronously averaged measured signal was able to indicate the presence of the gear defect.

Peng & Chu [92] compiled a comprehensive review of the application of the wavelet transform for condition monitoring and diagnostic purposes. Misiti *et al.* [93] developed a wavelet toolbox for use with Matlab incorporating several continuous and discrete wavelet transform algorithms.

1.2.11 System identification

It is possible to fit a difference equation representing an autoregressive moving average model if a system can approximately be represented by a linear differential equation.

Wu *et al.* [94] utilised such a model to detect defects such as unbalance on an electric motor through vibration measurements. The coefficients in the difference equation were fitted sequentially on the observed data from the electrical machine and the spectrum of the data can be estimated from the model coefficients. Note that the model coefficients are fitted via a least squares estimate and therefore act as a filter to remove noise from the spectrum of the signal. Less time data therefore has to be captured in order to, obtain a repeatable spectrum when compared to conventional spectral analysis where a number of averages have to be taken in order to smooth out the noise in the spectrum.

Zhuge *et al.* [95] proposed the non-stationary analysis of the vibration signal measured on a hydraulic piston pump through the utilisation of a time variant autoregressive model. Power spectra were generated from the model. The amplitudes in the spectra at certain frequencies were selected as features in a similarity analysis. Four different fault conditions were imposed on the pump to generate data for the similarity analysis. The Mahalanobis distance from the known feature, vectors were calculated in order to conduct the similarity analysis. The approach was found to be very sensitive in detecting the fault conditions.

Baillie and Mathew [96] diagnosed bearing fault conditions by utilising autoregressive time series models. Vibration signals from rolling element bearings were measured to compare the reliability and performance of three different autoregressive modelling techniques. They concluded that back propagation neural networks outperformed radial basis function neural networks and traditional linear autoregressive models when only short time lengths are available. However, if there is no restriction on the length of the time data, linear autoregressive models can be considered. The performance of radial basis function neural networks was disappointing.

Li and Yoo [97] evaluated several vibration based gear diagnostic algorithms to diagnose gear tooth surface pitting and chipped gear teeth. Spectrum analysis, condition indices, energy operator analysis, narrow band demodulation, wide band demodulation, time frequency analysis and model prediction error methods utilising linear autoregressive modelling and non-linear autoregressive modelling was considered. They concluded that only the model prediction error methods could provide diagnostic information, which increased consistently with an increase in the extent of gear pitting.

McCormick *et al.* [98] applied periodic time varying autoregressive models to diagnose and detect fault conditions in rotating machinery through vibration measurement. The approach does not require data from the machine when a fault condition is present in order to diagnose the fault condition. Unexpected or unfamiliar failures, which cause changes in the structural vibration, can therefore be detected. A comparison was made between time varying and time invariant autoregressive models. The authors concluded that the time varying autoregressive models performed better than the time invariant models.

Wang and Wong [99] applied a linear prediction method to detect and diagnose gear faults. They assumed that the vibration signal measured on a gearbox without any defects could be modelled with a stationary linear autoregressive model. Local faults on a gear will cause sharp spikes in the vibration signal measured on a gearbox. These faults are non-stationary transient events and cannot be modelled by the linear autoregressive model. Therefore, a deviance between the predicted linear model response and the measured response will be obtained when a fault condition is present in the gear. This deviance is utilised to diagnose and detect a gear fault condition.

1.2.12 Artificial intelligence

Research in the field of fault detection severity classification focuses on the utilisation of artificial neural networks. Artificial neural networks are trained with feature sets, which indicate typical failure or degradation stages.

A large numbers of these data sets are required to successfully train a neural network. However once trained, the network has the ability to generalise and correctly classify inputs that was not seen during the training process.

The network also has the ability to deal with data that is corrupted or that has an added noise component. These features make the use of artificial neural networks extremely attractive in the field of condition monitoring. Artificial neural networks can be classified in two classes, namely supervised and unsupervised learning. Supervised learning refers to the instance when a network is trained with data sets in which condition indication features as well as the physical condition of the component is available to train the network in order to classify the condition.

Unsupervised learning is implemented in applications where no information regarding the failure modes is available. The self-organising map is an example of such networks and is used to monitor a deviance in the network-input data. Therefore, it is used as an alarm indicator on new machinery where no service history exists. Artificial neural networks are often used in co-operation with expert and rule based systems to form so-called hybrid systems. The expert and rule based systems are used to generate the feature spaces for the artificial neural networks. A hybrid system therefore combines the power of expert and rule based systems with the generalisation and noise tolerant capabilities of neural networks.

Monsen *et al.* [100] developed helicopter gearbox health monitoring systems based on artificial neural networks. A discrete Fourier transform was used to pre-process the data measured from a single accelerometer before inputting the data into the artificial neural network. Three levels of fault characterisation were used and 100% fault detection and classification was obtained for the experimental data set used. Both rolling element bearing and gear tooth defects were investigated in an intermediate tail rotor gearbox.

Worden *et al.* [101] confirmed the conclusion of Monsen *et al.* [100] by applying artificial neural networks to detect local tooth faults on spur gears. Spectra of measured acceleration data was used as input data to the networks and the gear faults could successfully be diagnosed. Results improved when averaging the time data prior to the calculation of the spectra.

Xu *et al.* [102] indicated that artificial neural networks could be trained from raw time domain vibration data to classify six different helicopter transmission fault conditions. No form of pre-processing was performed.

McCormick and Nandi [103] investigated the utilisation of artificial neural networks to detect rotor rub and unbalance. Higher order statistical analysis of the vibration waveform, complex time series, radii distribution, spectrum analysis and time smoothing methods were used to generate input features for the artificial neural networks. The utilisation of the higher order statistics as input features allowed a classification success rate of 70% and the complex time series analysis features allowed a classification success rate of 80%. Features extracted from the higher order statistics and complex time series analyses did not effectively detect rubbing. However, the features generated through the application of the higher order statistics on the smoothed time series data could detect rubbing effectively. The various features were combined to obtain a classification success rate of 90%.

Jammu *et al.* [104, 105] introduced a diagnostic method for helicopter gearboxes that used knowledge of the gearbox structure and characteristics of the vibration features to define the influences between the features and faults. This method brings together the areas of dynamic modelling, fuzzy systems and neural networks to model the gearbox, represent diagnostic knowledge and to perform diagnosis. A simplified multi degree of freedom lumped parameter mass model of the gearbox and a procedure to obtain diagnostic influences from the model is introduced.

A structure based connectionist network using the influences as connection weights is presented as a method to do diagnosis. The system was tested on data measured on a helicopter gearbox and it was concluded that several gearbox faults could be diagnosed.

Paya *et al.* [106] investigated the condition of a model driveline consisting of a vehicle gearbox, electrical motor, disc brake and bearing housings. Single and multiple faults were introduced into the gearbox and bearing housing. The vibration signals were pre-processed with wavelet transforms. It is shown that by using multiplayer artificial neural networks the pre-processed wavelet transform data can be utilised to detect and classify multiple fault condition in the model driveline. An overall classification rate of 96% was achieved.

Essawy *et al.* [107, 108] developed a health monitoring system for the main power transmission of a navy CH-46E helicopter. Vibration data was collected using eight accelerometers mounted at different locations on the gearbox. Frequency domain and wavelet analysis techniques were used to analyse the vibration data and to extract the necessary fault features for neural network inputs. Self-organising map neural networks were used to cluster the features from the different sensors to distinct locations on a two dimensional map. Feed forward back propagation neural networks were used to identify the different faults according to where they cluster on the two dimensional map. A fuzzy sensor fusion algorithm was developed to process information from different neural network based fault identifiers and to produce a unified decision about the health of the monitored system. The fuzzy fusion sensor system had a classification rate of 100%.

Dellomo [109] investigated the use of artificial neural networks to detect and classify fault conditions on the main gearbox of a helicopter. The measured data was order tracked and the signal demodulated. A spectrum of the signal modulation was calculated and features were extracted for input to the artificial neural network. It was concluded that two layers in the network was sufficient to address the classification and detection problem. Additional layers only improved the artificial neural network performance slightly. A classification rate of approximately 100% was obtained.

Demuth and M. Beale [110] developed an artificial neural network toolbox for use with Matlab incorporating several artificial neural network architectures algorithms.

1.2.13 Chaos theory

Golnaraghi *et al.* [111] applied non-linear time series analysis to identify cracks in gear teeth. The investigation showed that the measured vibration signal is chaotic. The crack in the gear tooth alters the vibration response and hence the chaotic signature. Correlation dimension and Lyapunov exponents were used to quantify the change in the measured vibration signal with and without the gear defect present. It was concluded that non-linear time series analysis has great potential in the investigation of faulty gearboxes and other rotating machines.

Lin *et al.* [112] investigated a non-linear dynamical system approach for crack detection in a gearbox system. The study is based on the assumption that the modulation of the narrow band enhanced vibration signal measured on a gearbox, describes some degree of chaos in the gear mesh dynamics. It was concluded that it was possible to detect a 15 % crack by making use of the dimensions approach.

1.2.14 Fault detection through instantaneous angular speed measurement

Smith and Echeverria-villagomez [113] measured the torsional vibration on the wheel of a gearbox with an optical encoder on a free shaft end and with an accelerometer mounted tangentially on an auxiliary flange. The results were compared and it was concluded that there was good agreement between the results. The aim of the work was to investigate the measurement of transmission error and no attempt at gear fault detection was made in the investigation.

Yang *et al.* [114] investigated the use of instantaneous angular speed measurements to diagnose combustion related faults in a diesel engine. Typical fault conditions such as fuel and valve leakage was considered. A dynamic model for simulating the instantaneous angular speed of a four-cylinder diesel engine is presented. It is stated that the gas pressure and vertical imbalance inertial force have a great influence on the instantaneous angular speed. The simulation results were experimentally verified. It was concluded that diesel engine faults related to gas pressure in the cylinders could be detected through measurement of the instantaneous angular speed.

Sasi *et al.* [115] investigated the detection of cracked rotor bars in induction motors through the measurement of instantaneous angular speed. An advantage of utilising the instantaneous angular speed for fault diagnostic and detection purposes is the fact that in many applications the instantaneous angular speed is measured for control purposes. Furthermore, the instantaneous angular speed is less affected by the transmission path of the torsional vibration in comparison with conventional vibration measurements on machine casings. Two levels of broken rotor bar severity were seeded in an induction motor. It was concluded that the broken rotor bar could be detected through measurement of the instantaneous angular speed under load and no load operating conditions.

1.2.15 Gearbox fault detection under varying load conditions

Smith [116] states that gearboxes should not be monitored under conditions where the angular acceleration multiplied by the effective moment of inertia of the system exceeds the steady load torque. Randall [117] states that the amplitude of the vibration of the gearbox casing, caused by the meshing of the gears, is modulated by the fluctuation in the torque load. McFadden [21, 22] mentions that changing load conditions influenced the results he obtained for his time domain synchronised averaged vibration.

Bauer et al. [118] developed a vibration monitoring system to monitor large industrial gearboxes in the mineral mining industry. Rotational speed and load was measured in order to trigger the measurement of vibration signals at specific speed and load conditions in order to ensure that measurements were taken under constant speed and load conditions. Conventional fault detection techniques were used to analyse the data.

Wang and Wong [99] stated that the linear prediction method, which they developed, could diagnose fault conditions independent of the load conditions, but the precise influence that the load fluctuation has on the measured signal was not documented.

Baydar and Ball [119] showed that spectral analysis could not track the degradation in the condition of the gear under different nominal load conditions. The spectral content changes dramatically if the nominal load conditions change. Consequently, they employed the instantaneous power spectrum to detect local faults on the teeth of a gear under different nominal load conditions. The presence of the gear defect imposed could be seen in the instantaneous power spectrum under different loading conditions. However, the similarity between the instantaneous power spectrum plots under different loading conditions could complicate diagnosis of a fault condition.

1.2.17 Dynamic modelling of gear systems

Ozguven and Houser [120] wrote a comprehensive review on dynamic gear models. Publications over the last three decades were considered. The aim of the majority of the publications were to investigate bending stresses, contact stresses, pitting, scoring, transmission efficiency, radiated noise, estimation of loads exerted on other machine elements such as bearings, vibration motion, whirling, reliability and life. The models proposed by the investigators show considerable variation in the effects, which are included in to the model and the basic assumptions made. Models were classified into five groups namely simple dynamic factor models, models with tooth compliance, models for gear dynamics, models for geared rotor dynamics and models for torsional vibration.

Most of the models reviewed are lumped parameter mass models and the dynamic gear models include time varying mesh stiffness.

Howard et al. [121] developed a simplified dynamic gear model to explore the effect of friction on the resultant gear case vibration. The model incorporates the effects of variation in gear meshing stiffness. The meshing stiffness was calculated via finite element analysis. A method to introduce the frictional forces between the teeth in to the model is presented. Simulations were conducted with and without the frictional forces between the gear teeth. The effect of a gear defect on the gear case vibration is shown.

Bartelmus [122] reviewed current possibilities of using mathematical models and computer simulation to investigate the dynamic properties of gearbox systems. A model of a single stage gearbox with torsional degrees of freedom was considered. It is stated that the dynamics of the motor, couplings and driven machine has to be taken into account when simulating the dynamics of the gearbox. The influence of cracked gear teeth was investigated. Simulation results were compared with experimental results.

1.3 Research objectives

The first effect of fluctuating load conditions, which was observed, is the change in rotational speed associated with the change in load. Most electrical motors and internal combustion engines will rotate slower if the load on the motor or engine is increased. If the load is decreases, the electric motor or internal combustion engine will rotate faster. When a spectrum of a signal measured under changing speed conditions is calculated a smearing of the frequency content in the spectrum is observed. The effect of spectral smearing is perhaps the most detrimental and therefore it was the first issue addressed by researchers. Hardware order tracking methods were consequently developed to avoid spectral smearing under slowly varying speed conditions.

Potter and Gribler [3], Fyfe and Munck [4] as well as Bossley *et al.* [5] developed computed order tracking methods which was able to compensate for rapid speed fluctuation conditions. However, various authors such as Randall [117], McFadden [21, 22], Bauer et al. [118], Wang and Wong [99] indicated that the amplitude of the measured signal is influenced by fluctuating load conditions. Intuitively the measured structural response should increase if the load increases and decrease as the load decreases. Baydar and Ball [119] conducted the first experimental tests where vibration measurements were taken under different nominal load conditions. Their work indicated that spectral methods couldn't be used to monitor deteriorating fault conditions under fluctuating load conditions since the similarity between the spectra calculated under different load conditions varied dramatically. They applied a time frequency technique refereed to as the instantaneous power spectrum that indicated the presence of a fault condition in the time frequency plot of the distributions. However, the similarity between the plots under different loading conditions could complicate the diagnosis of a fault condition under different loading conditions.

Baydar and Ball [119] stated in their publication that it appears that no work has been done to evaluate how load conditions can effect the detection capability of vibration monitoring techniques. This observation was confirmed by the literature survey. From the literature survey, it can be concluded that order tracking should be applied to data measured under fluctuating load conditions. Time frequency analysis techniques are better suited to detect fault conditions under fluctuating load conditions. No experimental work was conducted under rapidly fluctuating load conditions.

The first objective of the research was set to build an experimental test rig, which was able to apply fluctuating load conditions to a spur gear test gearbox. Vibration measurements were taken on the test rig under different fluctuating load conditions. With this work, the effect of the fluctuating load on the measured acceleration could be determined. The experimental work indicated that the measured acceleration is amplitude modulated by the fluctuating load conditions.

Consequently, a load normalisation procedure should to be developed in order to compensate for the effect of the load without compromising diagnostic capability. A time synchronous averaging program, which incorporates, computed order tracking had to be programmed in order to eliminate spectral smearing and to reduce noise when analysing experimental data. Based on the literature review the data should be analysed with a pseudo Wigner-Ville distribution since it has good time frequency resolution. The developed normalisation technique should be applied to the data prior to the calculation of the pseudo Wigner-Ville distribution in order to improve the similarity between the distributions under different loading conditions. A single parameter, which could indicate deterioration in gear condition independent of the loading, should be extracted from the pseudo Wigner-Ville distribution.

The effect of the vibration transmission path from the gear to the point of measurement should be considered under fluctuating load conditions. However, it was postulated that the effect could be greatly reduced by measuring the instantaneous angular speed directly on the shaft with a shaft encoder. A simplified dynamic model of a gearbox should be developed to indicate the validity to measure the instantaneous angular speed and to simulate the effect of the fluctuating load conditions on the vibration measured on the gearbox casing as well as the instantaneous angular speed. The instantaneous angular speed and gearbox vibration should be measured experimentally on the same test gearbox under the same fluctuating load conditions to validate the postulate that the instantaneous angular speed is less influenced by the transmission path when compared to the vibration measured on the gearbox casing.

The effect of the transmission path under fluctuating load conditions should be investigated and a methodology should be developed to compensate for the transmission path effects. The methodology should be implemented on experimentally measured data to prove the efficiency of the developed methodology.

1.4 Document overview

A literature survey on gear vibration monitoring is presented in Chapter 1 as well as the objectives of the research conducted. In Chapter 2 the influence of load, fluctuation on the amplitude of the measured vibration signal is experimentally established on a spur gear test rig. Experimentally measured vibration waveforms measured under fluctuating load conditions are shown. From theses figures it is clear that the measured vibration waveform is amplitude modulated by the load on the gearbox. A load demodulation normalisation approach is proposed which estimates the modulation of the signal. The effect of the load on the modulation is estimated and the signal is then normalised by dividing the signal with the load modulation in order to obtain a load normalised acceleration signal. The signal is order tracked and synchronously averaged prior to the load normalisation approach and therefore the pseudo Wigner-Ville distribution can be calculated for the normalised data without being influenced by spectral smearing. Several statistical parameters are extracted from the distributions, which indicate a progression in gear damage under different load conditions.

A lumped parameter mass model of a simplified gear system is presented in Chapter 3 to model the effect of fluctuating load conditions on the structural response and instantaneous angular speed of a gear shaft. Simulation results indicate that the instantaneous angular speed can be used to monitor gear condition. Both the instantaneous angular speed and conventional gearbox casing vibration is amplitude modulated by the fluctuation in the applied load. It is proved through experimental measurements taken on a helical gear test rig that the instantaneous angular speed can be utilised to monitor a deteriorating gear fault condition under different loading conditions. The experimental results indicate that the instantaneous angular speed converges to a stable synchronous average in a fewer amount of shaft rotations when compared to the conventional vibration measurements measured on the gearbox casing. This phenomenon indicates that the conventional vibration measurements measured on the gearbox casing is influenced by the transmission path under fluctuating load conditions. A distinction is however made between cyclic stationary and non-cyclic stationary load conditions.

Chapter 4 introduces the phase smearing phenomenon, which occurs when applying synchronous averaging under fluctuating load conditions. The phenomenon is discussed and a phase domain averaging procedure is proposed to resolve the problem. Signal amplitudes are plotted as a function of the phase of the analytical signal prior to averaging in order to compensate for the phase shift induced by the transmission path when the rotational speed of the gear changes. An average of the signal amplitudes as a function of signal phase rather than degree of shaft rotation is calculated. A comparison is made between the phase domain averaging technique and conventional synchronous averaging combined with order tracking by applying the signal processing techniques to experimental data measured on the helical gear test rig.

The work is concluded in Chapter 5 and recommendations for further research are discussed. The experimental test rigs and measurement instrumentation utilised during the research are described in the Appendix.

Chapter 2

A load demodulation normalisation approach for vibration monitoring of gears operating under fluctuating load conditions

2.1 Introduction

In this chapter the influence of load fluctuation on the amplitude of the measured vibration signal is experimentally established through experiments conducted on a spur gear test rig. Vibration waveforms were measured on the test rig that indicated that the measured vibration waveform is amplitude modulated by the load on the gearbox. A rotation domain averaging process is proposed which combines synchronous averaging and order tracking to compensate for the fluctuation in rotational speed as well as to reduce the noise content in the measured signal.

In order to resolve the load modulation issue a load demodulation normalisation approach is proposed which estimates the modulation of the signal. The modulation of the signal is calculated by taking the absolute value of the signal's analytical signal. Load modulation of the signal will occur at a narrower frequency band in the low frequency region of the modulation when compared to the modulation caused by the presence of defects, which induces a wider frequency band modulation. The load modulation frequency band is obtained through an optimisation process described further on in the chapter. Modulation caused by the load is consequently obtained by low pass filtering the modulation of the signal. A load normalised acceleration signal is calculated by dividing the measured signal with the load modulation.

The literature survey indicated that the pseudo Wigner-Ville distribution has increased time frequency resolution characteristics in comparison with other time frequency techniques. Furthermore it was indicated that spectral analysis methods are unsuitable to monitor deteriorating fault conditions under fluctuating load conditions. Therefore the pseudo Wigner-Ville distribution was applied to the test data obtained from the spur gear test rig, in order to determine whether a deteriorating fault condition could be monitored with the distribution when calculating the distribution of the load normalised acceleration signal. Contour plots of the pseudo Wigner-Ville distribution data are presented, which indicate that the normalisation approach enables the detection of local gear tooth faults under fluctuating load conditions.

Statistical parameters and various other features are extracted from the distribution to indicate the linear separation of the values for the various fault conditions, once the vibration waveform normalisation approach has been applied. Feature vectors were compiled for the various fault and load conditions. Mahalanobis distances were calculated between the various feature vectors and an average feature vector was compiled from the data measured on the undamaged gearbox. The feature combination approach gives a single parameter, which can readily be monotonically trended to indicate the progression of a fault condition under fluctuating load conditions.

A single-layer perceptron network was trained by means of the perceptron-learning rule, within a finite number of iterations. This endorses the fact that the data are linearly separated between load conditions by the normalisation approach to vibration waveforms. The trained network can distinguish between the fault severities of a load condition that was not presented during the training of the network.

2.2 Experimental set-up

The experimental set-up consisted of a single-stage spur gearbox, driven by a 5 hp Dodge silicon controlled rectifier motor. A 5.5 kVA Mecc alte spa three-phase alternator was used for applying the load. Figure 2.1 illustrates the test rig.

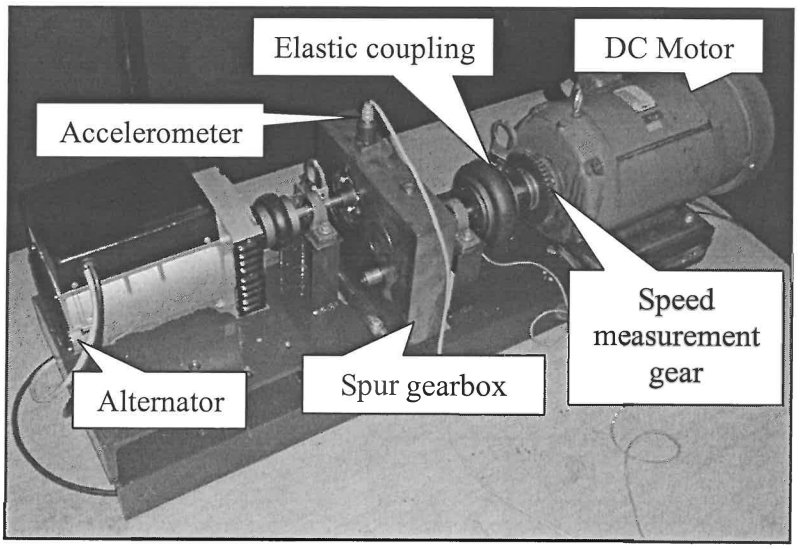

Figure 2.1 Experimental set-up

The gears each had 69 teeth. The Alternating Current (AC) generated by the alternator was rectified and dissipated over a large resistive load, which was kept constant during the tests. The Direct Current (DC) fields of the alternator were powered by an external DC supply in order to control the load that was applied to the gears. A single-phase voltage feedback from the alternator was used in conjunction with Proportional Integral (PI) compensation to regulate the torque applied by the alternator. A command signal input was incorporated into the controller so that a signal generator could be used to perform load control. Load fluctuation rates of up to 3 Hz could be applied.

The fluctuation in load changes the rotational speed of electrical motors. Therefore the rotational speed of the system was measured with a Deuta-Werke magnetic speed sensor, which was set on a gear with 50 teeth. The speed measurement gear was mounted on the output shaft of the electric motor. Gear teeth counters were utilised since they present a reliable and robust approach to speed measurement in practice. The average shaft speed during experimentation was 13 Hz.

A synchronising pulse was measured by means of a proximity switch on the key of the shaft. Acceleration measurements were taken in the vertical direction with a 500 mV/g PCB Integrated Circuit Piezoelectric (ICP) industrial accelerometer and a Siglab model 20-42 signal analyser. Vibration measurements were taken for five different load conditions and three different levels of damage severity, in order to develop and evaluate a signal-processing procedure that would be more sensitive to changes in the condition of the gears than to fluctuations in the load conditions.

Table 2.1 lists the specifications for the loading conditions. A sinusoidal load was selected to evaluate a slowly changing load condition, in contrast to the square load condition that creates a rapid change in load. The chirp load condition refers to a sinusoidal load condition where the frequency increases as time progresses. The chirp load condition therefore represents a wider frequency band of the applied load.

TABLE 2.1 Load case specifications

Load Case	Load Function	Frequency	Minimum Load	Maximum Load
1	Constant	0 Hz	14.4 Nm	14.4 Nm
2	Constant	0 Hz	15.9 Nm	15.9 Nm
3	Sine	0.5 Hz	6.6 Nm	18.6 Nm
4	Square	0.5 Hz	6.8 Nm	20.1 Nm
5	Chirp	0.1- 2 Hz	10.3 Nm	17.3 Nm

The initial vibration measurements were taken without any induced damage. Then face wear was induced on one of the gear teeth by artificially removing material from the gear face. In addition, a crack was sawed on the opposite side of the gear. The damage details are presented in Table 2.2. The fault severity conditions are expressed as the fraction of the root crack length over the 4 mm tooth thickness.

For further information with regards to the experimental set-up and measurement instrumentation refer to the appendix.

TABLE 2.2 Induced damage specifications

	Fault severity 25%	Fault severity 50%
Material removed from face	0.15 mm Nominally	0.3 mm Nominally
Crack length	1 mm	2 mm

2.3 Order tracking and synchronous averaging

Braun [6] introduced the use of time domain synchronised averaging on rotating machinery to filter out the measured acceleration caused by machine components, which are non-synchronous with the rotation of the shaft that is being analysed. McFadden [21, 22] employed the technique to monitor the condition of gears in helicopter gearboxes. The technique is based on the fact that the signal is cyclic stationary, since the same number of acceleration samples should be sampled during each revolution of the shaft to calculate the average signal.

Order tracking is a signal-capturing or sampling procedure, which is used to sample a vibration signal on rotating machinery with varying shaft speed. The sampling frequency of the logger is changed in accordance with a tacho pulse signal that indicates the speed of the shaft. A spectrum of the measured signal is calculated and expressed in terms of the shaft rotations, which are called orders. The order spectrum is therefore calculated independently of the shaft speed. In general the average of the order spectra is calculated in the order domain.

Time domain order tracking and synchronous averaging are approaches where the shaft speed, synchronising pulse and acceleration are measured at a constant sampling rate. The acceleration is calculated at constant angular positions of the shaft through interpolation. Several shaft rotation angles at constant increments of shaft rotation are initially selected in order to obtain the same number of data points for each shaft revolution.

The angle of shaft rotation for the sampled vibration is determined through the integration of the speed signal. A rotation-synchronised average is calculated from the acceleration in the rotation domain. The rotation-synchronised average vibration combines the properties of order tracking and synchronised averaging. The procedure enforces a pseudo-cyclic stationary condition on the data. A spectrum of the data is expressed in terms of shaft orders. The data were sampled at a high enough sampling frequency in order to avoid aliasing during the interpolation. The procedure was implemented in Matlab and 1 024 points were selected per revolution. Data from 276 shaft rotations were used to calculate the Rotation Domain Average (RDA) for each load condition and damage severity condition.

2.4 Load demodulation normalisation

The load variation manifests as a low-frequency band amplitude modulation on the Measured Acceleration Signal (MAS). The effect is displayed in Figure 2.2(a). The torque of an electrical machine decreases as the load frequency increases. Figures 2.3(a) to (c) illustrate the concept on the MAS when a chirp load condition is imposed on the system. The chirp load command signal, which is increased from 0.1 Hz to 2 Hz over a period of 5 seconds, can clearly be distinguished in the amplitude modulation that is low-pass filtered at 2Hz, as shown in Figure 2.3(c). The load modulation clearly indicates the decrease in amplitude as the load frequency increases. However the interaction and dynamic behaviour of the system due to the fluctuation in the load will modulate the amplitudes at higher frequencies.

A Load Demodulation Normalisation (LDN) procedure was adopted to manipulate the signal in order to reduce the effect of load fluctuation. A local defect on a gear tooth will modulate the MAS for a short duration in time. Gear systems are designed with contact ratios of more than 1.2 which means that more than one pair of teeth share the load during operation [123].

Gear systems that operate under fluctuating load conditions are generally designed with a contact ratio of greater than two in order to reduce noise levels and the possibility that teeth may impact on one another. Therefore the load will modulate the MAS for longer durations than a local tooth defect on a gear.

Consequently local tooth defects manifest in a wider frequency band amplitude modulation of the MAS with higher frequency content when compared with the smaller frequency band amplitude modulation caused by the load variation.

A fundamental part of the LDN signal manipulation procedure is to remove the modulation frequency band, which is influenced by the load variation, as will be discussed further on in the chapter. The procedure is suited to monitoring gear systems that operate under fluctuating load conditions and the results of experiments proved the hypothesis was valid.

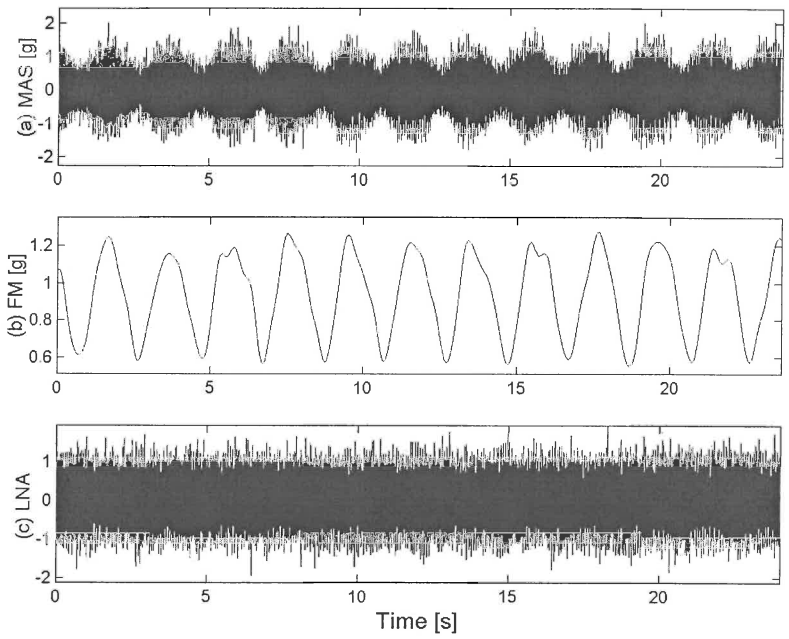

Figure 2.2 Load Demodulation Normalisation procedure
(a) Measured Acceleration Signal (b) Low pass Filtered Modulation of the signal
(b) Load Normalised Acceleration

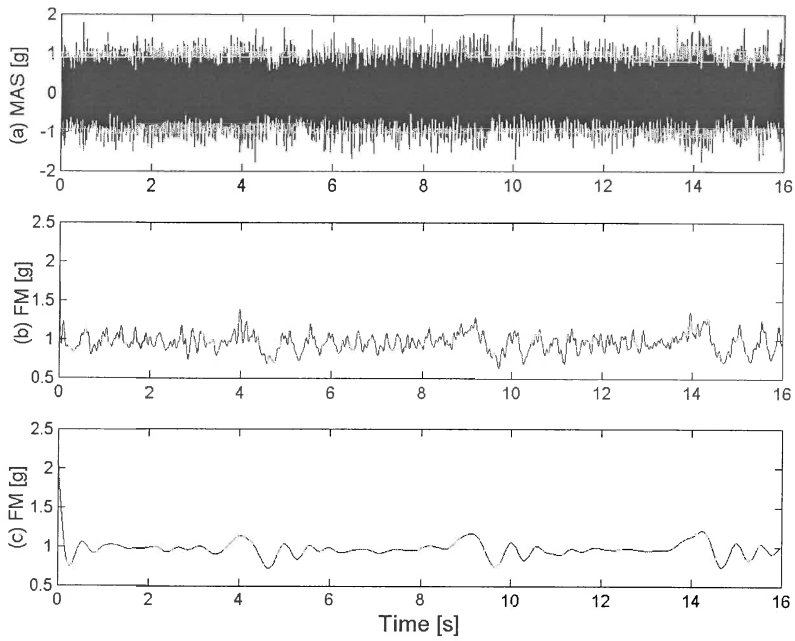

Figure 2.3 (a) Measured Acceleration Signal during chirp load excitation (b) Signal modulation low pass filtered at 10 Hz (c) Signal modulation low pass filtered at 2 Hz

The analytical signal of the MAS is calculated in order to obtain the amplitude modulation of the MAS. An analytical signal is a complex time signal comprising a real part equal to the real signal and the imaginary part is the Hilbert transform of the real part. The signal is expressed in Equation (2.2)

$$\tilde{a}(t) = H\{a(t)\} \tag{2.1}$$

$$\bar{a}(t) = a(t) + j\tilde{a}(t) \tag{2.2}$$

where $\tilde{a}(t)$ denotes the Hilbert transform of the real signal, $\bar{a}(t)$ the analytical signal, $a(t)$ the real signal and $j = \sqrt{-1}$. The Hilbert transform can be obtained by multiplying the positive frequency components of a signal's Fourier transform by –j (phase shift of minus 90 degrees) and the negative frequency components by +j (phase shift of plus 90 degrees). It is similar to frequency domain integration except that scaling with the frequency is not performed in the Hilbert transform.

The absolute value of the analytical signal represents the amplitude modulation of the signal. Randall [1] documents the procedure for retrieving the amplitude modulation. The amplitude modulation signal is low pass filtered to obtain the modulation of the MAS, which is influenced by the fluctuating load. The modulation frequency band, which is influenced by the load variation, will be referred to as the load-modulating frequency bandwidth. A Load Normalised Acceleration (LNA) signal is subsequently obtained by dividing the original signal by the Filtered Modulation (FM) signal. The concept is illustrated in Figures 2.2(a) to (c).

An optimisation procedure is followed to determine the load-modulating frequency bandwidth. It entails the calculation of the deviation in statistical properties between several LNA signals that were measured under different load conditions on an undamaged gearbox. The objective function of the optimisation procedure is therefore expressed as the sum of the relative differences between selections of statistical parameters as a function of the load-modulating frequency bandwidth. The objective function is shown in Equation (2.3)

$$OFV(f) = \sum_{s=1}^{S} \sum_{a=1}^{N} \sum_{b=1}^{N} \left[SP_{sa}(f) - SP_{sb}(f) \right] \qquad (2.3)$$

where OFV denotes the objective function value, SP the statistical parameter, S the number of statistical parameters, N the number of load conditions and f the low pass filter frequency or shaft order.

The time domain data are initially optimised by utilising the Root Mean Square (RMS) and variance as statistical parameters. Multiple local optima can be found in the Objective Function Values (OFV) for the load-modulating frequency bandwidth.

The RDA is calculated for each of these local optima since the non-synchronous components of the measured acceleration were present when the optimal load-modulating frequency bandwidth was being estimated. A post-processing optimisation is performed on the RDA signals once the non-synchronous components have been removed by means of the averaging procedure. Thus the optimal load-modulating bandwidth of the shaft order is determined. The statistical parameters used in the post-processing optimisation are based on the Pseudo Wigner-Ville (PWV) distribution of the rotation domain average and will be discussed in the following section of the chapter. Figure 2.4 shows a flow diagram of the optimisation procedure.

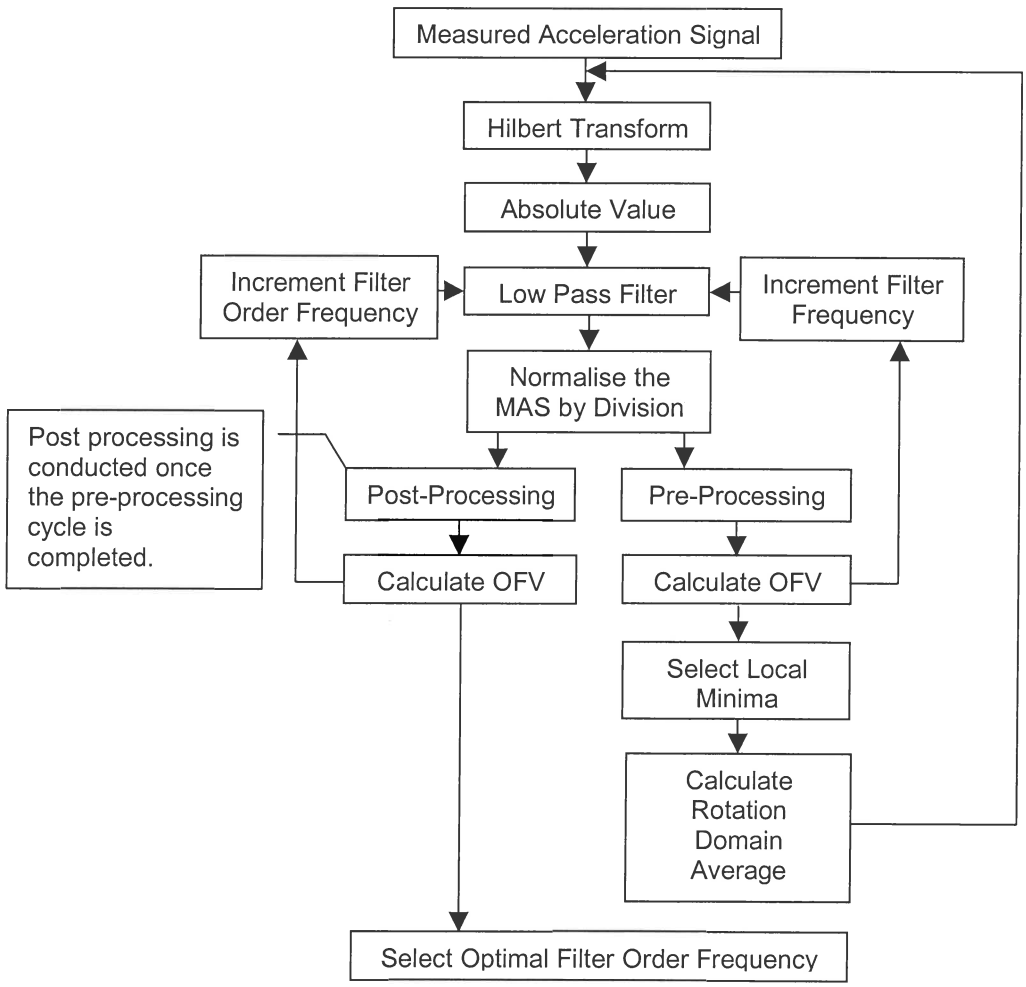

Figure 2.4 Flow diagram of the optimisation of load demodulation normalisation

Figure 2.5 presents the OFV for the pre-processing optimisation. The OFV and load-modulating frequency bandwidth for the local optima are shown in Table 2.3 which presents the post-optimisation results based on each of the local optima in the pre-processing optimisation. Note that the lowest OFV for the pre-optimisation procedures do not correlate with the lowest OFV obtained during the post-optimisation procedure. This is why all the local optima obtained in the pre-processing optimisation were selected. The local optima in the pre-processing optimisation do however indicate the load normalisation frequency bandwidths, which render LNA signals with increased similarity under different loading conditions. Therefore the best post-optimisation results will be obtained with data pre-normalised at these frequency bandwidths.

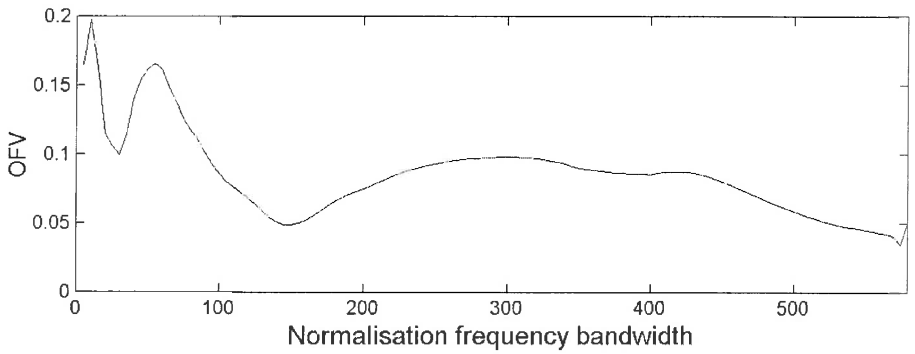

Figure 2.5 Objective function values for the various normalisation frequency bandwidths

TABLE 2.3 Results of optimal normalisation bandwidth

Frequency bandwidth	OFV	Shaft order bandwidth	OFV
0-29 Hz	0.099	0-21 Orders	6.208
0-144 Hz	0.048	0-23 Orders	6.361
0-578 Hz	0.034	0-11 Orders	9.062

The best optimisation result was obtained for a 21-order load modulating bandwidth, which was processed on a 29 Hz load-modulating frequency bandwidth. Figure 2.6 presents the OFV as a function of the load modulating normalisation bandwidth of the shaft order. The OFV was calculated for discrete steps of the shaft order. Note the steep increase in the OFV for larger load modulating normalisation frequency bandwidths, which indicates a decrease in statistical similarity for LNA signals with load-modulating shaft order bandwidths that are too wide.

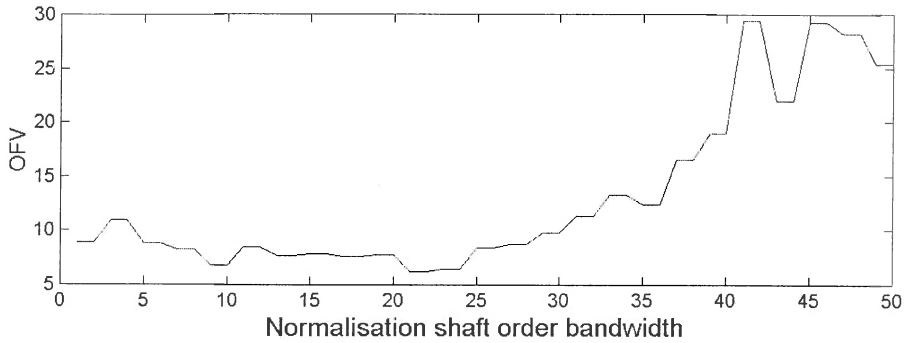

Figure 2.6 Objective function values for the various normalisation shaft-order bandwidths

2.5 Pseudo Wigner-Ville Distribution

In the literature survey it is indicated that time frequency analysis is the three-dimensional time, frequency and amplitude representation of a signal, which is inherently suited to indicating transient events in a signal. The Wigner distribution and its various permutations is such an analysis technique, and has been used by various authors to detect the presence of local gear faults by means of vibration signal analysis.

The Wigner distribution is derived by generalising the relationship between the power spectrum and the autocorrelation function for non-stationary time-variant processes. A Wigner-Ville distribution is obtained by applying the Wigner distribution to an analytical signal. This is done to account for all frequencies since the amplitudes of the negative frequencies in the analytical signal are equal to zero.

However the distribution is influenced by so-called cross-terms that are an inherent property of the distribution. Therefore a frequency-smoothing window is applied which relieves some of the interference and cross-term effects. The application of the frequency-smoothing window results in a Pseudo Wigner-Ville (PWV) distribution and is defined by Equation 2.4

$$PWV_a(t,f) = \int_{-\infty}^{+\infty} h(\tau)\bar{a}(t+\tau/2)\bar{a}^*(t-\tau/2)e^{-j2\pi f\tau}d\tau \qquad (2.4)$$

where t denotes the time, f the frequency, τ the time delay and h the frequency-smoothing window.

Local gear fault conditions will cause an impact, which modulates the measured acceleration signal. The transient signal modulation will be manifested as a dispersion of energy in the frequency domain of the distribution.

The PWV distribution was calculated on RDA signals, which were not load-normalised. The time domain component of the distributions indicates the degree of shaft rotation; the frequency component is expressed in orders since the distributions are calculated on the order-tracked data in the rotation domain. These distributions were normalised by using the maximum value of the distribution, based on the fact that previous authors have done this to detect the presence of gear defects in gearboxes through vibration monitoring. Figures 2.7 and 2.8 display contours of the distributions for the 25% and 50% fault severity situation without LDN.

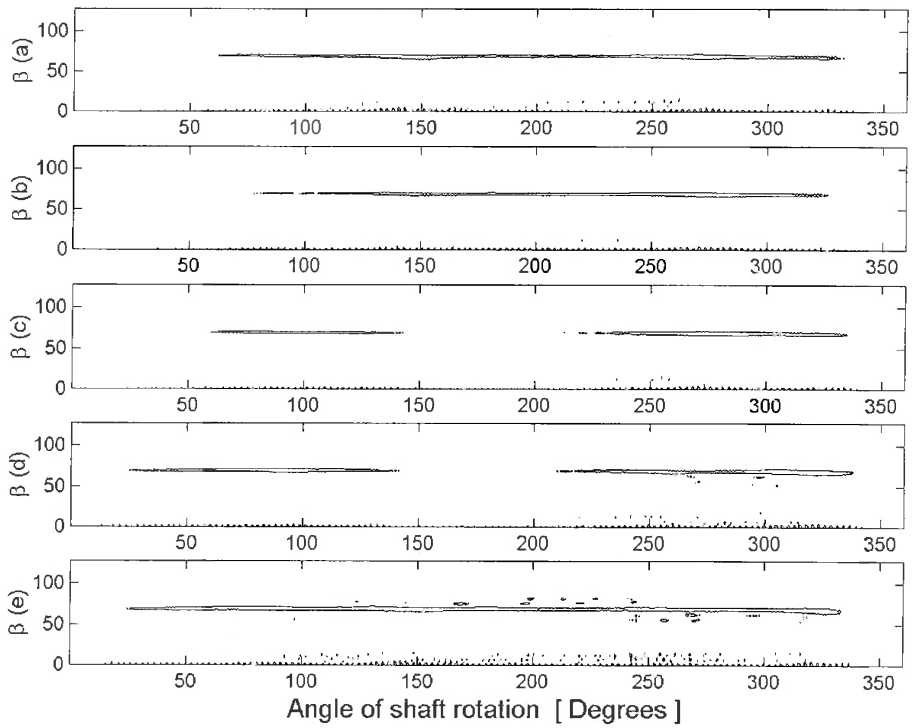

Figure 2.7. RDA PWV distribution contour. The contour level is calculated at 17 times the mean value of the distribution and represents the 25% fault severity condition. (a) Load Case 1; (b) Load Case 2; (c) Load Case 3; (d) Load Case 4; (e) Load Case 5.

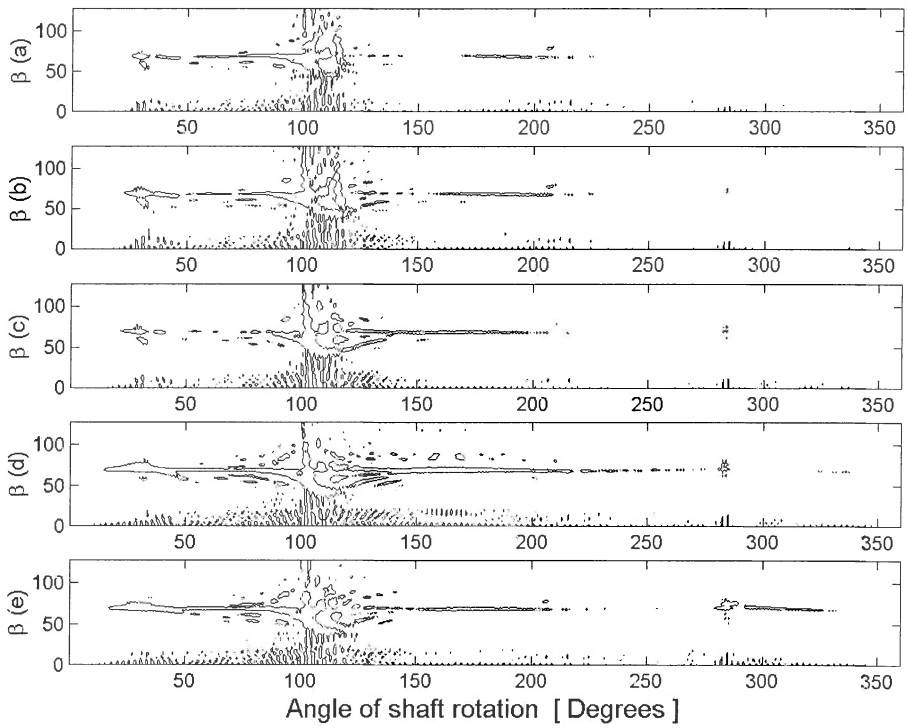

Figure 2.8. RDA PWV distribution contour. The contour level is calculated at 10 times the mean value of the distribution and represents the 50% fault severity condition. (a) Load Case 1; (b) Load Case 2; (c) Load Case 3; (d) Load Case 4; (e) Load Case 5.

Contours for the PWV distributions of the RDA LNA signals are displayed in Figures 2.9 and 2.10. The contours for the 25% and 50% fault severity condition are calculated at 17 and 10 times the mean value of the distribution. The fluctuation in the amplitude of the gear mesh order without LDN can be clearly seen in Figure 2.7 when compared to Figure 2.9.

The contour plot of the maximum value of the normalised PWV distribution at 50% fault severity indicates the inability of the distribution to detect the presence of the induced flank wear without LDN. The deviation in the energy distribution between the different load conditions of the mean normalised PWV distribution is more than the deviation in the energy distribution of the PWV distributions calculated from the LDN data.

The PWV distributions of the RDA signals were calculated with the Time-Frequency Toolbox for Matlab [80].

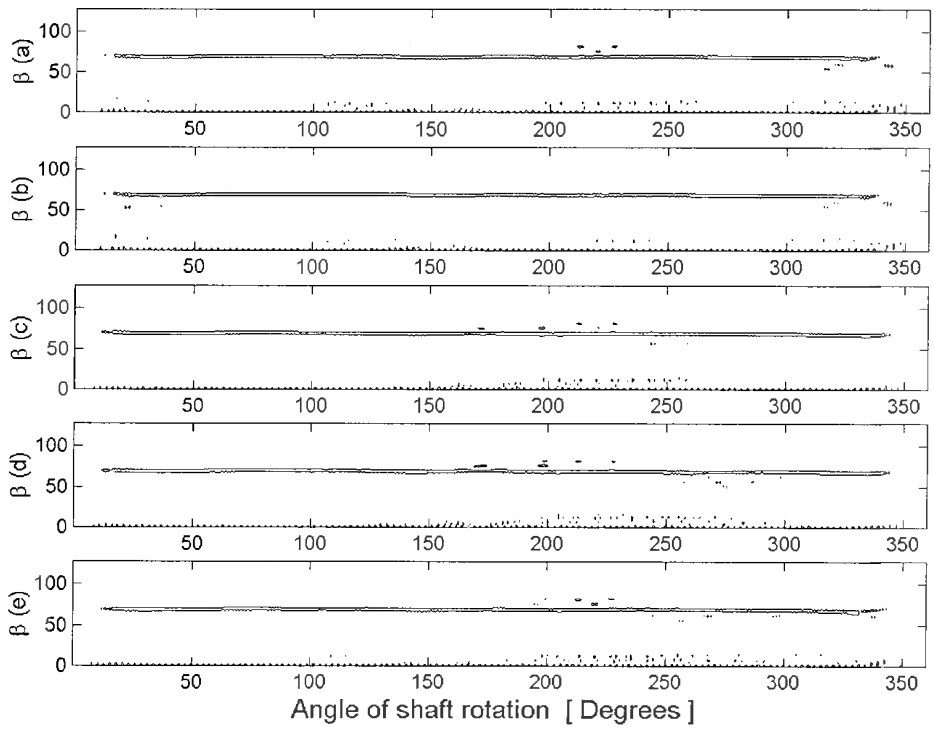

Figure 2.9. LDN RDA PWV distribution contour. The contour level is calculated at 17 times the mean value of the distribution and represents the 25% fault severity condition. (a) Load Case 1; (b) Load Case 2; (c) Load Case 3; (d) Load Case 4; (e) Load Case 5.

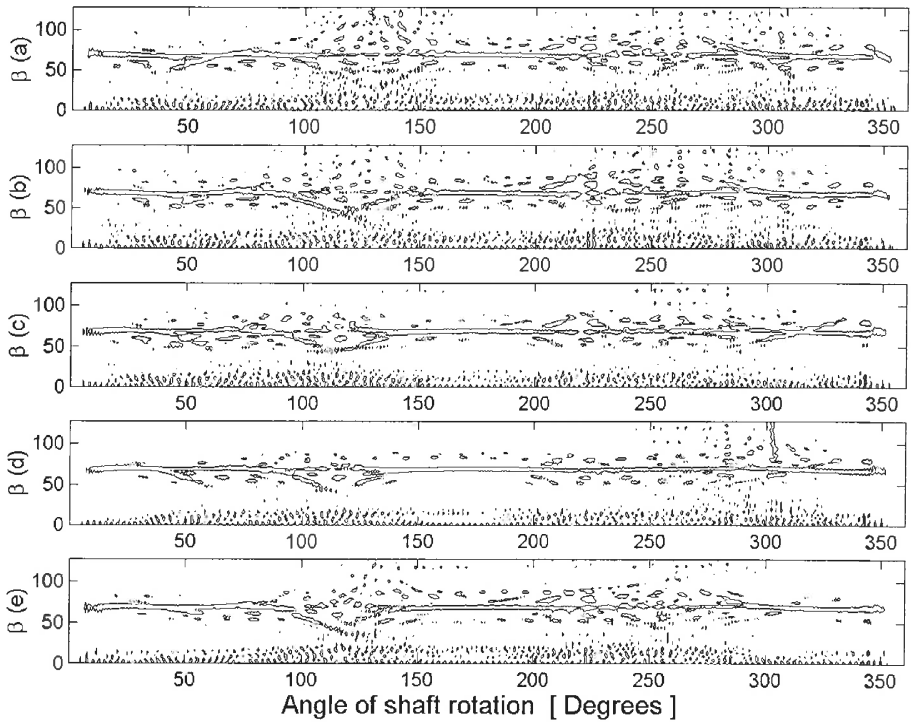

Figure 2.10. LDN RDA PWV distribution contour. The contour level is calculated at 10 times the mean value of the distribution and represents the 50% fault severity condition. (a) Load Case 1; (b) Load Case 2; (c) Load Case 3; (d) Load Case 4; (e) Load Case 5.

2.6 Statistical Features of the PWV distribution

A selection of statistical parameters was calculated for the various PWV distributions with and without load normalisation to indicate the effect of the LDN procedure under varying load conditions.

The rotation marginal of the PWV distribution is defined by Equation 2.5 and corresponds to the instantaneous power of the signal [80]

$$m_{\beta}(\theta) = \int_{-\infty}^{+\infty} PWV_a(\theta, \beta) d\beta \qquad (2.5)$$

where β denotes the order and θ the angle of shaft rotation.

The mean, standard deviation, variance and maximum values of the rotation marginal of the PWV distribution were calculated. A peak factor is defined as the ratio of the maximum value to the mean value of the time marginal. Table 2.4 lists the statistical parameters of the rotation marginal data.

Table 2.5 shows the energy of the various PWV distributions, calculated in accordance with Equation 2.6.

$$E = \int_{-\infty}^{+\infty} \int_{-\infty}^{+\infty} PWV_a(\theta, \beta) d\beta d\theta \qquad (2.6)$$

Table 2.5 also indicates the mean of the variance and the standard deviation of the amplitude of the order domain of the distribution. An area level ratio is defined as the area of the distribution that attains amplitudes higher than a specified contour level over the entire area of the distribution. Table 2.5 gives the data on the area level ratio for the distributions for a contour level that is ten times the mean value of the specific distribution.

The values of the statistical parameters calculated on the LNA RDA signal PWV distributions clearly indicate linear separation between the different levels of fault severity. A monotonic increase in the values is obtained for each load condition as the fault severity increases.

There are slight variations in the values between each fault condition but, the deviation is less than the deviation in the values caused by the increase in fault severity. The statistical parameters that are calculated on the mean normalised distributions are not linearly separated between the levels of fault severity.

This implies that the values of the parameters for a certain load condition at 0% fault severity might be more or less than the value at 25 % fault severity for a different load condition.

The order marginal of the PWV distribution is defined by Equation 2.7 and corresponds to the spectral density of the energy of the signal [80].

$$m_\theta(\beta) = \int_{-\infty}^{+\infty} PWV_a(\theta, \beta) d\theta \tag{2.7}$$

Equation 2.8 defines an order spectral energy density ratio and values for the distributions are given in Table 2.6.

$$ER = \frac{\sum_{\beta=60}^{80} m_\theta(\beta)}{\sum_{\beta=30}^{60} m_\theta(\beta) + \sum_{\beta=80}^{110} m_\theta(\beta)} \tag{2.8}$$

Note that the value of the ER is linearly separated between the load conditions for both of the normalised distribution cases. This is attributed to the fact that the ratio is inherently a normalised value without any form of normalisation on the distribution. The ER is defined over a wide range of orders to capture the dispersion of the energy due to a local fault condition, as shown in Figures 2.8 and 2.10.

TABLE 2.4 Results of rotation marginal feature anthology

Mean value of the LDN rotation marginal					
Fault severity	Load Case 1	Load Case 2	Load Case 3	Load Case 4	Load Case 5
0	0.5301	0.5273	0.5280	0.5253	0.5234
25%	0.5485	0.5426	0.5442	0.5415	0.5448
50%	0.6028	0.6095	0.5821	0.5631	0.5778
Mean value of the rotation marginal without LDN					
Fault severity	Load Case 1	Load Case 2	Load Case 3	Load Case 4	Load Case 5
0	0.0119	0.0112	0.0122	0.0132	0.0127
25%	0.0101	0.0089	0.0085	0.0103	0.0139
50%	0.0076	0.0089	0.0083	0.0112	0.0100
Standard deviation of the LDN rotation marginal					
Fault severity	Load Case 1	Load Case 2	Load Case 3	Load Case 4	Load Case 5
0	0.4591	0.4350	0.4310	0.4174	0.4208
25%	0.5297	0.5070	0.5144	0.5081	0.5279
50%	0.7289	0.7673	0.6336	0.5914	0.6585
Standard deviation of the rotation marginal without LDN					
Fault severity	Load Case 1	Load Case 2	Load Case 3	Load Case 4	Load Case 5
0	0.0134	0.0120	0.0121	0.0120	0.0124
25%	0.0114	0.0096	0.0090	0.0110	0.0151
50%	0.0186	0.0215	0.0209	0.0208	0.0195
Variance of the LDN rotation marginal					
Fault severity	Load Case 1	Load Case 2	Load Case 3	Load Case 4	Load Case 5
0	0.2108	0.1893	0.1857	0.1742	0.1771
25%	0.2806	0.2571	0.2646	0.2581	0.2787
50%	0.5313	0.5887	0.4014	0.3497	0.4336
Variance of the rotation marginal without LDN					
Fault severity	Load Case 1	Load Case 2	Load Case 3	Load Case 4	Load Case 5
0	0.1787	0.1438	0.1453	0.1440	0.1530
25%	0.1293	0.0929	0.0817	0.1208	0.2290
50%	0.3454	0.4620	0.4385	0.4311	0.3806
Peak factor of the LDN rotational marginal					
Fault severity	Load Case 1	Load Case 2	Load Case 3	Load Case 4	Load Case 5
0	4.2060	3.9358	3.9776	4.6599	3.8781
25%	5.8597	5.6956	5.8928	5.8693	5.8376
50%	7.5768	10.5802	7.3114	9.8727	7.7656
Peak factor of the rotation marginal without LDN					
Fault severity	Load Case 1	Load Case 2	Load Case 3	Load Case 4	Load Case 5
0	5.8409	6.9789	5.6969	4.6595	4.6652
25%	6.3101	6.2674	6.4693	5.7591	7.0030
50%	30.5872	21.7874	30.3159	22.1108	27.0636

TABLE 2.5 Results of the feature anthology

Energy of the LDN PWV distribution					
Fault severity	Load Case 1	Load case 2	Load case 3	Load Case 4	Load case 5
0	271.2579	269.7251	270.1939	268.8260	267.8423
25%	280.2933	277.0871	278.3292	276.9988	278.0602
50%	308.2603	311.7739	297.7140	287.3991	295.5083
Energy of the PWV distribution					
Fault severity	Load case 1	Load case 2	Load case 3	Load Case 4	Load case 5
0	6.0722	5.7478	6.2340	6.7488	6.5051
25%	5.1930	4.5673	4.3602	5.2900	7.0978
50%	3.8644	4.5705	4.2295	5.7454	5.1043
Mean of the amplitude variance in the order domain of the LDN PWV distribution					
Fault severity	Load case 1	Load case 2	Load Case 3	Load Case 4	Load Case 5
0	13.1775	13.0785	13.1200	12.9960	12.8708
25%	14.0273	13.6992	13.8744	13.7449	13.8757
50%	17.0021	17.3222	15.8747	14.9313	15.6247
Mean of the amplitude variance in the order domain of the PWV distribution					
Fault severity	Load Case 1	Load Case 2	Load Case 3	Load Case 4	Load Case 5
0	0.0066	0.0060	0.0069	0.0081	0.0075
25%	0.0055	0.0044	0.0040	0.0055	0.0098
50%	0.0038	0.0057	0.0047	0.0077	0.0063
Mean of the STD of the amplitude in the order domain of the LDN PWV distribution					
Fault severity	Load Case 1	Load Case 2	Load Case 3	Load Case 4	Load Case 5
0	3.5449	3.5321	3.5383	3.5258	3.5082
25%	3.6546	3.6144	3.6344	3.6234	3.6340
50%	4.0181	4.0455	3.8983	3.7874	3.8570
Mean of the STD of the amplitude in the order domain of the PWV distribution					
Fault severity	Load Case 1	Load Case 2	Load Case 3	Load Case 4	Load Case 5
0	0.0760	0.0723	0.0793	0.0861	0.0828
25%	0.0679	0.0601	0.0568	0.0685	0.0929
50%	0.0460	0.0542	0.0509	0.0732	0.0635
Area level ratio of the LDN PWV distribution					
Fault severity	Load Case 1	Load Case 2	Load Case 3	Load Case 4	Load Case 5
0	5.63%	5.24%	5.21%	5.14%	5.30%
25%	6.42%	5.99%	5.85%	6.30%	6.35%
50%	10.48%	10.68%	9.31%	8.62%	9.09%
Area level ratio of the PWV distribution					
Fault severity	Load Case 1	Load Case 2	Load Case 3	Load Case 4	Load Case 5
0	5.62%	5.12%	5.42%	5.61%	5.72%
25%	4.78%	3.70%	3.54%	4.79%	7.28%
50%	3.41%	4.54%	3.99%	6.43%	5.41%

TABLE 2.6 Results of the order spectral energy density ratio

Order spectral energy density ratio of the LDN PWV distribution					
Fault severity	Load Case 1	Load Case 2	Load Case 3	Load Case 4	Load Case 5
0	8.8791	10.9243	10.5386	11.8132	10.5999
25%	5.2951	6.0204	7.3664	6.2092	5.4004
50%	1.7644	1.7929	2.0292	2.7349	2.1879
Order spectral energy density ratio of the PWV distribution					
Fault severity	Load Case 1	Load Case 2	Load Case 3	Load Case 4	Load Case 5
0	9.2313	10.5225	10.3497	12.4929	11.1083
25%	6.5704	7.8579	8.7667	7.2788	5.8564
50%	1.7224	1.4050	1.2697	2.2282	1.8890

2.7 Divergence analysis

Divergence analysis was performed on the data in order to obtain a single parameter, which could be trended to indicate the degradation of the gears. To this end, feature vectors of the statistical parameters of the distributions were compiled.

The Mahalanobis distance is the weighted distance between two vectors and is used as a measure of the similarity between the vectors. The Mahalanobis distance is presented in Equation 2.9

$$d^2(\bar{x},\bar{y}) = \sum_{n=1}^{N}\left[\bar{x} - \bar{M}(\bar{y})\right]^T \frac{1}{s^2}\left[\bar{x} - \bar{M}(\bar{y})\right] \qquad (2.9)$$

$$m(\bar{y}) = \frac{\sum_{n=1}^{N}\bar{y}(n)}{N} \qquad (2.10)$$

where $\bar{x}$ denotes the vector to which the distance is calculated, $\bar{y}$ the mean reference vector. An average mean value vector $\bar{M}(\bar{y})$ of vector $\bar{y}$ is composed by inserting the mean scalar value $m(\bar{y})$ repetitively into the average mean value vector, in order to create a vector the size of $\bar{y}$. The distance between the two vectors are measured relative to the standard deviation s of the mean reference vector.

Weighting is performed in order to account for the scaling in the feature vectors. The value N refers to the number of values in the various vectors. Staszewski et al. [58, 59] used the weighted distance to indicate the degradation of gear integrity. The magnitude of the weighted distance indicates the degree of divergence from the reference vector.

A mean reference vector is compiled from a selection of the statistical parameters for the various load conditions at 0% fault severity. The weighted distance from the mean reference vector is therefore calculated to indicate the condition of the analysed gear. The weighted distance was calculated with the Statistical Toolbox of Matlab [124].

Table 2.7 shows the weighted distances for two selections of feature vectors, that was calculated and is shown in Table 2.8. The data indicate that the weighted distance procedure can readily show the monotonic trend of the condition of a gear under different loading conditions with a single parameter, if the statistical parameters are calculated from a PWV distribution of an LDN RDA signal.

The divergence analysis of the combined statistical parameters in a feature vector did not improve the linear separation between the load conditions for the parameters calculated from the mean normalised distribution.

TABLE 2.7 Feature vector compilation used in calculating the Mahalanobis distance

Feature Vector 1	Feature Vector 2
Area level ratio	Area level ratio
Mean variance of the distribution	Mean variance of the distribution
Mean value of the rotation marginal	Mean standard deviation of the distribution
Energy of the distribution	Standard deviation of the rotation marginal
	Mean value of the rotation marginal
	Peak factor of the rotation marginal
	Energy of the distribution
	Variance of the rotation marginal

TABLE 2.8 Results of the Mahalanobis distance of the divergence analysis

Mahalanobis distance of the LDN data of Feature Vector Number 1					
Fault severity	Load Case 1	Load Case 2	Load Case 3	Load Case 4	Load Case 5
0	3.04	3.00	3.01	2.98	2.96
25%	3.24	3.16	3.19	3.16	3.18
50%	3.90	3.99	3.64	3.39	3.58
Mahalanobis distance of the data without LDN for Feature Vector Number 1					
Fault severity	Load Case 1	Load Case 2	Load Case 3	Load Case 4	Load Case 5
0	2.95	2.57	2.95	3.35	3.25
25%	2.22	1.77	1.69	2.26	4.59
50%	1.58	1.94	1.73	3.21	2.42
Mahalanobis distance of the LDN data of Feature Vector Number 2					
Fault severity	Load Case 1	Load Case 2	Load Case 3	Load Case 4	Load Case 5
0	7.08	7.01	7.03	6.96	6.91
25%	7.55	7.38	7.45	7.37	7.43
50%	9.12	9.31	8.5	7.9	8.37
Mahalanobis distance of the data without LDN for Feature Vector Number 2					
Fault severity	Load Case 1	Load Case 2	Load Case 3	Load Case 4	Load Case 5
0	7.14	7.59	7.02	6.96	6.8
25%	6.31	5.39	5.43	5.9	10.83
50%	93.59	46.99	92.22	50.59	74.17

2.8 Neural networks

Neural Networks are multidimensional curve-fitting algorithms that attempt to mimic the structure of the brain and nervous systems of living creatures [125]. In general the fitted curve is used to recognise certain conditions in the input data. The fitting procedure is referred to as training. The perceptron network is an example of such a curve-fitting procedure and was utilised by Staszewski *et al.* [60] and many other authors to identify from pre-processed acceleration signal data the increase in the severity of gear faults.

The equations for a single-layer perceptron network are presented in Equations 2.11 and 2.12

$$\bar{n} = W\ \bar{p} + \bar{b} \tag{2.11}$$

$$\bar{a} = f_{Hard\,\lim}\{\bar{n}\} \tag{2.12}$$

$$f_{Hard\,\lim} = \begin{Bmatrix} 0\ if\ n < 0 \\ 1\ if\ n > 0 \end{Bmatrix}$$

where $\bar{n}$ denotes the input to the hard limit transfer function, W the weight matrix, $\bar{p}$ the input vector, $\bar{b}$ the bias vector and $\bar{a}$ the output vector.

The weight matrix and bias vector of Equation 2.11 are updated during training, in accordance with the perceptron learning rule presented in Equations 2.13 and 2.14

$$W^{new} = W^{old} + (\bar{t} - \bar{a})\bar{p} \tag{2.13}$$

$$b^{new} = b^{old} + (\bar{t} - \bar{a}) \tag{2.14}$$

where $\bar{t}$ denotes the target vector that is defined for the training procedure to indicate a certain level of fault severity. Input vectors that contain the feature data of the known fault severity condition are presented with the target vector during training. The weight matrix and bias vector will converge after a finite number of iterations with the learning data if the data is linearly separated. The precision with which the trained network can classify data is evaluated by simulating the network output for an input feature vector of known fault severity that was not presented during the learning process.

A single-layered perceptron network with five input items and three output items was trained to classify feature vectors according to fault severity, independently of the load conditions. The standard deviation, peak factor and variance of the rotation marginal as well as the energy ratio and area level values of the LDN PWV distributions were used in the input feature vectors.

The statistical parameters were normalised according to Equation 2.15 in conjunction with Equation 2.16 for those that increased with fault severity, and Equation 2.15 with Equation 2.17 for those that decreased with fault severity

$$NSP = \frac{SP - RP}{RP} \tag{2.15}$$

$$RP = s - \mu \tag{2.16}$$

$$RP = s + \mu \tag{2.17}$$

$$\mu = \frac{1}{N}\sum_{n=1}^{N} SP(n) \tag{2.18}$$

$$s = \left(\frac{1}{N-1}\sum_{n=1}^{N}\left(SP(n) - \mu\right)^2\right)^{\frac{1}{2}} \tag{2.19}$$

where NSP denotes the normalised statistical parameter, RP the reference parameter, μ the mean value of the statistical parameter under the various load conditions at 0% fault severity and s the standard deviation of the statistical parameter under the various load conditions at 0% fault severity.

The network was trained with the constant, sine and square load case excitation data. The weight matrix and bias vector converged within 60 passes of the training data set, confirming that the data are linearly separated. Table 2.9 lists the weight matrix and bias vector of the trained network. The network was able to classify the data on chirp-loading conditions according to fault severity. The results of the network evaluation on the chirp load data are listed in Table 2.10. The network was trained and evaluated by means of the Matlab Neural Network Toolbox [110].

TABLE 2.9 Weight and bias values of the neural network

	Neural Network Weight Matrix					Bias Vector
Node number	Network input number					
	1	2	3	4	5	
1	-3.7929	-3.8994	-2.8223	-6.0797	-7.5479	5
2	17.3752	-16.0945	2.5477	0.6228	-2.9946	-3
3	-0.2203	3.6407	1.2032	2.0124	4.4466	-9

TABLE 2.10 A Load Case 5: simulation input data

Normalised feature	Fault severity 0%	Fault severity 25%	Fault severity 50%
Standard deviation of the rotation marginal	0.0874	0.5351	0.8116
Peak factor of the rotation marginal	0.0382	0.2423	0.7794
Variance of the rotation marginal	0.0110	0.2684	0.5822
Energy ratio	0.0176	0.5318	1.0377
Area level ratio	0.0236	0.6112	1.5069

TABLE 2.10 B Load Case 5: simulation output results before and after the hard limit transfer function

Fault severity 0 %		Fault severity 25 %		Fault severity 50 %	
n	a	n	a	n	a
4.2033	1	-6.5786	0	-20.4439	0
-2.1274	0	1.5813	1	-3.8252	0
-8.7266	0	-4.1246	0	3.1483	1

Chapter 3

Instantaneous angular speed monitoring of gearboxes under non-cyclic stationary and cyclic stationary load conditions

3.1 Introduction

A simplified mathematical model was developed to determine whether the Instantaneous Angular Speed (IAS) of a shaft fitted with a gear would vary as the teeth meshed in and out of the gear mesh, and whether it could be used for diagnostic purposes under fluctuating load conditions. The model is based on the gear system modelling methodologies of Howard *et al.* [121] and Bartelmus [122]. Model simulations indicate that the IAS varies as the gear teeth mesh in and out of the gear mesh and that a fault condition in the form of reduced meshing stiffness can be detected by utilising the IAS. The IAS is measured in order to compensate for the fluctuation in speed caused by the varying load conditions. The vibration signal was previously measured on gearbox casings for monitoring purposes, but the IAS signal can be used as a substitute because the signal can reflect changes in the gear meshing stiffness for monitoring purposes. Gear condition can therefore be monitoring without taking the conventional vibration signal measured on the casing to indicate the deterioration in gear condition under fluctuating load conditions. The IAS measurement can be used for both diagnostic and order tracking purposes. Monitoring cost can therefore be reduced by utilising the IAS.

Varying load conditions were applied to the gear model. Both the IAS and conventional vibration measurements exhibited the modulation caused by the load fluctuation. A distinction was made between cyclic stationary load conditions and non-cyclic stationary load conditions. It was found that non-cyclic stationary load modulation could be averaged out with RDA. Once the RDA had converged and the modulation effect of the non-cyclic stationary load had been removed, the signal still had to be normalised in order to compensate for the nominal difference in the load. The inherent advantage of dealing with non-cyclic stationary load conditions is that the low pass filter frequency does not have to be determined through an optimisation process. However, LDN has to be applied to cyclic stationary load conditions to remove the modulation caused by the load modulation, and a low pass filter frequency has to be determined to suppress the load modulation effects.

A test rig was built to apply non-cyclic stationary load conditions to a test gearbox. Measurements were taken with an accelerometer and a shaft encoder for three different levels of induced flank wear on the gear wheel. Convergence studies were conducted with both the accelerometer and shaft encoder data under different loading conditions. The results indicated that the dissimilarity between rotation domain averaged data under different non-cyclic stationary loading conditions decreased as the number of averages increased. The postulate that the non-cyclic stationary load modulation is diminished with an increase in the number of rotation domain averages was proven valid.

The convergence studies indicated that the IAS converge faster than normal vibration measurements because the measurement is less susceptible to the transmission of forces from surrounding rotating equipment, as these forces contribute to the response measured with conventional vibration instrumentation. This aspect simplifies the diagnosis of gear fault conditions and makes the utilisation of the IAS an attractive option for monitoring the condition of gears.

Smoothed Pseudo-Wigner-Ville (SPWV) distributions were calculated for the experimental data to which the RDA process was applied for diagnostic purposes. An energy ratio value was defined to obtain a single parameter to indicate the degradation in the condition of the gear. Linear separation between the energy ratio values for the three levels of gear damage severity was obtained under different loading conditions.

3.2 Dynamic gear model

Figure 3.1 is a diagram of a simplified dynamic gear model. The model comprises four degrees of freedom and was developed to explore the utilisation of the IAS for the purposes of monitoring the condition of gears. A unique feature of the model is the incorporation of a translating mass. This degree of freedom is utilised to represent conventional vibration monitoring on the gear-case, which is compared with IAS monitoring. The equations of motion describing the model are presented in Equations 3.1 to 3.4. The selected model parameters, which are representative of typical values for a gearbox, are given in Table 3.1.

$$M_1\ddot{X}_1 + (C_1 + C_2)\dot{X}_1 + (K_1 + K_2)X_1 - C_2\dot{X}_2 - K_2X_2 = 0 \tag{3.1}$$

$$\begin{aligned} M_2\ddot{X}_2 + (C_2 + C_3)\dot{X}_2 + (K_2 + K_3)X_2 - C_2\dot{X}_1 - K_2X_1 - C_3R_g\dot{\theta}_2 - K_3R_g\theta_2 \\ + C_3R_p\dot{\theta}_1 + K_3R_p\theta_1 = 0 \end{aligned} \tag{3.2}$$

$$\begin{aligned} I_1\ddot{\theta}_1 + R_p{}^2C_3\dot{\theta}_1 + R_p{}^2K_3\theta_1 - R_pR_gC_3\dot{\theta}_2 - R_pR_gK_3\theta_2 \\ + R_pC_3\dot{X}_2 + R_pK_3X_2 = T_1 \end{aligned} \tag{3.3}$$

$$\begin{aligned} I_2\ddot{\theta}_2 + R_g{}^2C_3\dot{\theta}_2 + R_g{}^2K_3\theta_2 - R_gR_pC_3\dot{\theta}_1 - R_gR_pK_3\theta_1 \\ - R_gC_3\dot{X}_2 - R_gK_3X_2 = -T_2 \end{aligned} \tag{3.4}$$

The gear mesh stiffness is approximated as a 2 % sinusoidal variation of the nominal mesh stiffness in order to simulate the fundamental gear-meshing harmonic. The percentage variation in gear meshing stiffness is adopted from the work of Howard *et al.* [121]. Model damping is approximated as being viscous for simplification purposes. A unity input torque T_1 is applied to the input pinion of the model with a 10 % variation in time in order to simulate the fluctuating load conditions on the model.

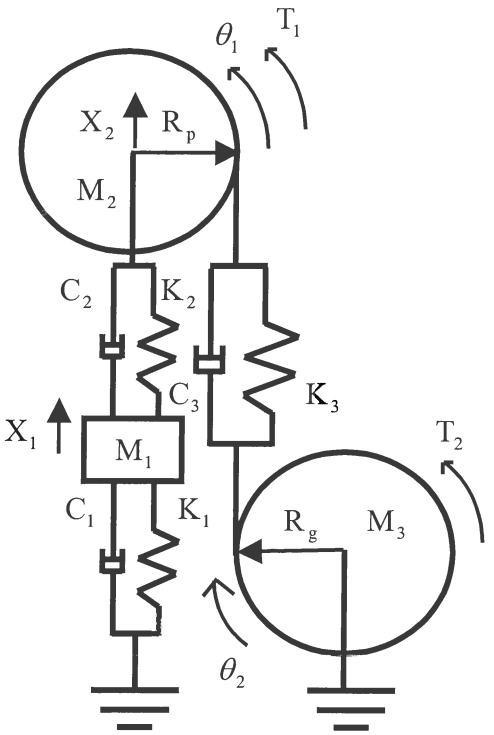

Figure 3.1. Diagram of the dynamic gear model

The load on the system is set proportional to the square of the gearwheel speed, which enables the system to accelerate up to a nominal speed during simulation. There is an increase in the applied load as the rotational speed of the system increases. A proportional constant K_s is selected to control the resultant nominal steady state rotational speed of the system.

The mathematical expression for the applied toque is presented in Equation 3.5 and the proportional constant K_s was set equal to 16,2 in order to obtain a nominal system rotational speed of 1 500 rpm for the simulation results shown.

$$T_2 = K_s \times \dot{\theta}_2^2 \tag{3.5}$$

TABLE 3.1 Model parameters

Model parameter	Description	Value
M_1	Translating mass	0.05 kg
M_2	Pinion mass	0.05 kg
M_3	Gearwheel mass	0.05 kg
K_1	Structural stiffness	100 kN/m
K_2	Bearing stiffness	100 kN/m
K_3	Gear mesh stiffness	$100 \times \{1 - 0.01 \times \sin(N \times \theta_1)$ kN/m
C_1	Structural damping	1.2 Ns/m
C_2	Bearing damping	1.2 Ns/m
C_3	Gear mesh damping	1.2 Ns/m
R_p	Pinion base circle radius	0.01 m
R_g	Gearwheel base circle radius	0.01 m
N	Number of gear teeth	10
GR	Gear ratio	1:1
I_1	Pinion inertia	$0.5\ M_2R_p^2$
I_2	Wheel inertia	$0.5\ M_3R_g^2$

A gear fault was introduced into the model by reducing the meshing stiffness K_3 to 99,7% of the nominal gear meshing stiffness for five degrees of the shaft rotation. The model was written into state space format and implemented in MATLAB for simulation purposes, with the ode45 differential equation solver.

The fluctuation in loading causes a fluctuation in the IAS $\dot{\theta}_1$ of the model as indicated in Figure 3.2. Note that the low frequency fluctuation can also be observed in the velocity $\dot{X}_1$. A higher frequency band of activity caused by the fluctuation in the mesh stiffness is present in both the velocity $\dot{X}_1$ and the IAS $\dot{\theta}_1$. The amplitude modulation caused by the fluctuating load becomes visible in the time domain when the signals are high pass filtered to remove frequencies below 200 Hz as shown in Figure 3.3.

Conventional vibration monitoring strategies rely on the amplitude ratio between the fundamental gear mesh frequency and the sidebands surrounding the gear mesh frequency to detect the modulation caused by a gear defect under constant load and angular speed conditions. The spectra of the simulation results under fluctuating load conditions are shown in Figures 3.3 (b) and (d). Multiple peaks are observed in the frequency region around the nominal gear mesh frequency which should be at 250 Hz. The phenomenon is known as spectral smearing and is due to the fluctuation in speed caused by the fluctuation in load. Figures 3.4 (b) and 5(b) indicate that these peaks are consolidated into a prominent peak at the gear meshing order once the COT process has been applied to the data.

The velocity $\dot{X}_1$ and the IAS $\dot{\theta}_1$ for one rotation of the shaft are shown in Figures 3.4 (a) and 3.5 (a). A deviation from the gear mesh response behaviour caused by the defect can be seen between 180 and 200 degrees of the shaft rotation. The results indicate that the IAS can detect a gear defect if the gear defect reduces the stiffness in the gear meshing. Note that the gear defect manifests as a modulation and the load modulates the velocity $\dot{X}_1$ and the IAS $\dot{\theta}_1$ signals. Therefore the sidebands around the gear mesh order in Figures 3.4 (b) and 3.5 (b) are caused by both the load and the defect modulation. LDN was applied to the velocity $\dot{X}_1$ and IAS $\dot{\theta}_1$ in order to obtain the load-normalised velocity $\dot{X}_1$ and IAS $\dot{\theta}_1$ signals.

The LDN procedure reduces the amplitude of the low frequency modulation sidebands close to the gear mesh order, relative to the amplitude of the gear mesh order. A separation between the modulation caused by the load and the defect is obtained by applying the LDN procedure. Figures 3.4 (d) and 3.5 (d) display the spectra of the load-normalised velocity $\dot{X}_1$ and IAS $\dot{\theta}_1$.

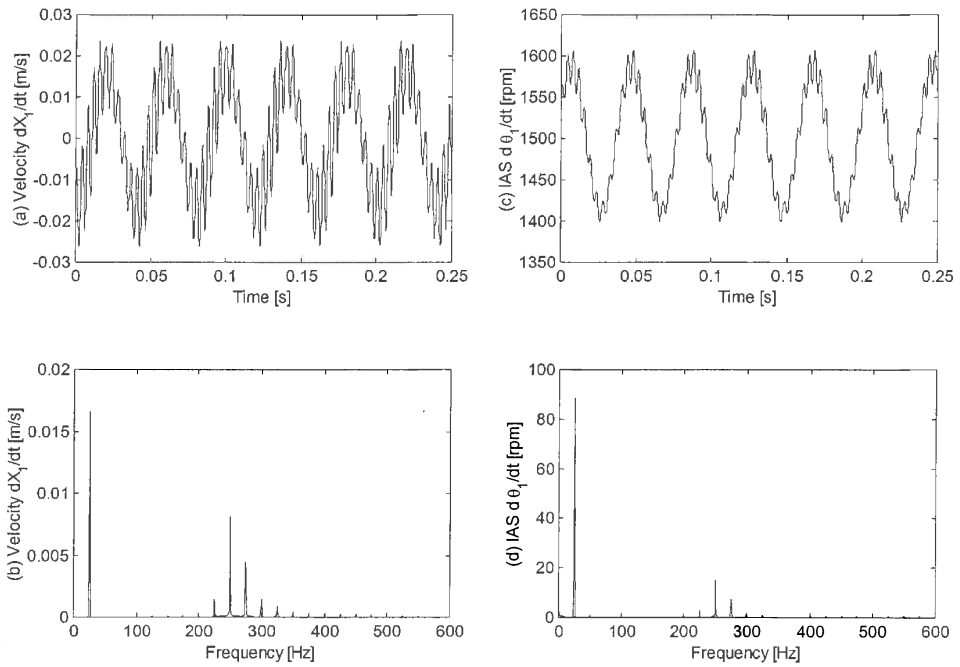

Figure 3.2. Gear model simulation results: (a) velocity time domain response; (b) velocity frequency domain response; (c) IAS time domain response; (d) IAS frequency domain response.

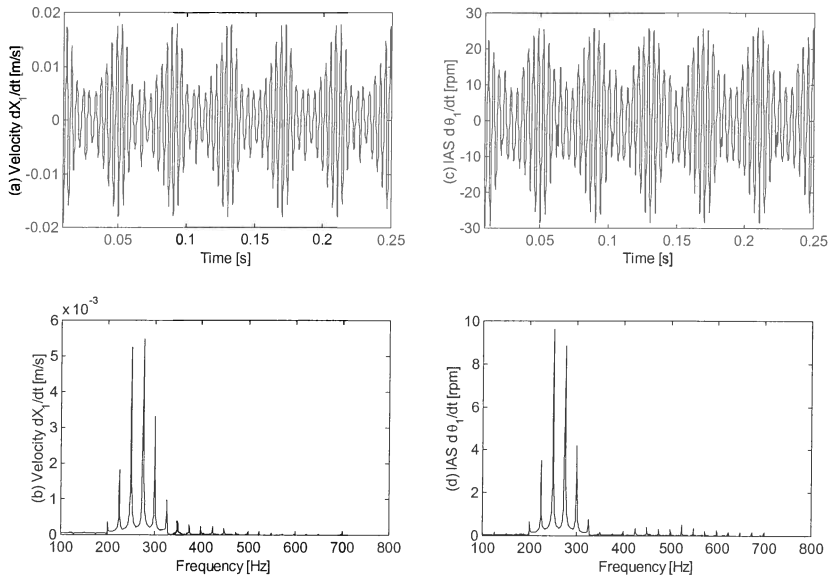

Figure 3.3. High pass filtered gear model simulation results: (a) velocity time domain response; (b) velocity frequency domain response; (c) IAS time domain response; (d) IAS frequency domain response.

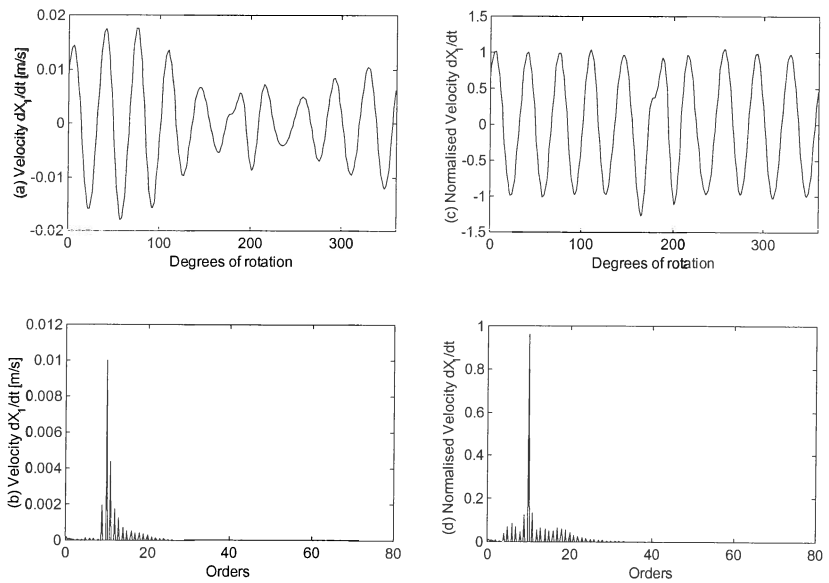

Figure 3.4. Computer order tracked and high pass filtered gear model simulation results: (a) rotation domain response; (b) order domain response; (c) load-normalised rotation domain response; (d) load-normalised order domain response.

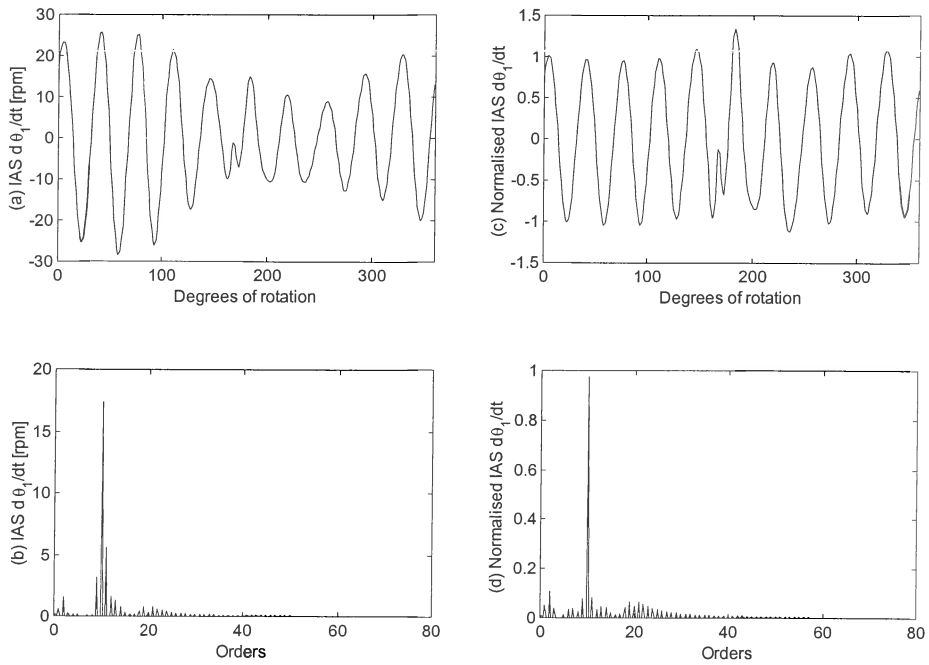

Figure 3.5. Computer order tracked and high pass filtered gear model simulation results: (a) rotation domain response; (b) order domain response; (c) load-normalised rotation domain response; (d) load-normalised order domain response.

3.3 Cyclic stationary and non-cyclic stationary load conditions

Cyclic stationary load conditions refer to instances where the modulation caused by the load fluctuation is stationary while the rotation of the gear is being monitored. In other words there is no phase shift in the modulation relative to the rotation of the gear. The phase of the modulation for non-cyclic stationary fluctuating load conditions will change relative to the rotation of the gear being analysed.

The distinction between the two scenarios becomes relevant when the RDA process is applied to data. Figures 3.6(a) and 3.6(b) display two signals where the phase of the modulation between the two signals is 180 degrees out of phase. The addition of the two signals in the rotation domain results in the signal shown in Figure 3.6(c) with reduced amplitude modulation.

Figure 3.6(f) displays the results of the addition of the two signals shown in Figures 3.6(d) and 6(e). Note that the modulation in Figure 3.6(f) is not reduced since there is no difference in the phase of the signals shown in Figures 3.6(d) and 6(e).

The modulation caused by non-cyclic stationary load conditions can therefore be averaged out with the RDA process, provided that enough averages are taken for the rate at which the phase of the modulation changes relative to the rotation of the shaft.

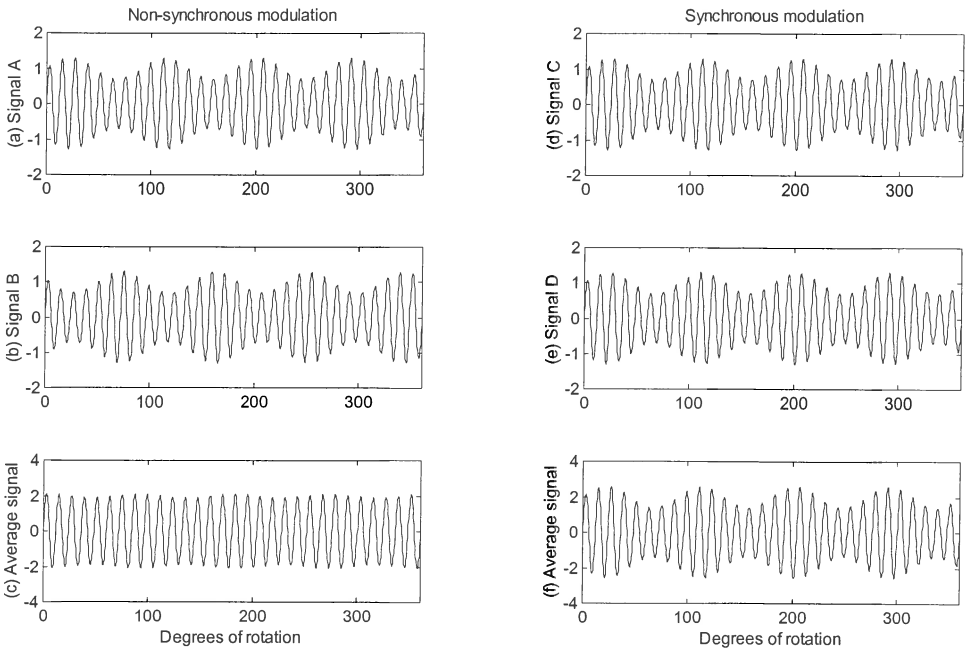

Figure 3.6. Comparison between cyclic stationary and non-cyclic stationary load modulation for RDA: (a) signal A non-cyclic stationary modulation; (b) signal B non-cyclic stationary modulation; (c) average of the non-cyclic stationary modulated signals; (d) signal C cyclic stationary modulation; (e) signal D cyclic stationary modulation; (f) average of the cyclic stationary modulated signals.

For cyclic stationary load conditions, the modulation of the signal being analysed is calculated in the LDN process. A low pass filter is applied to the modulation data in order to separate the modulation caused by the load from the modulation caused by the gear defect. The filter frequency is calculated in an optimisation process where the similarity between signals measured under different loading conditions is optimised.

A load-normalised signal is obtained by dividing the signal by the low pass filtered modulation. The signal is band pass filtered before the modulation is calculated, to ensure that there are no zero values in the filtered modulation signal, which would result in division by zero.

The modulation caused by a gear defect will always be cyclic stationary with the rotation of the shaft, and will not be suppressed by the RDA process. The RDA process provides a means to separate the frequency content of the cyclic stationary modulation caused by the gear defect from the frequency content of the modulation caused by the non-cyclic stationary load modulation. The approach will allow overlapping in the frequency bands of the load modulation and gear defect modulation, in contrast to the cyclic stationary loading case where no overlapping is possible since the signal modulation is low pass filtered in order to separate the modulation caused by the load and probable defects.

Note that RDA will suppress the non-cyclic stationary modulation and not the amplitude of the resulting signal. Therefore the non-cyclic stationary signals will still have to be normalised once the RDA process has been applied. However the low pass filter frequency of the LDN process can be set at one shaft order, since no separation has to be obtained between the modulation caused by the load and the modulation caused by the gear defect.

The final drive gear of a continuous miner cutter head gearbox is a typical application of cyclic stationary load condition. The rate at which the picks of the cutter head shear the coal from the coalface remain constant relative to the meshing of the gears since no relative movement between the picks and gear teeth will take place. Hence, if RDA is applied the modulation caused by the coal shearing action of the picks will not be averaged out since the modulation caused by the shearing of the coal from the coalface will remain cyclic stationary. The load on the drag gearboxes of a dragline will however change randomly since it depends on how the operator controls the dragline. For the dragline, application the load will therefore be non-cyclic stationary and the modulation caused by the load will be averaged out by the RDA process.

3.4 Convergence of rotation domain averaging

The convergence of the RDA process under non-cyclic stationary load conditions was investigated by applying the RDA process to two signals with different amplitude modulation characteristics. A Normalised Relative Difference Value (NRDV) was calculated according to Equation 3.6 in order to obtain a normalised comparison of the similarity and deviation in amplitude between the two signals in the rotation domain:

$$NRDV = \sqrt{\frac{1}{N_S}\sum_{n=1}^{N_S}\left(\left[\frac{Signal1(\theta) - Signal2(\theta)}{\frac{1}{2}\times\left[\sqrt{\frac{1}{N_S}\sum_{n=1}^{N_S}(Signal1(\theta)\times\Delta\theta)^2} + \sqrt{\frac{1}{N_S}\sum_{n=1}^{N_S}(Signal2(\theta)\times\Delta\theta)^2}\right]}\right]\times\theta\right)^2} \quad (3.6)$$

where N_S denotes the number of samples per shaft revolution, θ the rotation of shaft in degrees and $\Delta\theta$ the angular increment in degrees. The NRDV is essentially the Root Mean Square (RMS) value of the difference between two signals normalised by the average of their RMS amplitudes.

The NRDV was calculated as a function of the number of averages to indicate the convergence behaviour of the RDA process for various non-cyclic load modulation scenarios. Narrowband periodic, wideband periodic and random non-periodic modulation scenarios as well as the influence of non-stationary random noise were investigated.

A Gear Mesh Signal (GMS) was simulated based on a sinusoidal approximation of the gear meshing stiffness as indicated in Equation 3.7:

$$GMS(N,\theta) = \sin(N\times\theta) \quad (3.7)$$

where N represents the number of gear teeth and θ the degree of shaft rotation.

The narrow band periodic modulation is generated according to Equation 3.8:

$$\text{Modulation}(L_I, L_O, R_N, \theta, \phi, \alpha) = 1 + L_I \times \sin(L_O \times \theta - R_N \times \phi - \alpha) \quad (3.8)$$

where L_I denotes the load intensity, L_O the load order, R_N the rotation number, ϕ the modulation phase shift per revolution in degrees per rotation and α the constant modulation phase shift in degrees. Load intensity is proportionally related to the amplitude of the modulation. The load order represents the order-tracked frequency of the modulation. The phase shift per revolution for the modulation is introduced in Equation 3.8 by multiplying the rotation number by the modulation phase shift per revolution of the shaft ϕ in order to simulate the non-cyclic stationary load modulation effect.

A Narrowband Modulated Gear Mesh Signal (NMGMS) is obtained in Equation 3.9 by multiplying the GMS in Equation 3.7 by the modulation in Equation 3.8.

$$\text{NMGMS}(L_I, L_O, R_N, N, \theta, \phi, \alpha) = \text{GMS}(N, \theta) \times \text{Modulation}(L_I, L_O, R_N, N, \theta, \phi, \alpha) \quad (3.9)$$

The constant modulation phase shift will create a difference between the modulations of the signals. The phase shift per revolution of the shaft was kept constant for both the signals. Therefore the dissimilarity between the two signals can only be improved by the non-cyclic stationary averaging effect, which will reduce the magnitude of the amplitude modulation.

Two signals with a constant relative phase shift of 10 degrees in the modulation were generated for the simulation. The order of the modulation was set at 4 orders and the load intensity was set at 30 per cent of the peak value in the NMGMS. Fifteen gear teeth were selected for the simulation.

Convergence simulations were conducted for values of the modulation phase shift equal to 15 and 30, and for 45 degrees per revolution. Figure 3.7 indicates the results of the convergence simulation between two signals. It can be concluded from the simulation results that the number of averages required to reduce the amplitude of the non-cyclic stationary load modulation to zero is equal to 360^{o} divided by the phase shift per shaft revolution in degrees. However the conclusion is based on the assumptions that the load modulation is periodic, that there is no non-synchronous noise present in the signal and that the phase shift per revolution is constant.

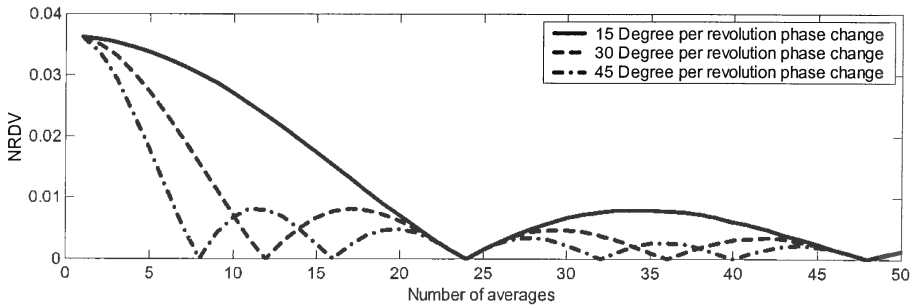

Figure 3.7. NRDV versus the number of rotation domain averages for a periodic load with an order of 4: load intensity 30 %; no non-synchronous noise.

A signal with a 90-degree phase shift per revolution was generated to illustrate the convergence process in the rotation domain within four averages. Figures 3.8 (a) to (d) show the data. Figures 3.8 (e) to (h) indicate the reduction in the amplitude modulation as the number of averages increases.

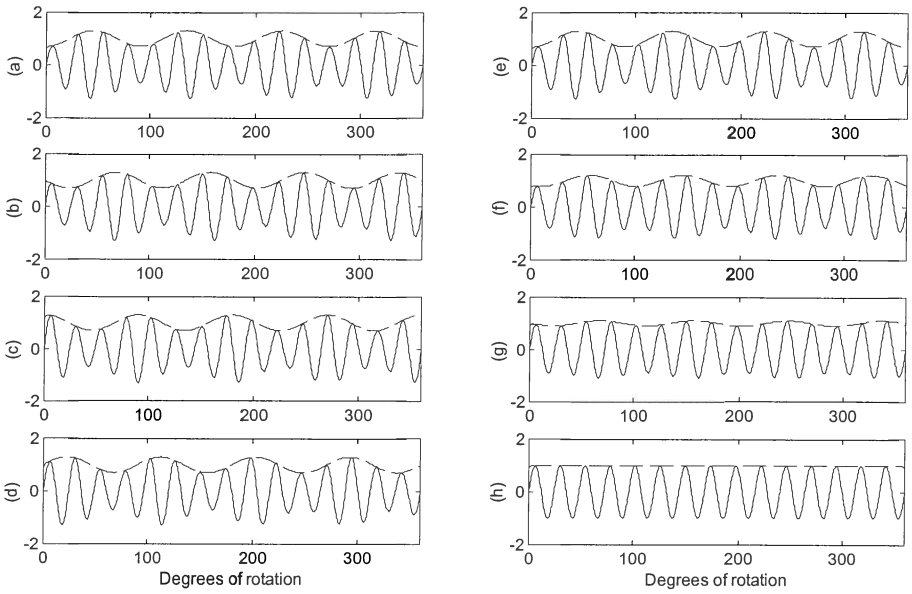

Figure 3.8. RDA example under non-cyclic stationary fluctuation load conditions: load intensity 30%; modulation order = 4; (a) rotation 1 with 0 degrees of phase change; (b) rotation 2 with 90 degrees of phase change; (c) rotation 3 with 180 degrees of phase change; (d) rotation 4 with 270 degrees of phase change; (e) one rotation domain average; (f) two rotation domain averages; (g) three rotation domain averages; (h) four rotation domain averages.

The influence of random non-synchronous noise on the convergence of the RDA process was investigated by adding random noise to the narrowband periodic modulation simulation. Noise was added, with a maximum amplitude of 25 % of the peak amplitude value in the NMGMS. The results shown in Figure 3.9 indicate that absolute similarity cannot be obtained between the signals by utilising the RDA process, once random non-synchronous noise has been added to the individual signals within a finite number of averages. In other words, the RDA process cannot completely attenuate or reduce the effect of random noise on a measurement taken within an economically feasibly number of shaft rotations.

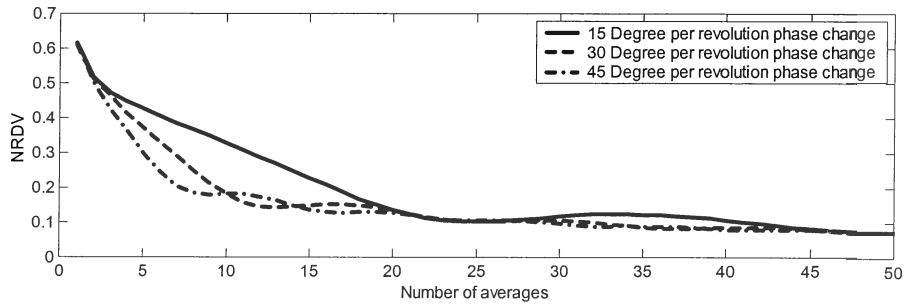

Figure 3.9. NRDV versus the number of rotation domain averages for a periodic load with an order of 4: load intensity 30 %; non-synchronous noise level of 25%.

Additional simulations were conducted in which the maximum amplitude of the non-synchronous noise was increased from 20 % to 100 %. The convergence simulations indicate that reduced similarity is obtained between two signals after a finite number of averages when the maximum amplitude of the non-synchronous noise is increased. The simulation results are shown in Figure 3.10.

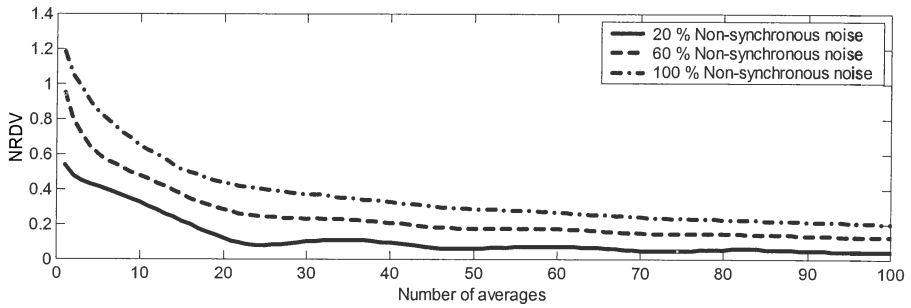

Figure 3.10. NRDV versus the number of rotation domain averages for a periodic load with an order of 4: load intensity 30 %; fifteen degrees of phase change per revolution.

Most of the fluctuating load scenarios found in practice inflict wideband modulation on the GMS. These modulations may or may not be periodic, depending on the particular situation. Simulation data for the periodic wideband scenario were generated by multiplying the GMS signal in Equation 3.6 by the same random modulation signal.

The modulation signal had a bandwidth of 1 to 7 orders and the phase of the signal was shifted for each revolution of the shaft. A constant modulation phase shift of 10 degrees was kept between the two signals used in the comparison studies. The convergence simulation results shown in Figure 3.11 indicate that the dissimilarity between the two wideband modulated signals can be reduced to zero within a finite number of averages, provided that there is no non-synchronous noise present in the signals, the modulation is periodic and that a sufficient number of averages are taken.

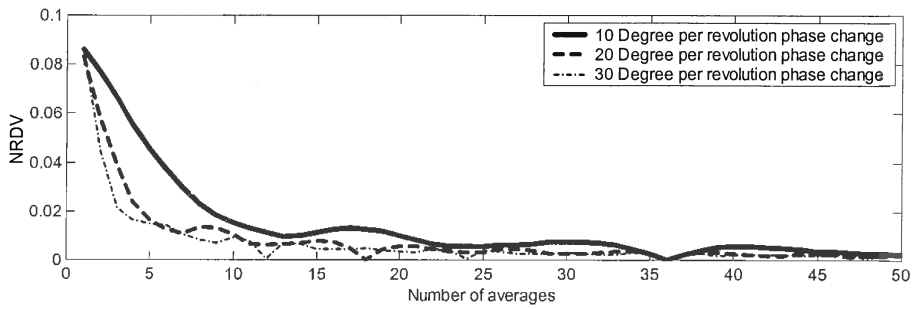

Figure 3.11. NRDV versus the number of rotation domain averages for a periodic load with an order bandwidth of 1 to 7 orders: load intensity 30%; no non-synchronous noise.

The rotation domain simulation results for a periodic wideband modulation scenario are shown in Figures 3.12 (a) to (h). A constant phase shift of 90 degrees per shaft revolution was chosen in order to obtain zero amplitude modulation after 4 averages. The results shown in Figure 3.12 (h) indicate that the modulation amplitude was reduced but not averaged out completely by applying the RDA process. Periodic wideband amplitude modulation will therefore not be averaged out to zero amplitude modulation if the phase shift per revolution is too large.

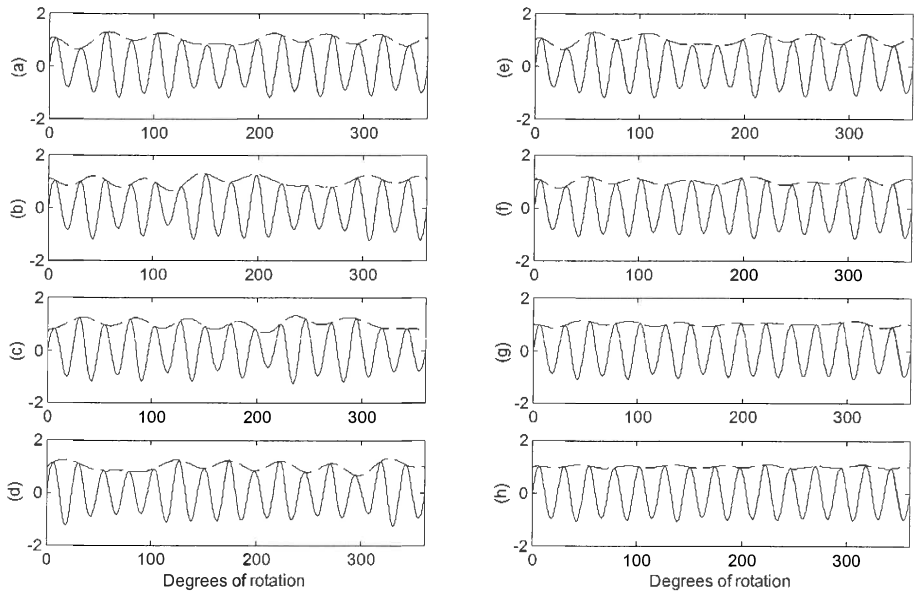

Figure 3.12. RDA example under non-cyclic stationary fluctuation load conditions: load intensity 30%; modulation band 1 to 7 orders; (a) rotation 1 with 0 degrees of phase change; (b) rotation 2 with 90 degrees of phase change; (c) rotation 3 with 180 degrees of phase change; (d) rotation 4 with 270 degrees of phase change; (e) one rotation domain average; (f) two rotation domain averages; (g) three rotation domain averages; (h) four rotation domain averages.

The GMS signal in Equation 3.6 was multiplied by different random noise signals in order to investigate the random non-periodic modulation scenario. New random modulation signals were generated for each revolution and the maximum amplitude of the modulation was 30% of the maximum GMS amplitude. The simulation results shown in Figure 13 indicate that the amplitude of a random non-periodic amplitude modulation cannot be reduced to zero within a finite number of averages by applying the RDA process.

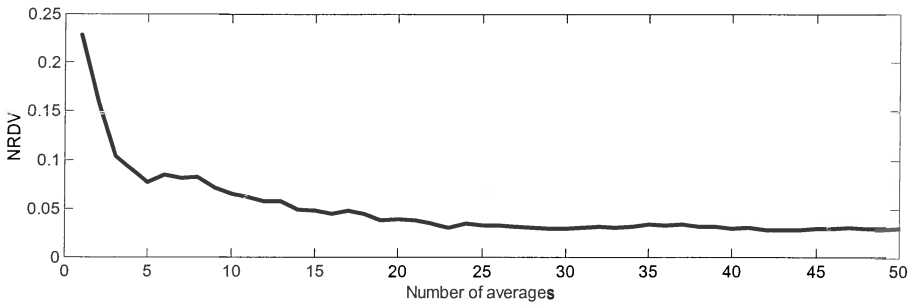

Figure 3.13. NRDV versus the number of rotation domain averages for a random load with an order bandwidth of 1 to 7 orders: load intensity 30%; no non-synchronous noise.

3.5 Implementation of the techniques on the gear model

Simulations were conducted on the dynamic gear model under sinusoidal cyclic stationary and non-cyclic stationary loading conditions. The load fluctuation frequency was set at 25 Hz for the non-cyclic stationary loading conditions and at 1 order for the cyclic loading condition. A 20 % variation in the load was applied.

RDA was applied to the simulation results to verify that RDA would suppress the modulation caused by non-cyclic stationary loading but not the modulation caused by cyclic loading. The simulation results for 4 averages are shown in Figures 3.14 (a) to (d). Note that the modulation caused by the load fluctuation can be observed for both the cyclic stationary and non-cyclic stationary loading conditions. Figures 3.15 (a) to (d) indicate the rotation domain results for 20 averages. The load modulation caused by the cyclic stationary load is not suppressed by an increase in the number of averages in the RDA process. Figures 3.15 (a) and (d) indicate that the modulation caused by the non-cyclic stationary load is suppressed by the increase in the number of averages in the RDA process for both the velocity at $\dot{X}_1$ and the IAS at $\dot{\theta}_1$.

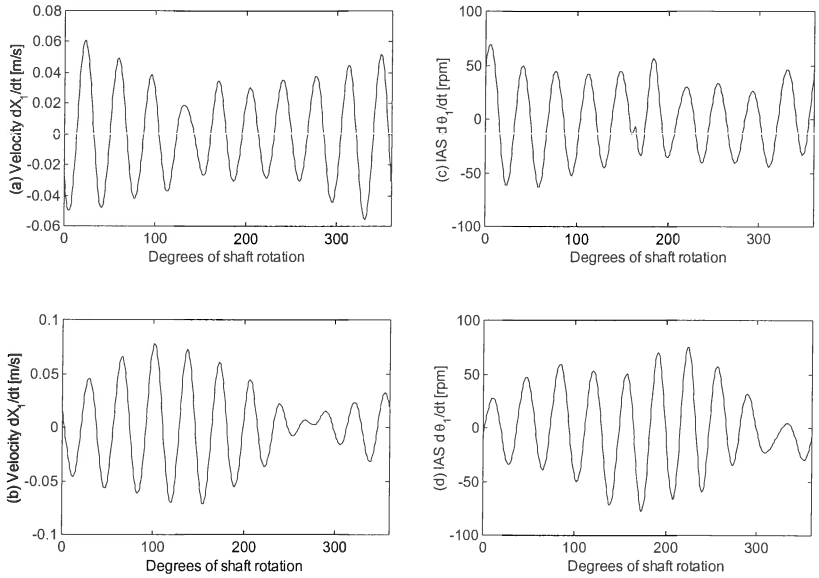

Figure 3.14. RDA results after 4 averages at 20 % variation in load: (a) non-cyclic stationary loading at 25 Hz; (b) cyclic stationary loading at 1 order; (c) non-cyclic stationary loading at 25 Hz; (d) cyclic stationary loading at 1 order.

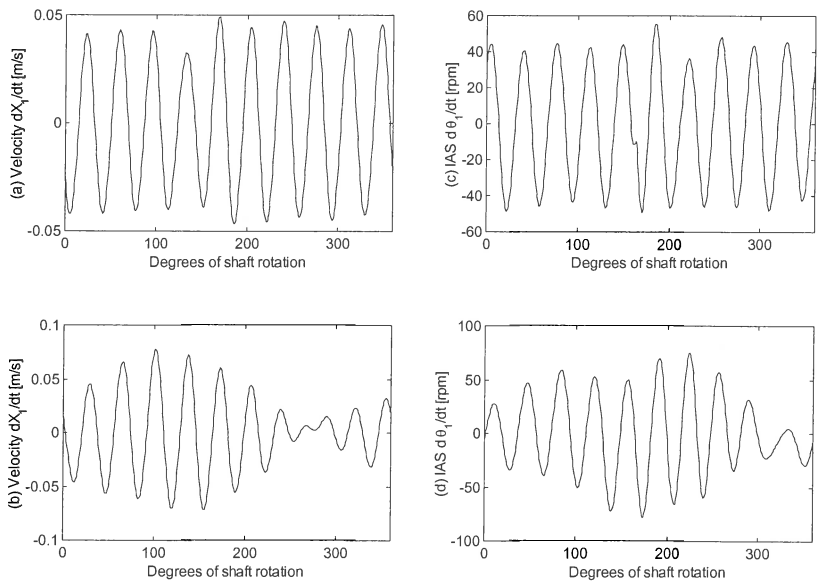

Figure 3.15. RDA results after 20 averages at 20 % variation in load: (a) non-cyclic stationary loading at 25 Hz; (b) cyclic stationary loading at 1 order; (c) non-cyclic stationary loading at 25 Hz; (d) cyclic stationary loading at 1 order.

3.6 Experimental set-up

The experimental set-up consisted of three Flender Himmel Motox helical gearboxes, driven by a 5,5 kW three-phase four-pole Weg squirrel cage electrical motor. A 5,5 kVA Mecc alte spa three-phase alternator was used for applying the load. Figure 3.16 illustrates the test rig. The gearbox test rig was designed to conduct accelerated gear life tests on the Flender E20A gearbox under varying load conditions.

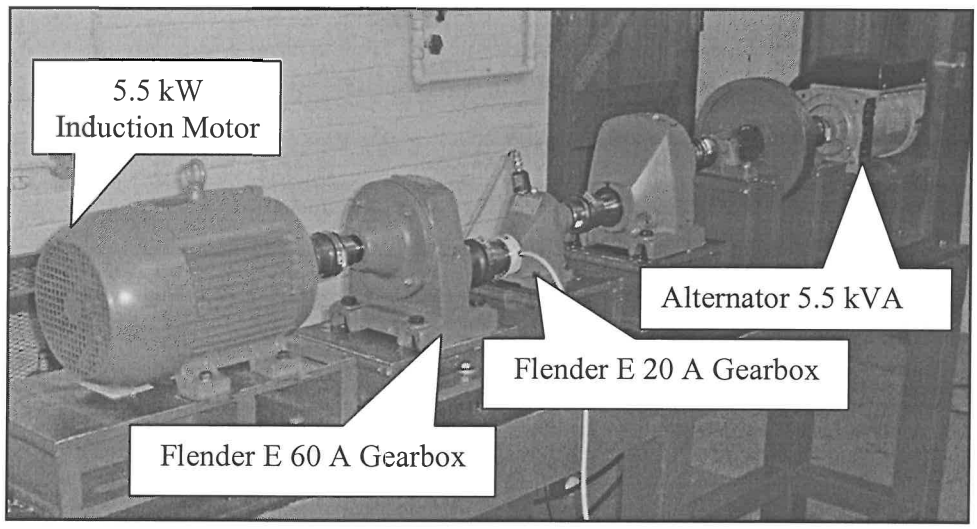

Figure 3.16. Experimental set-up.

Two additional Flender E60A gearboxes were incorporated into the design in order to increase the torque applied to the small Flender E20A gearbox. The rated load of the gears in the Flender E20A gearbox was 20 Nm. The same gear train loading system explained in paragraph 2.2 was utilised in the experimental set-up.

A Hengstler R176T01 1024ED 4A20KF shaft encoder, producing 1 024 pulses per revolution in the form of an analogue push-pull signal, was used for measuring the shaft speed. The reference point for the synchronous averaging was measured as a single pulse from the shaft encoder. Acceleration was measured in the vertical direction on the gear casing, by means of a 10 V/g PCB integrated circuit piezoelectric industrial accelerometer.

The measurements were taken with a Siglab model 20-42 signal analyser for five different load conditions and three different levels of damage severity. The specifications for the loading conditions are given in Table 3.2. During the experimentation, flank wear was progressively induced on one of the gear teeth in the gearwheel of the gearbox. Details of the amount of wear are presented in Table 3.3.

TABLE 3.2 Load case specifications

Load Case	Load Function	Frequency	Minimum Load	Maximum Load
1	Constant	0 Hz	10.7 Nm	10.7 Nm
2	Sine	1 Hz	7.4 Nm	14.7 Nm
3	Square	0.3 Hz	7.4 Nm	14.7 Nm
4	Chirp	0.1- 2 Hz	7.4 Nm	14.7 Nm
5	Random	0.1- 2 Hz	7.4 Nm	14.7 Nm

TABLE 3.3 Induced tooth face damage specifications

Fault condition	Tooth face removal
1	100 μm
2	200 μm
3	300 μm

The gearwheel of the test gearbox is the slowest rotating component in the test rig and has the lowest inertia, resulting in a relatively low gear mesh frequency amplitude compared with the overall vibration levels.

The anti-aliasing filter of the Siglab analyser has a constant cut-off frequency of 20 kHz. Therefore, an eighth-order analogue Butterworth filter with a cut-off frequency at 270 Hz was used as an analogue low pass filter. The high amplitude vibration in the higher frequency range was filtered out in this way, improving the digitisation range of the gear mesh signal.

For further information with regards to the experimental set-up and measurement instrumentation, refer to the appendix.

3.7 Experimental verification under non-cyclic stationary load conditions

A convergence study of the RDA process was conducted on the experimental data obtained from the test rig. Comparisons were made between the constant, random, chirp and sinusoidal non-cyclic stationary loading conditions.

The results are shown in Figure 3.17. Note that the signals measured under different loading conditions become more similar as the number of averages increases. The RDA process suppresses both the modulation caused by the varying load conditions and the non-synchronous noise. Figure 3.17 indicates that there is less similarity between the velocity measurements on the gear-case than between the IAS measurements for a low number of averages. This can be attributed to the fact that the velocity measurements are contaminated by more non-synchronous noise sources, because of the dispersion of forces through the structure from other rotating components in the system and the vibration must pass through a transmission path before being measured with the accelerometer.

The shaft encoder signal is measured as a push-pull signal and post-processed to obtain the IAS and will therefore only reflect the IAS associated with the rotation of the shaft under consideration.

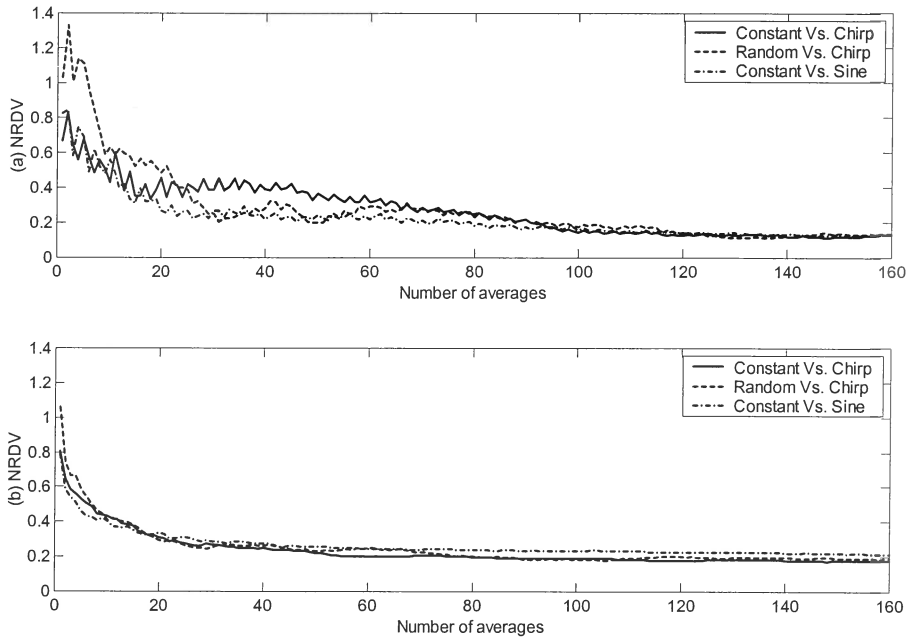

Figure 3.17. NRDV versus the number of rotation domain averages for the experimental data under constant, random, chirp and sinusoidal excitation: (a) velocity measured on the gearbox casing; (b) IAS.

The Smoothed Pseudo-Wigner-Ville (SPWV) algorithm proposed by Wang [62] was utilised to analyse the signals to which the RDA process was applied. Both time and frequency smoothing is utilised in the SPWV in contrast to the PWV in which only frequency smoothing is applied to attenuate the interference and cross terms. Thus better attenuation of the interference and cross terms will be obtained by utilising the SPWV distribution in comparison with the PWV distribution. Details of the number of data points used are presented in Table 3.4. Figures 3.18 and 3.19 indicate the SPWV distributions of the IAS signals for one rotation under the different loading conditions and levels of damage severity. No similarity was found between the distributions. However, the SPWV distributions of the IAS shown in figures 3.20 and 3.21 indicate similarity between the various distributions for the different loading cases when a rotation domain average from 160 rotations is calculated. The flank wear was induced between 50^{o} and 100^{o} of shaft rotation.

Note that the flank wear is indicated by increased amplitude levels that spread out over the order bandwidth at the position of the gear damage in the distribution of the IAS to which the RDA was applied.

TABLE 3.4 SPWV distribution specifications

Signal data point length	1024 data points
Pseudo window length	32 data points
Smoothing window length	4 data points

An energy ratio parameter was defined according to Equation 3.10 to exploit the phenomenon to trend the degradation of the gear condition as a single numerical value:

$$\text{Energy Ratio} = \frac{E_D}{E_{ND}} \tag{3.10}$$

where E_D represents the sum of the energy in the order band of the time frequency distribution in which the amplitude of the distribution increases when gear damage is introduced over 360^o of the shaft rotation; and E_{ND} the energy in the gear mesh order band of the time frequency distribution, which is present when no gear fault condition is induced over 360^o of the shaft rotation.

Energy ratio values were calculated from the SPWV distributions under the five different loading conditions and three different levels of damage severity.

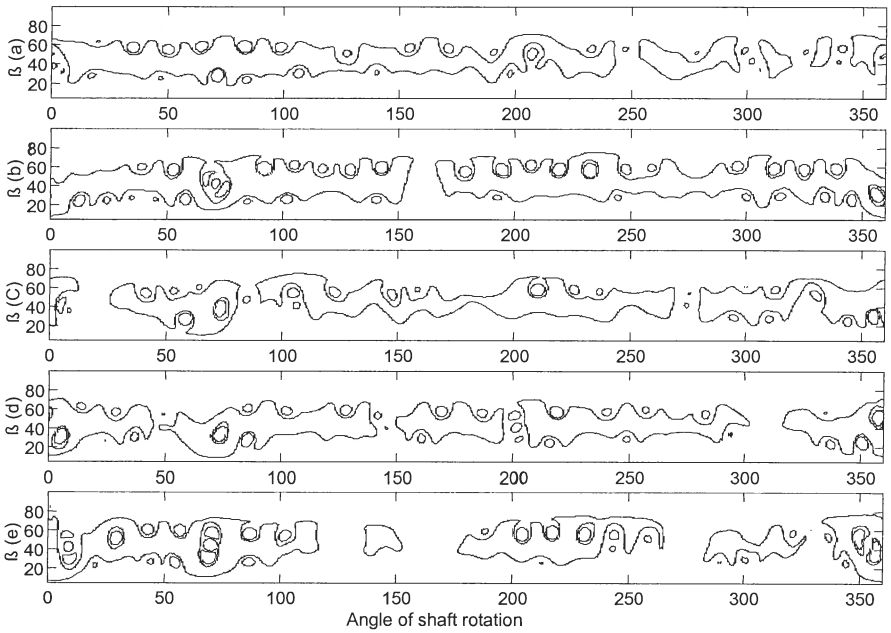

Figure 3.18. SPWV distributions for a single rotation of the experimental IAS measurements at damage level 2: (a) constant load; (b) random load; (c) chirp load; (d) sinusoidal load; (e) square load.

A linear separation between the energy ratio values for different levels of damage severity, under the various non-cyclic stationary loading conditions, was obtained for the measurements to which the RDA process was applied, as shown in Tables 3.5 A and B. The deterioration in gear condition can therefore be readily trended monotonically to indicate the progression of a gear fault condition under non-cyclic stationary varying load conditions by applying the SPWV distribution to the rotation domain averaged gear-case velocity and IAS measurements. The energy ratio values for the SPWV distributions calculated for a single shaft rotation are indicated in Tables 3.5 C and D. Note that no linear separation between the damage severity cases was obtained for the values under the different loading conditions when the computed order tracking (COT) process is applied.

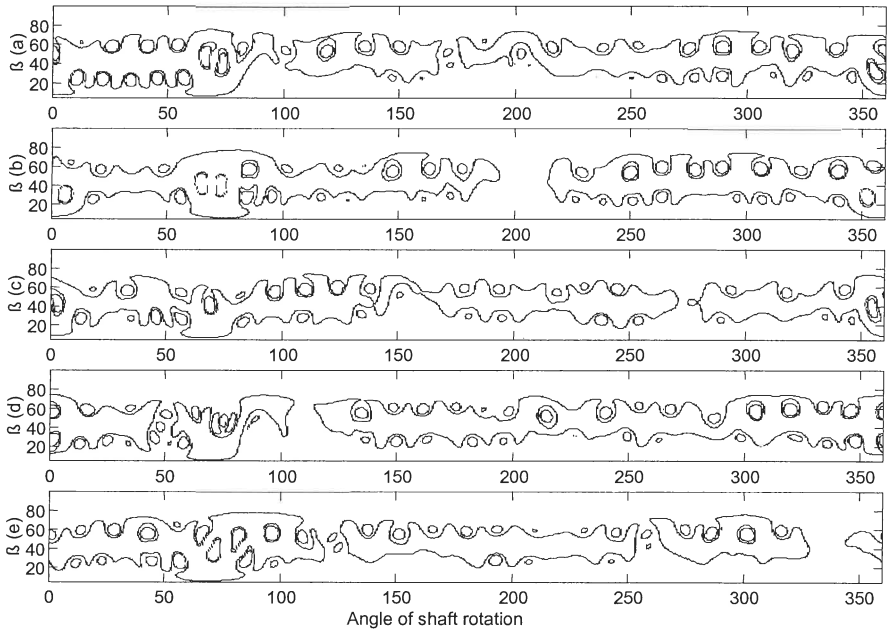

Figure 3.19. SPWV distributions for a single rotation of the experimental IAS measurements at damage level 3: (a) constant load; (b) random load; (c) chirp load; (d) sinusoidal load; (e) square load.

TABLE 3.5A Energy ratio of the rotation domain averaged gear-case velocity

Damage	Constant	Sine	Square	Chirp	Random
Level 1	0.1213	0.2256	0.2597	0.1365	0.1426
Level 2	0.8988	0.8232	0.8705	1.0649	0.9343
Level 3	1.1992	1.3697	1.2330	1.1691	1.2440

TABLE 3.5B Energy ratio of the rotation domain averaged IAS

Damage	Constant	Sine	Square	Chirp	Random
Level 1	0.0548	0.0622	0.0675	0.0593	0.0586
Level 2	0.0727	0.0793	0.0778	0.0722	0.0853
Level 3	0.1069	0.1089	0.1166	0.1223	0.1231

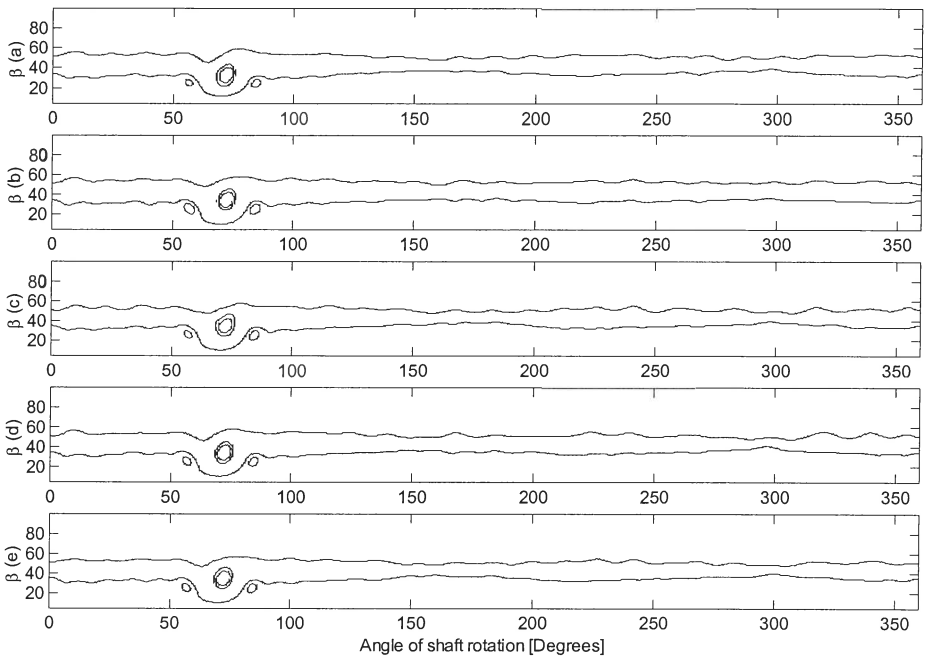

Figure 3.20. SPWV distributions for the experimental IAS rotation domain averaged measurements at damage level 2: (a) constant load; (b) random load; (c) chirp load; (d) sinusoidal load; (e) square load.

TABLE 3.5C Energy ratio of the gear-case velocity for a single rotation

Damage	Constant	Sine	Square	Chirp	Random
Level 1	0.3304	0.2331	0.3616	0.3176	0.3237
Level 2	0.5536	0.4452	0.4564	0.3572	0.5650
Level 3	0.7920	0.5827	0.4170	0.7233	0.7988

TABLE 3. 5D Energy ratio of the IAS for a single rotation

Damage	Constant	Sine	Square	Chirp	Random
Level 1	0.2728	0.2715	0.1741	0.3494	0.3235
Level 2	0.2519	0.2540	0.4351	0.2713	0.3145
Level 3	0.3120	0.2976	0.3294	0.3758	0.2954

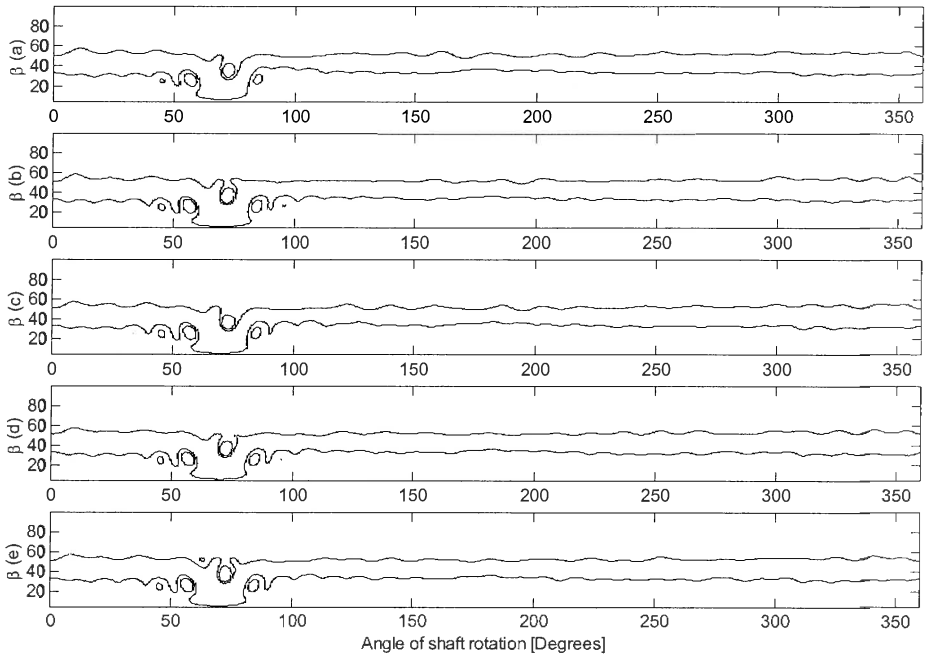

Figure 3.21. SPWV distributions for the experimental IAS rotation domain averaged measurements at damage level 3: (a) constant load; (b) random load; (c) chirp load; (d) sinusoidal load; (e) square load.

Chapter 4

Transmission path phase compensation for gear monitoring under fluctuating load conditions

4.1 Introduction

In chapter 3 it was established that the instantaneous angular speed measured by means of a shaft encoder with sufficient resolution, could be used to monitor a deteriorating fault condition on a gear under fluctuating load conditions. The results indicated much faster convergence of the rotation domain average, compared to the vibration measured with an accelerometer on the casing of the gearbox, due to the fact that the vibration must pass through a transmission path before being measured with the accelerometer. Various authors have investigated the problem of signal distortion due to transmission paths.

Powel [126] developed an inverse filtering technique to predict input forces acting on a component, from the vibration response measurements. This requires the Frequency Response Function (FRF) of the structure between the point of excitation and the response measurement point to be available. In most vibration monitoring applications it is either not financially viable or practically impossible to measure the required FRFs.

Kim [127] consequently considered the scenario where the required FRFs of the structure are not available. Cepstrum analysis was used to estimate an initial input. However the estimated signal was not accurate enough to diagnose a fault condition. Therefore a parameter modification process that utilises optimisation was applied to minimise the difference between the measured and estimated response.

Once the parameter modification process was applied a diagnosis of the fault condition could be made. Kim however concludes that the estimated and measured FRFs of the structure differed from one another by as much as 6 dB in magnitude and 20 radians in phase.

Consequently a method to reduce the effect of the transmission path phase on the measured response, was developed in order to improve the repeatability and diagnostic capability of the RDA and LDN methods currently used to conduct vibration monitoring under fluctuating load conditions. The LDN methodology will remove the amplitude modulation inflicted on the measured vibration signal by the transmission path at the rotational speed of the gear shaft. Hence, a methodology to compensate only for the phase distortion inflicted by the transmission path on the vibration measured signal, is required.

The proposed method entails representing the signal as a function of its phase rather than the angle of shaft rotation. Once the signal has been order tracked, the phase of the signal for each rotation of the shaft is calculated. The amplitudes of the signal are then sampled through an interpolation process at predetermined intervals of the phase. After the phase representation is calculated an average of the amplitudes in the pseudo phase representation is calculated. It is shown that this process is much more efficient and less data is required to obtain a converged synchronised average representation of the signal that can be utilised for diagnostic purposes.

4.2 Transmission path phase distortion

The transmission of excitation to response in a physical structure is always subjected to relative phase variation as well as amplification or attenuation depending on the structural mass, stiffness and damping characteristics. In general an averaged spectrum is calculated for condition monitoring purposes. Hence, the phase relationships in the signals are ignored and the magnitude of the amplitudes is monitored.

RDA is applied in gear monitoring applications where noise attenuation is required. A signal, which is synchronous with the rotation of the shaft of the gear being monitored, is measured in order to obtain a synchronising reference that is synchronous with the rotation of the shaft. Hence the synchronising reference signal remains synchronous with the excitation when the excitation frequency or shaft speed changes. However the response is not synchronous with the reference signal, due to the phase change imposed by the transmission path if the rotational speed of the machine changes. It is however only practically feasible to measure a reference signal which is synchronous with the excitation and shaft rotation.

The phase shift phenomena can be illustrated by means of a lumped parameter mass model with base excitation as described by Rao [128]. A diagram of the system is shown in figure 4.1. The equation of motion for the system is shown in equation 4.1

$$\begin{aligned} m\ddot{x} + c\dot{x} + kx &= F_y \\ m\ddot{x} + c\dot{x} + kx &= c\dot{y} + ky \end{aligned} \tag{4.1}$$

where x denotes the displacement of the mass m, c the viscous damping, k the stiffness, F_y the force applied with the base and y the displacement of the base.

Equation 4.1 can be mathematically manipulated in order to obtain the amplitude of the displacement transmissibility shown in equation 4.2 and the phase of the displacement transmissibility shown in equation 4.3

$$\frac{X}{Y} = \left[\frac{1+(2\zeta\, \mathrm{r})^2}{(1-r^2)^2 + (2\zeta\, \mathrm{r})^2} \right]^{1/2} \tag{4.2}$$

$$\phi = \tan^{-1}\left[\frac{(2\zeta\, \mathrm{r})^3}{1+(4\zeta^{\,2}-1)r^2} \right] \tag{4.3}$$

where r denotes the ratio of the excitation frequency relative to the natural frequency of the system and ζ the damping ratio.

Figure 4.2(a) illustrates the graphical representation of equation 4.2 and figure 4.2(b) the graphical illustration of equation 4.3, for damping ratios of 10% and 20 %. From the graphical illustrations, it is clear that the transmission path will induce amplitude amplification and attenuation as well as relative phase variation of the response, as functions of the frequency ratio.

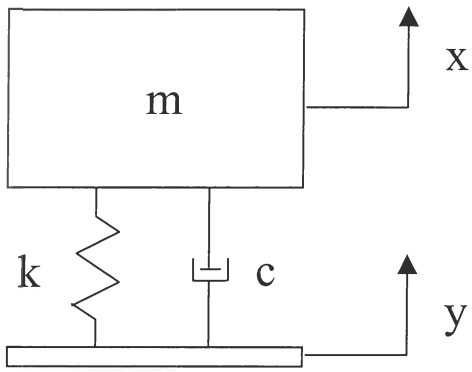

Figure 4.1. Lumped parameter mass model with base excitation.

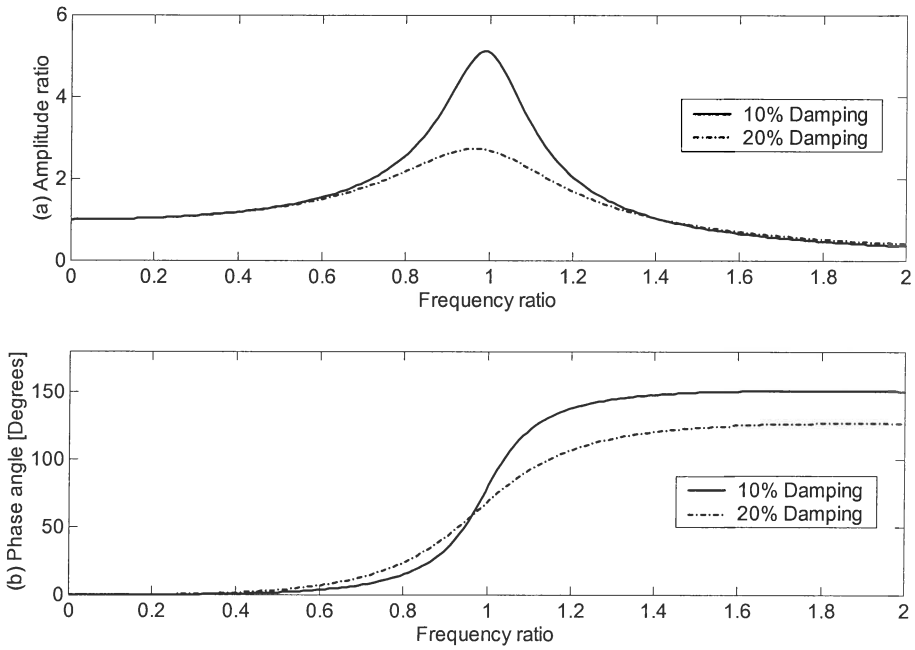

Figure 4.2. Transmissibility function of a lumped parameter mass model with base excitation: (a) Amplitude ratio of the displacement transmissibility; (b) Phase angle of the displacement transmissibility.

The concern with regards to phase shifting becomes apparent when RDA is performed. In the RDA process a constant number of samples are interpolated from the measured vibration signal for predetermined angles of shaft rotation. The angle of shaft rotation is calculated from the reference signal, which is synchronous with the shaft rotation. If the rotational speed of a gear being monitored changes, the RDA process will ensure that the order content in the signal remains correct but the phase shift will be neglected.

Figure 4.3(a) depicts two signals with amplitude modulation that are the same, except for the phase shift of ninety degrees relative to one another. The addition of the signals shown in figure 4.3(b) leads to the attenuation of the amplitude modulation. It can therefore be concluded that the possibility exists that modulation which is synchronous with excitation can be attenuated by the phase shifting effect of the transmission path. The phase shifting effect can furthermore lead to a total distortion of the RDA vibration signal that should represent the gear meshing stiffness for diagnostic purposes. Such distortions will affect repeatability and diagnostic capability.

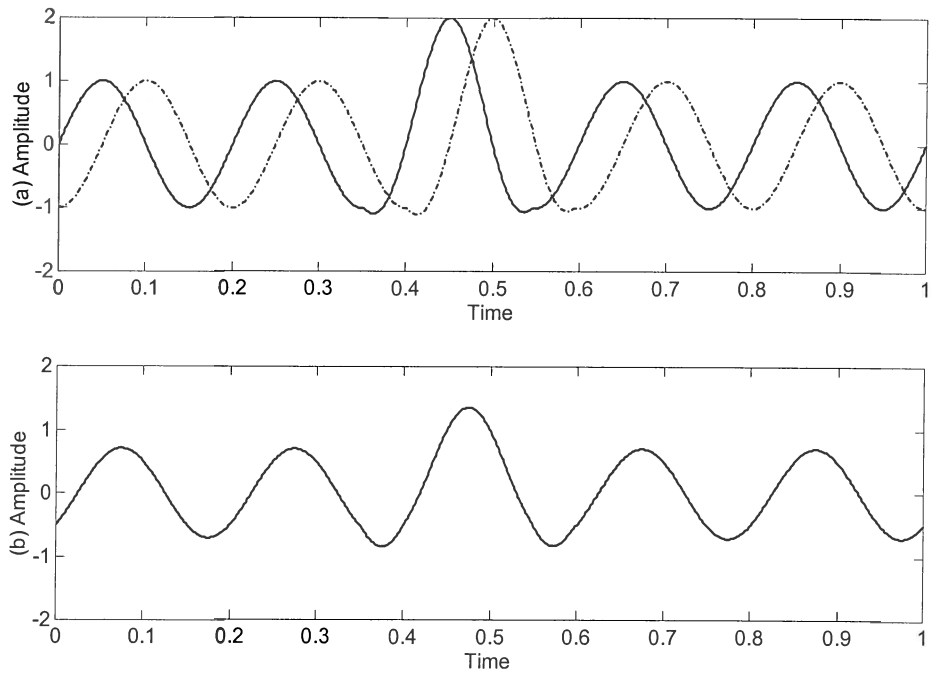

Figure 4.3. Phase effect on the addition of the same signal with a relative phase shift: (a) Signals 90 degrees out of phase; (b) Average of the out of phase signals.

4.3 Phase compensation methodology

In order to overcome the phase shift effect due to the transmission path, the real response signal $a(t)$ is transformed from the rotation domain in to the phase domain of the signal. This is accomplished by calculating the analytical signal as discussed in paragraph 2.4. An analytical signal can be visualized as a vector rotating in a complex plane over time. The absolute value of the analytical signal represents the amplitude modulation of the signal and the angle of vector rotation represents the phase of the signal.

Two signals are shown in Figure 4.4(a). The phase of the one signal is constant and the phase of the other signal changes with time. Figure 4.4(b) shows the amplitude of the two signals plotted as a function of each signal's phase, which was calculated from its analytical signal. It is clear that the signals are overlaid and that the phase shift is no longer visible. Consequently the effect of the transmission path phase distortion can be overcome by expressing the COT data in terms of the phase domain.

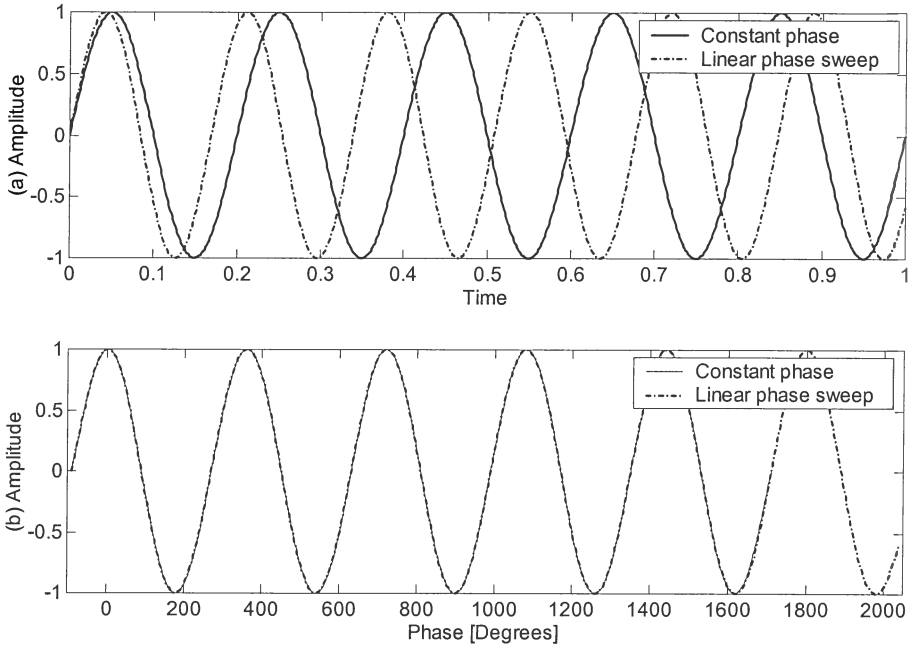

Figure 4.4. Amplitude representation of sinusoidal signals: (a) Amplitude versus time plot of the sinusoidal signals; (b) Amplitude phase plot of the sinusoidal signals.

The phase domain averaging process is described by the flow diagram in figure 4.5. Initially the data is measured and the conventional COT process is applied. The analytical signal of the COT signals for each rotation of the shaft is then calculated. From the analytical signal the corresponding phase of the signal is calculated. Unfortunately the scenario where the vector in the analytical signal counter-rotates does occur, which means that the phase of the signal reverses. This effect is eliminated through a process of narrowband enhancement. In other words, the signal is band-pass filtered around the fundamental gear-meshing harmonic of interest. The frequency band around the fundamental gear-meshing harmonic is narrowed until a sufficient number of shaft rotations are available from the COT data wherein phase reversal does not occur.

A minimum frequency bandwidth is set in order to avoid the scenario where too many gear-meshing sidebands are filtered from the signals. In general some 90 % of the captured data can be utilised once the data has been narrow band enhanced. The remaining data is discarded.

Once the phase for each signal has been calculated, the maximum and minimum phase value for the ensemble of signals is determined to establish the phase envelope. A number of points are selected at constant angle of phase over the phase envelope and the amplitudes of the signals are sampled through interpolation at the selected phase interval points. This is done in order to enable the averaging process for the shaft rotations over the phase envelope. The average signal is referred to as the Phase Domain Average (PDA). The phase envelope is normalised between zero and one for ease of use.

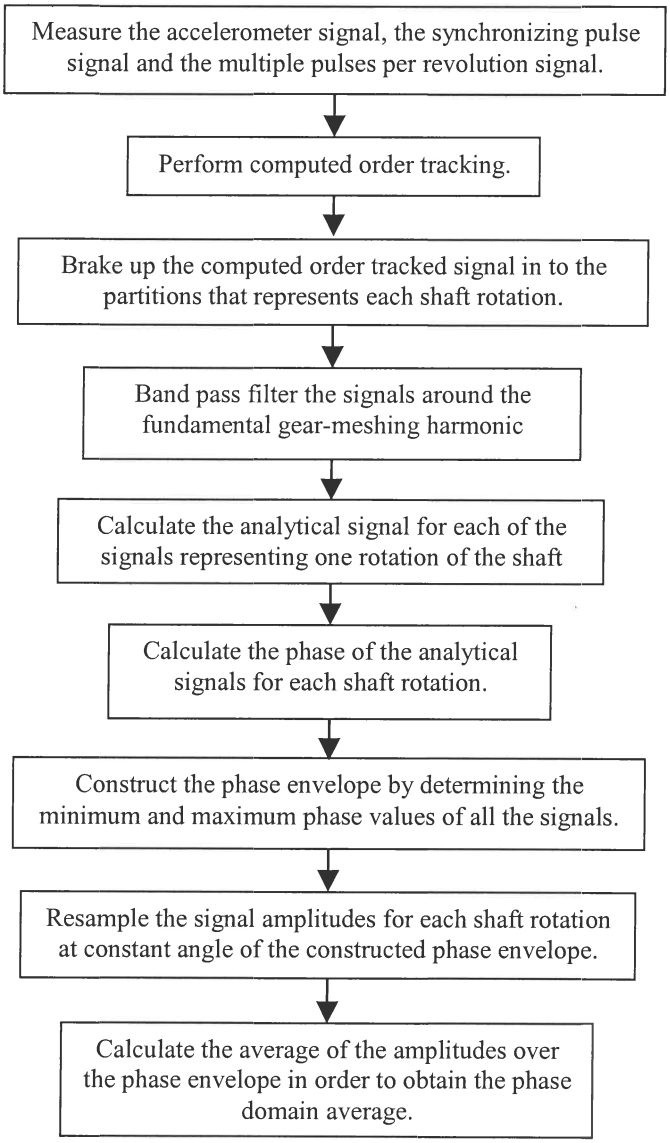

Figure 4.5. Phase domain-averaging flow diagram

4.4 Experimental investigation

Experimental measurements taken with the test set-up in paragraph 3.6 was utilised in the investigation. Measurements taken under a sinusoidal load condition where the load varied from 7.4 Nm to 14.7 Nm at a frequency of 1 Hz were utilised. The phase compensation methodology described in the previous paragraph of the chapter was

applied to the experimental measurements taken on the test rig, for three levels of damage severity. The accelerometer measurements where computer order tracked and band pass filtered to avoid counter-rotation of the analytical signal vector. The band pass order range was determined to be between 33 and 53 shaft orders, since the gearwheel had 43 teeth. Hence, sufficient bandwidth was available to incorporate the modulation of the fundamental gear-meshing harmonic representing the gear meshing stiffness.

The NRDV was calculated as a function of the number of averages to indicate the convergence behaviour of the RDA and PDA processes. An averaging process will converge faster if the order bandwidth is decreased by band pass filtering or narrow band enhancement. Therefore the signals that were used for the RDA process were band-pass filtered between 33 and 53 shaft orders, in order to make a fair comparison between the RDA and PDA approaches. Figures 4.7 (a) and (b) indicate the convergence behaviour for the processes applied to the experimental measurements for damage levels 1 and 2. It is evident that PDA process converges much faster with much less erratic behaviour, compared to the RDA process.

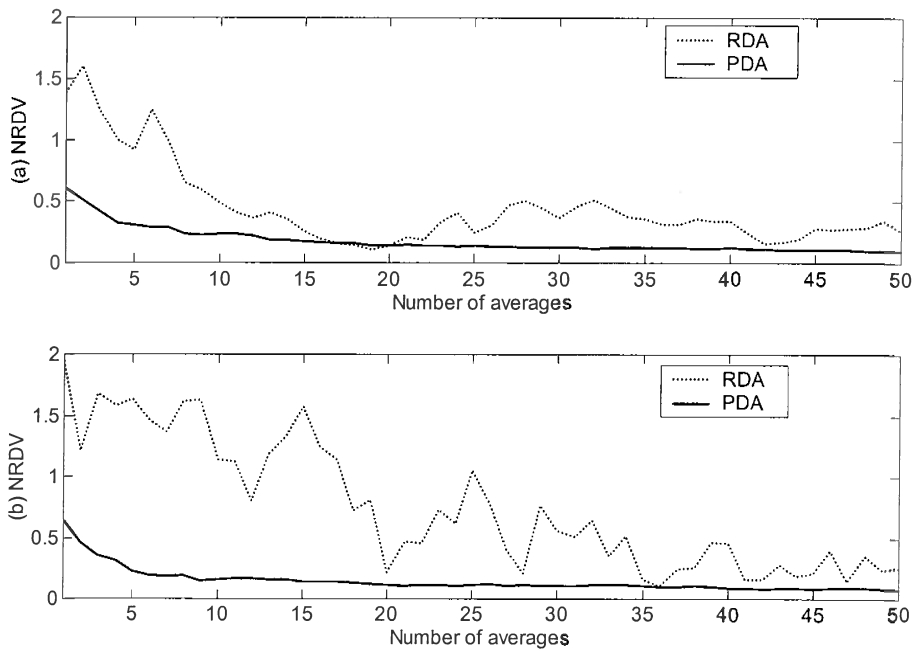

Figure 4.7. NRDV versus the number of averages for the RDA and PDA process: (a) Damage level 1; (b) Damage level 2.

It can furthermore be concluded that the PDA process requires much less data to converge to a stable average. The erratic convergence of the RDA process can be attributed to the inability of the RDA process to deal with the phase changes in the response measurements, due to the fluctuating speed conditions.

Figures 4.8 (a) and (b) indicate the averaged signals for damage levels 2 and 3 obtained through the RDA process and figures 4.8 (c) and (d) show the signals obtained through the PDA process. The induced damage is indicated by the severe modulation at approximately ninety degrees of the shaft rotation and twenty five percent of the phase envelope. This is evident for the averaged signals obtained through RDA and PDA. However the averaged signals obtained through the RDA process shows increased modulation activity compared to the signals obtained through the PDA process, which may complicate fault detection and prognosis when detecting incipient gear damage.

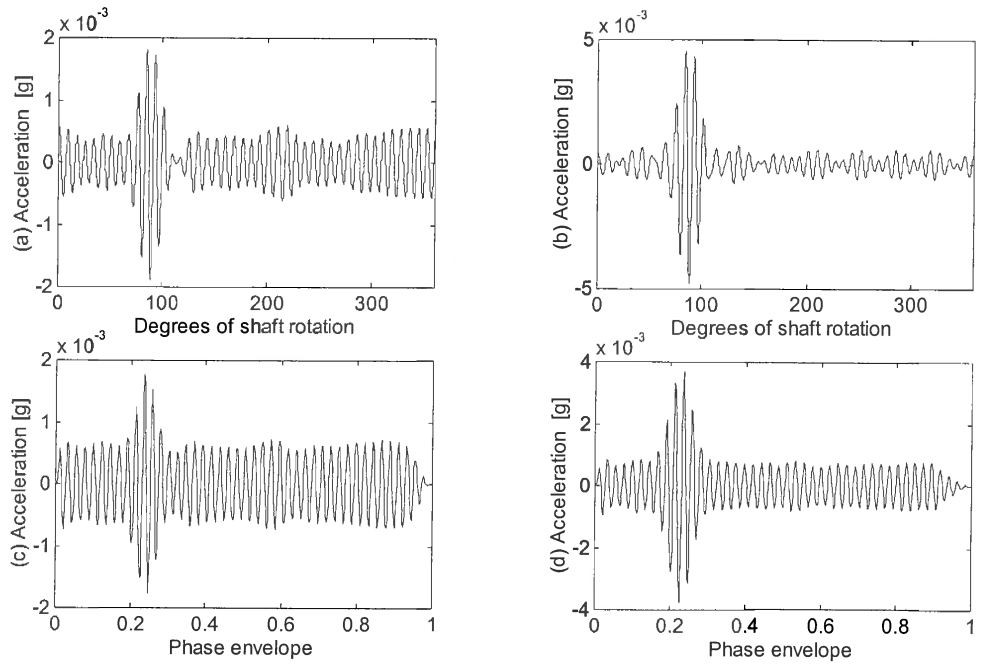

Figure 4.8. Synchronously averaged vibration signals measured on the test rig: (a) RDA at damage level 2; (b) RDA at damage level 3; (c) PDA at damage level 2; (d) PDA at damage level 3.

The SPWV algorithm proposed by Wang [62] was applied to the averaged signals obtained by utilising the RDA and PDA processes. Details of the number of data points used are presented in Table 4.1. Figures 4.9 (a) to (c) and 4.10 (a) to (c) indicate the contour plots of the SPWV distributions at the same amplitude level for the three levels of damage severity. The distributions calculated from the PDA signals produce smoother contours compared to the distributions calculated from the RDA signals. It can therefore be concluded that it is easier to diagnose and trend a deteriorating fault condition by utilising signals obtained from the PDA process.

TABLE 4.1 SPWV distribution specifications

Signal data point length	512 data points
Pseudo window length	32 data points
Smoothing window length	4 data points

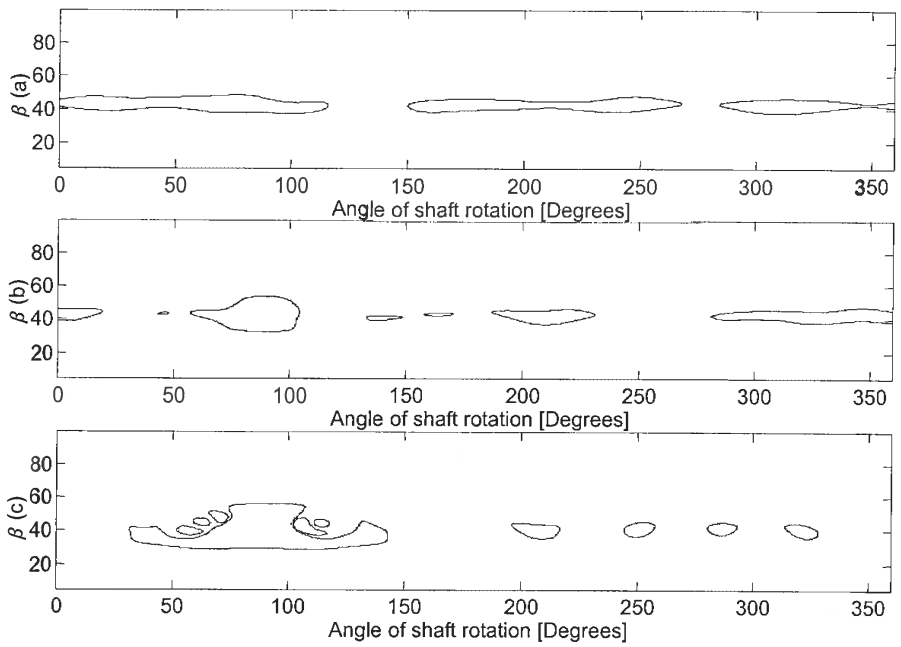

Figure 4.9. Smoothed Pseudo Wigner Ville contour plot of the RDA signals: (a) Damage level 1; (b) Damage level 2; (c) Damage level 3.

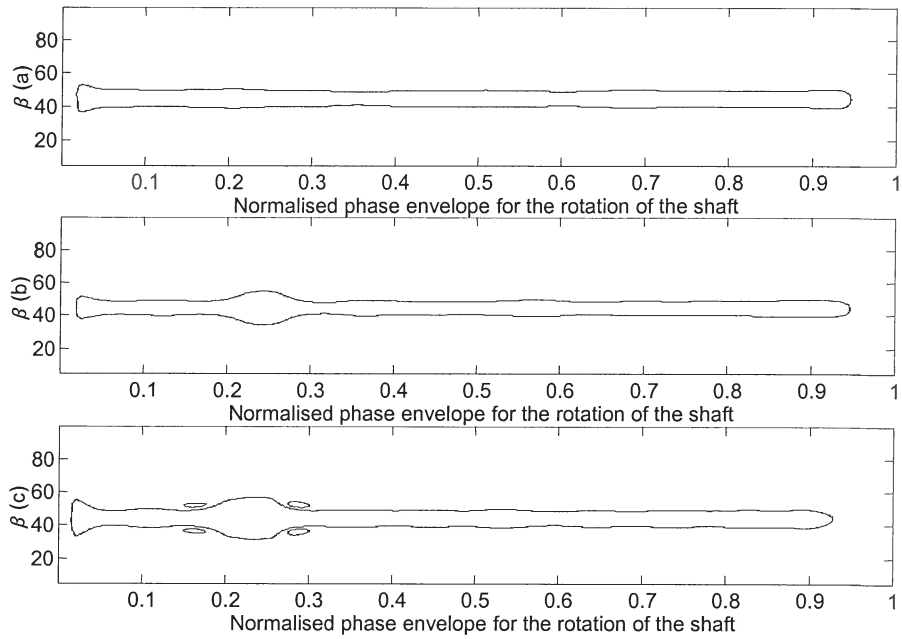

Figure 4.10. Smoothed Pseudo Wigner Ville contour plots of the PDA signals: (a) Damage level 1; (b) Damage level 2; (c) Damage level 3.

Chapter 5

Conclusion and recommendations for further research

5.1 Conclusion

A signal-processing approach to load demodulation normalisation was devised to monitor the condition of gears operating under fluctuating load conditions. The procedure was tested on experimental data measured during constant, sinusoidal, step and chirp load fluctuations for different levels of damage severity. Statistical parameters were calculated from the pseudo-Wigner-Ville distributions, which had been calculated for the load-normalised acceleration signals averaged in the rotation domain. These parameters were linearly separated between the fault severity levels under different loading conditions. It was indicated that the Mahalanobis distance could be utilised to combine the parameters into a single-value parameter, which can readily be monotonically trended to indicate the progression of fault severity. A neural network could also be trained on the parameters to classify the severity of faults, on data of a load condition, which had not been used during training.

A simplified mathematical model was developed to simulate the structural response and the instantaneous angular speed of a gear system under cyclic stationary and non-cyclic stationary load fluctuation. The instantaneous angular speed will change as the gear teeth mesh in and out of the gear mesh, owing to the fluctuation in meshing stiffness. A fault condition of reduced gear meshing stiffness was considered, resulting in a change in the instantaneous angular speed, which indicated that the instantaneous angular speed could be used to detect and monitor the presence of a gear defect.

The amplitude of both the gearbox casing vibration and the instantaneous angular speed will be modulated by the fluctuating load conditions. However, if the modulation is non-cyclic stationary it will be suppressed if a sufficient number of averages are taken when applying the rotation domain averaging process. Once the signal has been rotation domain averaged, it will still have to be normalised in order to compensate for the variation in nominal load. The rotation domain averaging process will not remove the load modulation effect if the load is cyclic stationary with the rotation of the shaft. Therefore, a load demodulation normalisation approach should be followed to remove the effect of cyclic stationary load modulation.

There are two inherent advantages of non-cyclic stationary load fluctuation. The first is that an optimal load normalisation frequency does not have to be determined and the second is that an overlap in the frequency band of the gear defect modulation and the load modulation can be tolerated. Experimental results were obtained from a test rig built to apply non-cyclic stationary load fluctuation to a test gearbox. The experimental results confirmed the conclusions made regarding the instantaneous angular speed monitoring and the non-cyclic stationary load modulation, which are suppressed through the process of rotation domain averaging.

The effect of the transmission path phase characteristics on synchronous averaging was explained under fluctuating load and speed conditions. It is indicated that the effect cannot be neglected when conducting synchronised averaging in the rotation or time domain. A methodology is proposed to eliminate the effect of the phase variation by calculating an, amplitude versus signal phase representation of the computer order tracked signal. It is indicated that the average of the amplitude versus phase representation converges with fewer shaft rotations compared to conventional rotation domain averaging. Consequently, less data needs to be captured for monitoring purposes when applying the amplitude versus phase representation of the signal. It is shown that the amplitude versus phase representation of the signal can be utilised for diagnostic purposes.

It is indicated that the average amplitude versus phase representation has less abrupt modulation compared to the conventional rotation domain averaging. The abrupt modulation is caused by the effect of the phase variation in the transmission path, which reduces repeatability and complicates the diagnosis of a fault condition.

5.2 Recommendations for further research

Currently very little to no research has been conducted to establish criteria that will indicate the required accuracy and resolution with which the instantaneous angular speed has to be measured for diagnostic purposes. The criteria should enable the specification of shaft encoder resolution or the number of pulses per revolution that it will produce. Shaft encoder resolution should be specified for a range of rotational speed conditions as well as the frequency at which the measured signal should be digitised for post processing purposes.

The reason for the phase reversal in the phase of the analytical signal obtained through the utilisation of the Hilbert Transform is unknown. The phenomenon needs to be investigated. Reasons for the occurrence need to be established in order to enable further research in resolving the phase reversal phenomenon.

It is postulated that the phase of the signal can be used for order tracking purposes and that the accurate measurement of the instantaneous angular speed is not necessary. Only the synchronising pulse can be measured and the phase of the analytical signal can be used to estimate the speed fluctuation between the pulses.

It is envisaged that the moving windows utilised in most time frequency techniques can be modified in order to incorporate normalisation in the window. This will reduce pre and post processing and might increase defect detection sensitivity.

References

1. R.B. Randall 1987 *K. Larsen and Son, Denmark.* Frequency Analysis.
2. R. Potter 1990 *Sound and Vibration 24. 30-34* A new order tracking method for rotating machinery.
3. R. Potter and M. Gribler 1989 *SAE Noise and Vibration Conference. 63-67.* Computer order tracking methods obsoletes older methods.
4. K.R. Fyfe and E.D.S. Munck 1997 *Mechanical Systems and Signal Processing 11(2)*, 187-205. Analysis of computed order tracking.
5. K.M. Bossley, R.J. Mckendrick, C.J. Harris and C. Mercer 1999 *Mechanical Systems and Signal Processing 13(4)*, 627-641. Hybrid computed order tracking.
6. S.G. Braun 1975 *Acustica 32(2)*, 69-77. The extraction of periodic waveforms by time domain averaging.
7. S.G. Braun and B.B. Seth 1979 *Journal of Sound and Vibration 65(1),* 37-50. On the extraction and filtering of signals acquired from rotating machines.
8. P.D. Mcfadden 1987 *Mechanical Systems and Signal Processing 1(1)*, 83-95. A revised model for the extraction of periodic waveforms by time domain averaging.
9. P.D. Mcfadden 1989 *Mechanical Systems and Signal Processing 3(1)*, 87-97. Interpolation techniques for time domain averaging of gear vibration.
10. B.D. Forrester 1996 *A thesis submitted for the examination for the degree Doctor of Philosophy, University of Melbourne, Australia.* Advanced vibration analysis techniques for fault detection and diagnosis in geared transmission systems.
11. R.M. Stewart 1977 *University of Southampton Report MHM/R/10/77.* Some useful data analysis techniques for gearbox diagnostics.
12. N.S. Swanson, B.D. Forrester and I.M. Howard 1989 *Proceedings of the Australian Aeronautical Conference, Melbourne, October 1989.* Fault detection in helicopter transmissions: Trends in health and usage monitoring.
13. G.P. Succi 1991 *Supplemental contract report R9110-001-RD Technology Integration Incorporated.* Synchronous averaging for gearbox vibration monitoring.

14. C.J. Stander, P.S. Heyns and W. Schoombie 2002 *Mechanical Systems and Signal Processing 16(6)*, 1005-1024. Using vibration monitoring for local fault detection on gears operating under fluctuating load conditions.
15. P.D. McFadden 2000 *Mechanical Systems and Signal Processing 14(5)*, 805-817. Detection of gear faults by decomposition of matched differences of vibration signals.
16. G.K. Chaturvedi and D.W. Thomas *1981 Journal of Sound and Vibration 76(3)*, 391-405. Adaptive noise cancellation and condition monitoring.
17. P.G. Bremer 1990 *A thesis submitted for the examination for the degree master of science in engineering, University of Cape Town, South Africa.* Adaptive noise cancellation applied to machine condition monitoring.
18. G. Gelle, M. Colas and G. Delaunay 2000 *Mechanical Systems and Signal Processing 14(3)*, 427-442. Blind source separation applied to rotating machines monitoring by acoustical and vibrations analysis.
19. J.D. Smith 1999 *Marcel Dekker Inc., New York.* Gear noise and vibration.
20. P.D. McFadden and J.D. Smith 1985 *Proceedings of the Institute for Mechanical Engineers 199(C4), 287-292.* A signal processing technique for detecting local defects in a gear from the signal average of the vibration.
21. P.D. McFadden April 1986 *Journal of vibration, Acoustics, Stress and Reliability in Design 108,* 165-170. Detecting fatigue cracks in gears by amplitude and phase demodulation of the meshing vibration.
22. P.D. McFadden 1987 *Mechanical Systems and Signal Processing 1(2)*, 173-183. Examination of a technique for the early detection of failures in gears by signal processing of the time domain average of the meshing vibration.
23. P.D. McFadden 1988 *Mechanical Systems and Signal Processing 2(4)*, 403-409. Determining the location of a fatigue crack in a gear from the phase of the change in the meshing vibration.
24. J. Ma and C.J. Li 1994 *Manufacturing Science and Engineering ASME PED 68(1),* 299-306. A new approach to gear vibration demodulation and its application to defect detection.

25. D. Brie, M Tomczak, H. Oehlmann and A. Richard 1997 *Mechanical Systems and Signal Processing 11(1)*, 149-167. Gear crack detection by adaptive amplitude and phase demodulation.
26. W. Wang 2001 *Mechanical Systems and Signal Processing 15(5)*, 887-903. Early detection of gear tooth cracking using the resonance demodulation technique.
27. K. R. N. Al-Balushi 1995 *A thesis submitted for the examination for the degree Doctor of Philosophy, Cranfield University, United Kingdom*. The use of high frequency stress waves for monitoring gears.
28. D. Birch 1994 *A thesis submitted for the examination for the degree master of science in engineering, University of Cape Town, South Africa*. A review of vibration signal processing techniques for use in a real time condition monitoring system.
29. S.N. Engin 1998 *A thesis submitted for the examination for the degree Doctor of Philosophy, University of Hertfordshire, United Kingdom*. Condition monitoring of rotating machinery using wavelets as a preprocessor to artificial neural networks.
30. F.A.R. Andrade 1999 *A thesis submitted for the examination for the degree Doctor of Philosophy, Brunel University, United Kingdom*. New techniques for vibration condition monitoring: Volterra kernel and Kolmogorov-smirnov.
31. H. Komura, K. Shibata, K Shimomura, Y. Kawabe and T. Toyota 2000 *Proceedings of the 13th International Congress on Condition Monitoring and Diagnostic Engineering Management Houston Texas 3-8 December*, 165-174. New technology of machine diagnosis without using the trend data.
32. H.R. Martin, F. Ismall and F. Omar 1992 *Mechanical Systems and Signal Processing 6(4)*, 317-327. Algorithms for statistical moment evaluation for machine health monitoring.
33. F. Ismall, H.R. Martin and F. Omar 1995 *Proceedings of the ASME Design and Technical Conferences Boston USA 17–20 September,* 1413-1418. Statistical index for monitoring tooth cracks in a gearbox.
34. D.C.D. Oguamanam, H.R. Martin and J.P. Huissoon 1995 *Applied Acoustics 45,* 247-261. On the application of the beta distribution to gear damage analysis.

35. I.M. Howard 1990 *Proceedings of the Institute of Engineers Australia Vibration and Noise Conference Melbourne 18-20 September*, 171-178. Epicyclic Transmission Fault Detection by Vibration Analysis.
36. F.A. Andrade, I. Esat and M.N.M. Badi 2001 *Journal of Sound and Vibration 240(5)*, 909-919. A new approach to time domain vibration condition monitoring: Gear tooth fatigue crack detection and identification by the Kolmogorov-smirnov tests.
37. N. Baydar, Q. Chen, A. Ball, U. Kruger 2001 *Mechanical Systems and Signal Processing 15(2)*, 303-321. Detection of incipient tooth defect in helical gears using multivariate statistics.
38. S. Goldman 1999 *Industrial Press, New York.* Vibration spectrum analysis second edition.
39. T.M. Hunt 1996 *Chapman and Hall, London UK.* Condition Monitoring of Mechanical and Hydraulic Plant: A Concise Introduction and Guide.
40. B.K.N. Rao 1996 *Elsevier Science Ltd.* Handbook of Condition Monitoring First Edition.
41. A. Davis 1998 *Chapman and Hall, London UK*. Handbook of Condition Monitoring: Techniques and Methodology.
42. M. Angelo 1987 *Naerum Offset, Denmark.* Bruel and Kjaer Technical Review Vibration Monitoring of Machines.
43. R.B. Randall 1980 *Proceedings of the 2nd International Conference on Rotating Machinery Cambridge UK,* 169-174. Advances in the application of cepstrum analysis to gearbox diagnosis.
44. D.G. Childers, D.P. Skinner and R.C. Kemerait 1977 *Proceedings of the IEEE Vol 65 Number 10*, 1428-1443. The cepstrum a guide to processing.
45. M.Q. Wu and M.J. Crocker 1989 *Proceedings of the 1st International Machinery Monitoring and Diagnostics Conference Las Vegas Nevada USA*, 79-85. The modified cepstrum for machinery monitoring.
46. L. Debao, Z. Hongcheng, Z. Yuanyun, W. Bo, L. Lingsheng and L. Jing 1989 *Proceedings of the 1st International Machinery Monitoring and Diagnostics Conference Las Vegas Nevada USA*, 596-598. Cepstrum analysis and the fault diagnosis of rotating machine.

47. D.J. Van Dyke and W.A. Watts 1990 *Proceedings of the 2nd International Machinery Monitoring and Diagnostics Conference Los Angeles USA*, 554-559. Automated rolling contact bearing fault detection using cepstrum analysis.
48. M. El Badaoui, J. Antoni, F. Guillet, J. Danière and P. Velex 2001 *Mechanical Systems and Signal Processing 15(5)*, 873-885. Use of the moving cepstrum integral to detect and localize tooth spalls in gears.
49. C.J. Li, J. Ma, Bhwang and GW Nickerson 1991 *Proceedings of the 3rd International Machinery Monitoring and Diagnostics Conference Las Vegas Nevada USA*, 225-231. Bispectral analysis of vibration for bearing condition monitoring.
50. T. Ning, Y.S. Kung and F.S. Wei 1996 *Proceedings of the International Conference on Industrial Electronics, Control and Instrumentation New York USA, 1960-1965.* Detection of distributed gear faults with a new bispectral analysis.
51. I.M. Howard 1997 *Journal of Aerospace Engineering 211(G4)*, 211-219. Higher order spectral techniques for machine vibration condition monitoring.
52. B.E. Parker, H.A. Ware, D.P. Wipf, W.R. Tompkins, B.R. Clark and E.C. Larson. 2000 *Mechanical Systems and Signal Processing 14(4)*, 561-570. Fault diagnosis using statistical change detection in the bispectral domain.
53. D. Kocur and R Stanko 2000 *Mechanical Systems and Signal Processing 14(6)*, 871-890. Order bispectrum: a new tool for reciprocated machine condition monitoring.
54. L. Cohen 1995 *Prentice Hall, New Jersey USA*. Time frequency analysis.
55. S. Qian and D. Chen 1996 *Prentice Hall, New Jersey USA*. Joint time frequency analysis methods and applications.
56. B.D. Forrester 1989 *Proceedings of the ASSPA 89 Signal Processing, Theories, Implementations and Applications Conference Adelaide Australia 17-19 April,* 78-82. Use of the Wigner-Ville distribution in helicopter fault detection.
57. B.D. Forrester 1990 *Proceedings of the 44th Meeting of the Mechanical Failures Prevention Group Virginia Beach USA 3-5 April,* 225-234. Analysis of gear vibration in the time frequency domain.
58. W.J. Staszewski 1994 Department of Engineering, Manchester University,_PhD thesis. *The application of time variant analysis to gearbox fault detection.*

59. W.J. Staszeweski and G.R. Tomlinson 1997 *Mechanical Systems and Signal Processing 11(3)*, 331-350. Local fault detection in gearboxes using a moving window procedure.

60. W.J. Staszewski, K.Worden and G.R. Tomlinson 1997 *Mechanical Systems and Signal Processing 11(5)*, 673-692. Time-frequency analysis in gearbox fault detection using the Wigner-Ville distribution and pattern recognition.

61. P.D. McFadden 1981 *Proceedings of the fifth international symposium on air breathing engines Bangalore India 16 –21 February 10-1 – 10-10.* Investigation into the vibration of the starter gearbox of an aircraft turbine engine.

62. W.J. Wang 1993 Department of Engineering Science, Oxford University, PhD thesis. *Gearbox condition monitoring and early damage diagnosis by two and three dimensional vibration analysis.*

63. W.J. Wang and P.D. McFadden 1993 *Mechanical Systems and Signal Processing 7(3)*, 193-203. Early detection of gear failure by vibration analysis – 1. Calculation of the time frequency distribution.

64. W.J. Wang and P.D. McFadden 1993 *Mechanical Systems and Signal Processing 7(3)*, 205-215. Early detection of gear failure by vibration analysis – 2. Interpretation of the time frequency distribution using image-processing techniques.

65. W.J. Wang and P.D. McFadden 1993 *Proceedings of the 16th Annual Energy-Sources Technology Conference and Exhibition, Structural Dynamics and Vibration PD-52, Houston Texas 31 January – 4 February,* 91-99. Analysis of gear motion excitation by kinematic modeling and three –dimensional energy spectrum of structural responses.

66. W.J. Wang and P.D. McFadden 1993 *Proceedings of the5th International Congress on Condition Monitoring and Diagnostic Engineering Management Bristol UK July*, 79-84. Gear diagnostics by interpreting images of time-frequency energy distribution of vibration signals.

67. G.T. Zheng and P.D. McFadden 1999 *Journal of Vibration and Acoustics 121*, 328-333. A time frequency distribution for analysis of signals with transient components and its application to vibration analysis.

68. I. Yesilyurt, P.J. Jacob and A.D. Ball 1996 *Proceedings of the 9th International Congress on Condition Monitoring and Diagnostic Engineering Management Sheffield UK*, 477-486. Fault detection in helical gears using Pseudo Wigner-Ville, instantaneous power spectrum and Choi-Williams distributions. Part 1: Performance comparison of time frequency distributions.
69. N. Baydar, F. Gu and A. Ball 1999 *Proceedings of the first International Conference on the Integration of Dynamics, Monitoring and Control Manchester UK 1-3 September,* 109-115. Helical gear fault detection and diagnosis using a varying-time frequency distribution.
70. N. Baydar and A. Ball 2001 *Mechanical Systems and Signal Processing 15(6)*, 1091-1107. A comparison study of acoustic and vibration signals in detection of gear failures using Wigner-Ville distributions.
71. N. Baydar 2000 Department of Mechanical Engineering, University of Manchester, PhD thesis. *The vibro-acoustic monitoring of gearboxes.*
72. Y.S. Han and C.W. Lee 1999 *Mechanical Systems and Signal Processing 13(5)*, 723-737. Directional Wigner distribution for order analysis in rotating / reciprocating machines.
73. S.K. Lee and P.R. White 1997 *Mechanical Systems and Signal Processing 11(4)*, 637-650. Higher order time frequency analysis and its application to fault detection in rotating machinery.
74. H. Oehlmann, D. Brie, M. Tomczak and A. Richard 1997 *Mechanical Systems and Signal Processing 11(4)*, 529-545. A method for analyzing gearbox faults using time-frequency representation.
75. Q. Meng and L. Qu 1991 *Mechanical Systems and Signal Processing 5(3)*, 155-166. Rotating machinery fault diagnosis using Wigner distributions.
76. G.W. Rossano, J.F. Hamilton and Y.S. Shin 1990 *Proceedings of the 2nd International Machinery Monitoring and Diagnostics Conference Las Angeles USA*, 167-173. The Pseudo Wigner-Ville distribution as a method for machinery condition monitoring of transient phenomena.
77. M. Chiollaz and B. Favre 1993 *Mechanical Systems and Signal Processing 7(5)*, 375-400. Engine noise characterization with Wigner-Ville time frequency analysis.

78. F.K. Choy, S. Huang, J.J. Zakrajsek, R.F. Handschuh and D.P. Townsend 1996 *Journal of Propulsion and Power 12(2),* 289-295. Vibration signature analysis of a faulted transmission system.
79. Y.H. Kim 1991 *Mechanical Systems and Signal Processing 5(6)*, 461-473. Fault detection in a ball bearing system using a moving window
80. F. Auger, P Flandrin, P. Goncalvès and O. Lemoine 1996 CNRS France and Rice University USA. *Time-frequency toolbox for use with Matlab.*
81. W.J. Wang and P.D. McFadden 1993 *ASME Structural Dynamics and Vibration* Vol. 52, 13-20. Application of the wavelet transform to gearbox vibration analysis.
82. W.J. Wang and P.D. McFadden 1995 *Mechanical Systems and Signal Processing* 9(5), 497-507. Application of orthogonal wavelets to early gear damage detection.
83. W.J. Wang and P.D. McFadden 1996 *Journal of Sound and Vibration* 192(5), 927-939. Application of wavelets to gearbox vibration signals for fault detection.
84. S.T. Lin and P.D. McFadden 1997 *Mechanical Systems and Signal Processing* 11(4), 603-609. Gear vibration analysis by B-spline wavelet-based linear wavelet transform.
85. W.J. Wang 2001 *Mechanical Systems and Signal Processing* 15(4), 685-696. Wavelets for detecting mechanical faults with high sensitivity.
86. W.J. Staszewski and G.R. Tomlinson 1994 *Mechanical Systems and Signal Processing.* 8(3), 289-307. Application of the wavelet transform to fault detection in a spur gear.
87. W.J. Staszewski 1998 *Journal of Sound and Vibration* 211(5), 735-760. Wavelet based compression and feature selection for vibration analysis.
88. I. Yesilyurt and A.D. Ball 1997 *Maintenance and Asset Management* 12(4), 28-32. An advanced approach to the detection of bending fatigue in spur gears.
89. D. Boulahbal, M.F. Golnaraghi and F. Ismail 1999 *Mechanical Systems and Signal Processing* 13(3), 423-436. Amplitude and phase wavelet maps for the detection of cracks in geared systems.
90. W.Q. Wang, F. Ismail and M.F. Golnaraghi 2001 *Mechanical Systems and Signal Processing* 15(5), 905-922. Assessment of gear damage monitoring techniques using vibration measurements.

91. G. Dalpiaz, A. Rivola and R. Rubini 2000 *Mechanical Systems and Signal Processing* 14(3), 387-412. Effectiveness and sensitivity of vibration processing techniques for local fault detection in gears.

92. Z.K. Peng and F.L. Chu 2004 *Mechanical Systems and Signal Processing* 18(2), 199-221. Application of the wavelet transform in machine monitoring and fault diagnostics: a review bibliography.

93. M Misiti, Y. Misiti, G. Oppenheim and J.M. Poggi 1997 User guide *MathWorks Inc.*, 1.3-1.13. Wavelet toolbox for use with MATLAB.

94. S.M. Wu, T.H. Tobin and M.C. Chow 1980 *Journal of Mechanical Design 102*, 217-221. Signature analysis for mechanical systems via dynamic data systems monitoring technique.

95. Q. Zhuge, Y. Lu and S Yang 1990 *Mechanical Systems and Signal Processing 4(5)*, 355-365. Non-stationary modeling of vibration signals for monitoring the condition of machinery.

96. D.C. Baillie and J. Mathew 1996 *Mechanical Systems and Signal Processing 10(1)*, 1-17. A comparison of autoregressive modeling techniques for fault diagnosis of rolling element bearings.

97. C.J. Li, J Limmer and J. Yoo 1996 *Manufacturing Science and Engineering ASME MED 4,* 595-603. Gear pitting and chipping assessment via model based algorithms-A case study.

98. A.C. McCormick, A.K. Nandi and L.B. Jack 1998 *Journal of Mechanical Engineering Science 212(C6)*, 417- 428. Application of time varying autoregressive models to the detection of bearing faults.

99. W. Wang and A.K. Wong 2000 *Proceedings of the 13th International Congress on Condition Monitoring and Diagnostic Engineering Management Houston Texas 3-8 December*, 797-807. Linear prediction and gear fault diagnosis.

100. P.T. Monsen, E.S. Manolakos and M. Dzwonczyk 1993 *Proceedings of the 27th Asilomar Conference on Signals, Systems and Computers Pacific Grove USA,* 381-385. Helicopter gearbox fault detection and diagnosis using analogue neural networks.

101. K. Worden, W.J. Staszewski and A.G. Star 1994 *Proceedings of the 8th International Congress on Condition Monitoring and Diagnostic Engineering Management*, 418-426. Gear fault detection and severity classification using neural networks.

102. X. Xu, H. Vanderveldt and R. Allen 1997 *IEEE International Conference on Neural Networks San Diego USA, Volume 4 Number 4*, 2434-2438.An ANS helicopter transmission diagnostic system.

103. A.C. McCormick and A.K. Nandi 1997 *Proceedings of the Institute for Mechanical Engineering, Volume 12 Part C*, 439-450. Classification of the rotating machine condition using artificial neural networks.

104. V.B Jammu, K. Danai and D.G. Lewicki 1995 *Proceedings of the ASME International Mechanical Engineering Congress and Exposition Part 2, San Francisco USA*, 12 – 17 November, 747-757. Fuzzy connectionist network for fault diagnosis of helicopter gearboxes.

105. V.B Jammu, K. Danai and D.G. Lewicki 1997 *Proceedings of the 53rd annual forum of AHS Part 2 Virginia Beach USA, 29 April – 1 May,* 1297-1307. Unsupervised connectionist network for fault diagnosis of helicopter gearboxes.

106. B.A. Paya, I.I. Esat and M.N.M. Badi 1997 *Mechanical Systems and Signal Processing 11(5)*, 751-765. Artificial neural network based fault diagnostics of rotating machinery using wavelet transform as a pre processor.

107. M.A. Essawy, S. Diwakar, S. Zein-Sabbato and M. Bodruzzaman 1997 *Intelligent Engineering Systems through Artificial Neural Networks, Volume 7,* 661-666. Helicopter transmission fault diagnosis using neuro-fuzzy techniques.

108. M.A. Essawy, S. Diwakar and S. Zein-Sabbato 1998 *Proceedings of the Artificial Neural Networks in Engineering Conference, St. Louis Missouri USA, 1-4 November,* 767-772. Wavelet versus Fourier pre processing for neuro-fuzzy systems for fault diagnosis in helicopter gearboxes.

109. M.R. Dellomo 1999 *Journal of Vibration and Acoustics Volume 121,* 265-272. Helicopter gearbox fault detection: A neural network based approach.

110. H. Demuth and M. Beale 1998 Math Works Inc. *Neural network toolbox for use with Matlab.*

111. M. F. Golnaraghi, D. Lin and P. Fromme 1995 *Proceedings of the ASME Design and Technical Conferences, Boston USA, 17–20 September,* 121-127. Gear damage detection using chaotic dynamics techniques: A preliminary study.

112. D.C. Lin, M.F. Golnaraghi and F Ismail 1997 *Journal of Sound and Vibration 208(4)*, 664-670. The dimension of the gearbox signal.

113. J. D. Smith and J. S. Echeverria-villagomez 1990 *Proceeding of the First International Conference on Gear Noise and Vibration*, 43-49. Comparing encoder and accelerometer measurement of transmission error or torsional vibration.

114. J. Yang, L. Pu, Z. Wang, Y Zhou and X. Yan 2001 *Mechanical Systems and Signal Processing 15*, 549-564. Fault detection in a diesel engine by analysing the instantaneous angular speed.

115. A.B. Sasi, B. Payne, F. Gu and A. Ball 2001 *Proceedings of the 14th International Congress on Condition Monitoring and Diagnostic Engineering Management Manchester UK 4-6 September*, 311-318. The exploitation of instantaneous angular speed for condition monitoring of electric motors.

116. J.D. Smith 1999 *Gear Noise and Vibration*, 143-150. New York: Marcel Dekker Inc.

117. R.B. Randall 1982 *Journal of Mechanical Design 104*, 259-267. A new method of modelling gear faults.

118. B. Bauer, B. Geropp and A Seeliger 1997 *Proceedings of IFAC Symposium on Fault Detection, Supervision and Safety for Technical Processes, Kingston upon Hull UK, 26- 28 August.* Condition monitoring and predictive maintenance in mining industry using vibration analysis for diagnosis of gearboxes.

119. N. Baydar and A. Ball 2000 *Mechanical Systems and Signal Processing 14(6)*, 907-921. Detection of gear deterioration under varying load conditions by using the instantaneous power spectrum.

120. H. N. Ozguven and D. R. Houser 1988 *Journal of Sound and Vibration 121(3),* 383-411. Mathematical models used in gear dynamics –a review.

121. I. Howard, S. Jia and J. Wang 2001 *Mechanical Systems and Signal Processing 15(5)*, 831-853. The dynamic modelling of a spur gear in mesh including friction and a crack.

122. W. Bartelmus 2001 *Mechanical Systems and Signal Processing 15(5)*, 855-871. Mathematical modelling and computer simulation as an aid to gearbox diagnostics.

123. J.E. Shigley 1986 *Mechanical Engineering Design*, pp. 478-479 New York: McGraw-Hill Book Company.

124. B. Jones 1999 *Statistical toolbox for use with Matlab*, The Math Works Inc.

125. A. Cichocki and R. Unbehauen 1994 *Neural Networks for Optimisation and Signal Processing*, 38. Stuttgart: John Wiley and Sons Ltd and B.G. Teubner.

126. R.E. Powel 1982 *A thesis submitted for the examination for the degree Doctor of Science, Massachusetts Institute of Technology*. Multi-channel inverse filtering of machinery vibration signals.

127. J.T. Kim 1987 *A thesis submitted for the examination for the degree Doctor of Philosophy, Massachusetts Institute of Technology*. Source and path recovery from vibration response recovery.

128. S.S. Rao 1995 *Addison –Wesley Publishing Company, USA*. Mechanical Vibrations Third Edition.

Appendix

Experimental test rigs and measurement instrumentation

A.1 Introduction

Two experimental test rigs where developed to determine the influence of fluctuating load conditions on structural response measurements. Spur gears and helical gears were considered in the test rigs. Different levels of gear damage were induced onto the gears of the rigs in order to generate measurement data under different loading conditions, to validate the signal processing procedures presented in chapters 2, 3 and 4.

A.2 Load control

The load on the gearbox test rigs were applied with a 5.5 kVA Mecc alte spa three-phase alternator. An analogue controller was designed to manipulate the electromagnetic field strength in the alternator in order to change the load, which was applied to the system. Figure A.1 shows a schematic diagram of the loading system.

The Alternating Current generated by the alternator is rectified and dissipated over a large resistive load, which is kept constant during tests. A single-phase voltage feedback from the alternator is measured in order to give an indication of the current, which is drawn from the alternator since the resistance was kept constant. The current drawn from the alternator is related to the torque applied by the alternator onto the system. Hence, the voltage feedback serves as an indication of the torque applied by the alternator.

A reference or command torque signal is used as an input to the controller, which manipulates the electromagnetic field strength in the alternator by switching the current flow to the DC field coils of the alternator with a transistor in order to follow the command signal. An external Direct Current (DC) power supply is utilised to provide the power for the DC field coils of the alternator. The controller utilises Proportional Integral (PI) compensation. Figure A.2 shows the load controller and DC rectification circuits. The resistive bank and external DC power supply is shown in figure A.3.

Note that the amplitude of load fluctuation decreases as the loading frequency or rate of load change increases due to the inertia and inductance in the system. The excitation frequencies during experiments were therefore kept below 3 Hz in order to obtain maximum load fluctuation amplitudes.

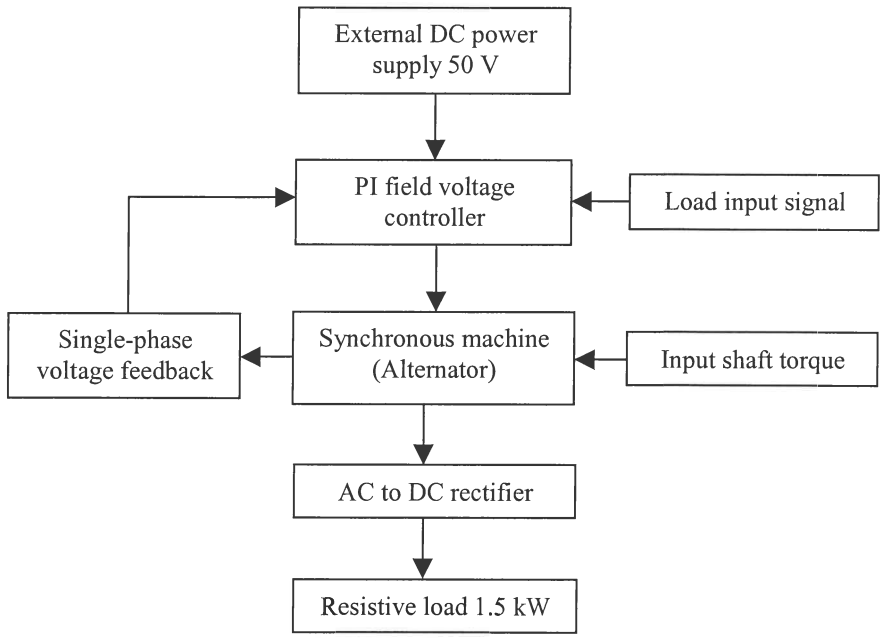

Figure A.1 Schematic diagram of the gearbox test rig loading system.

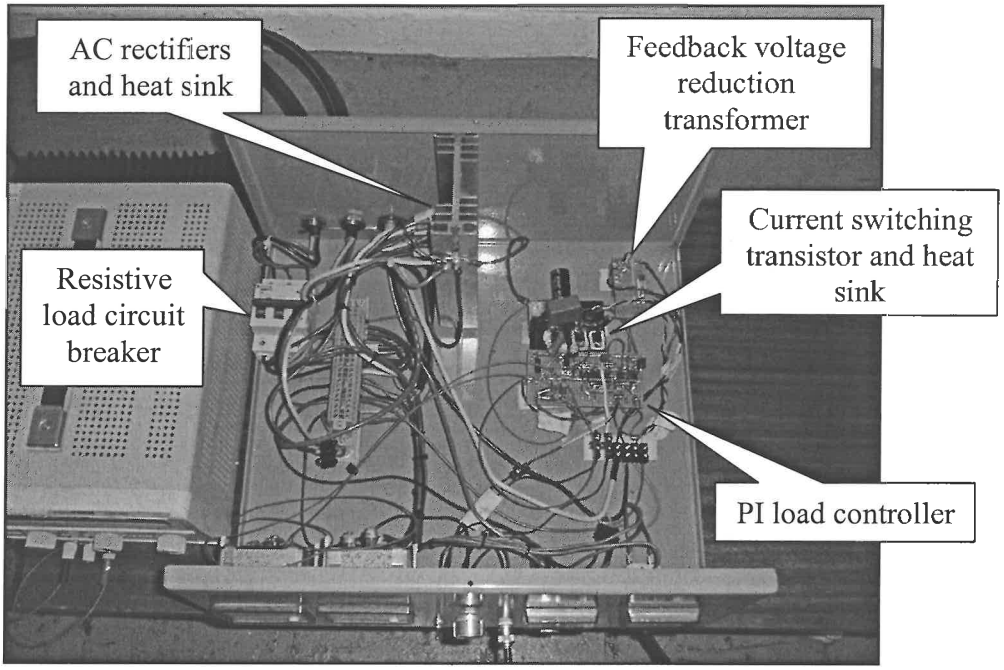

Figure A.2 Load controller electronic circuit

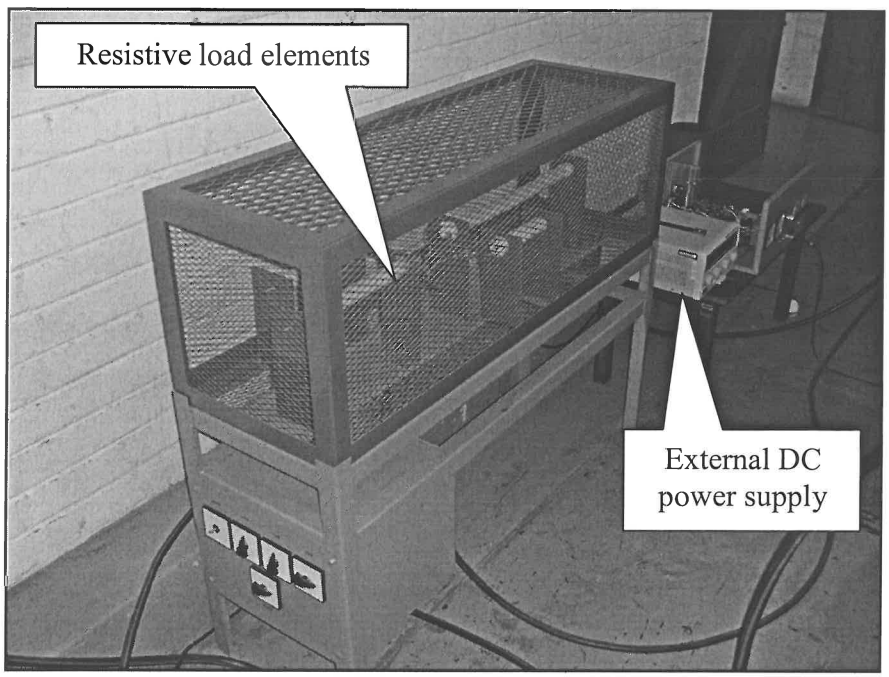

Figure A.3 Resistive load

A.3 Measurement system and instrumentation

The measurements were taken with a Siglab model 20-42 signal analyser and a Pentium 200 MMX Personal Computer (PC) with 64MB of Random Access Memory (RAM) shown in figure A.4. Four Analogue to Digital (A/D) channels where used to measure the key phasor, gearbox casing vibration, shaft speed and electric motor current signals. The virtual function generator was used to generate the load command signals for the load controlling system on the test rigs.

Integrated Circuit Piezo (ICP) accelerometers with a signal conditioner unit was utilised to measure the gearbox casing vibration. An accelerometer with higher sensitivity was utilised for measurements on the helical gearbox test rig due to the low amplitude response of the test gearbox casing vibration.

A magnetic speed sensor was user to measure the speed on the spur gear test rig. The shaft encoder was introduced in the helical gear test rig in order to improve the accuracy of the speed measurement from 50 pulses per revolution to 1024 pulses per revolution, which enabled the use of the IAS as a diagnostic measurement.

A schematic diagram of the measurement and load control system is shown in figure A.5. Table A.1 presents a table of the instrumentation with the specifications, which were used during experimentation on the two test rigs.

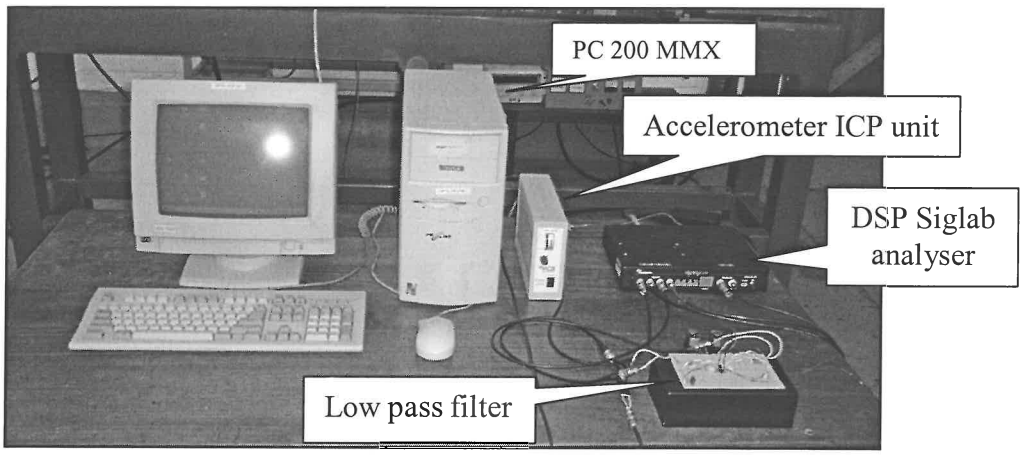

Figure A.4 Measurement system

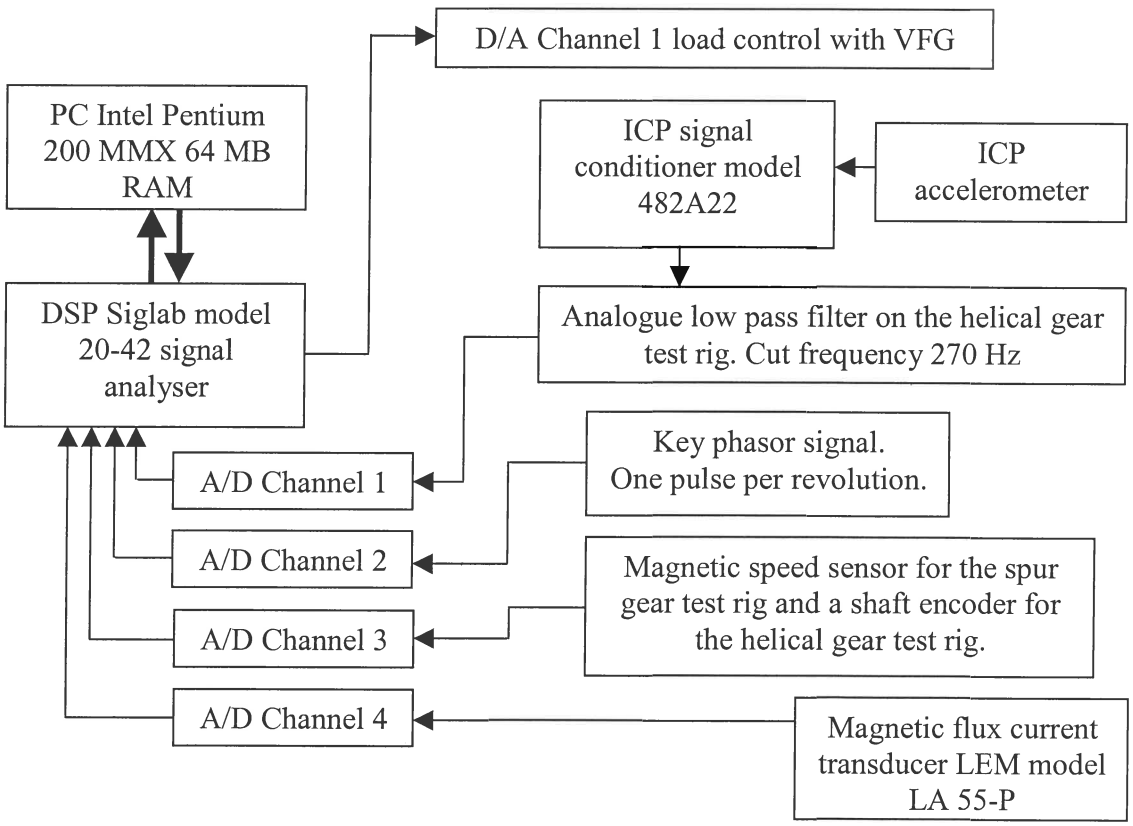

Figure A.5 Schematic diagram of the measurement and control system

Table A.1 Instrumentation

Instrument	Specification	Test rig
Signal analyser	DSP Siglab model 20-42	Helical & spur gear test rig
Personal Computer	Intel Pentium 200 MMX	
ICP Signal conditioner	PCB model 482A22	
Current transducer	LEM model LA 55-P	
Accelerometer 1	Entek 500 mV/g model E326A02	Spur gear test rig
Accelerometer 2	PCB 10 V/g model U393B12	Helical gear test rig
Magnetic speed sensor	Deuta-Werke model BM1/1A M14×1×50mm	Spur gear test rig
Shaft encoder	Hengstler model R176T01 1024ED 4A20KF	Helical gear test rig
Low pass filter	8^{th} Order Butterworth	Helical gear test rig

A.4 Low pass filter

The gear wheel of the test gearbox in the helical gear test rig is the slowest rotating component in the test rig with the lowest inertia which resulted in a relatively low gear mesh frequency amplitude when compared to the overall vibration levels. The anti-aliasing filter of the Siglab analyser has a constant cut off frequency of 20 kHz. An eighth order analogue Butterworth filter with a cut off frequency at 270 Hz was therefore designed and implemented as an analogue low pass filter. The high amplitude vibration in the frequency range above 270 Hz was therefore filtered out and the digitisation range of the gear mesh signal was improved.

The filter was designed with Microchip Filter Lab version 1.0.40. A frequency response function of the filter is shown in figure A.6. The schematic diagram of the filter with the component specifications is shown in figure A.7 and the physical hardware is shown in figure A.8. Two 9 Volt batteries was used to power the operational amplifiers of the active filter.

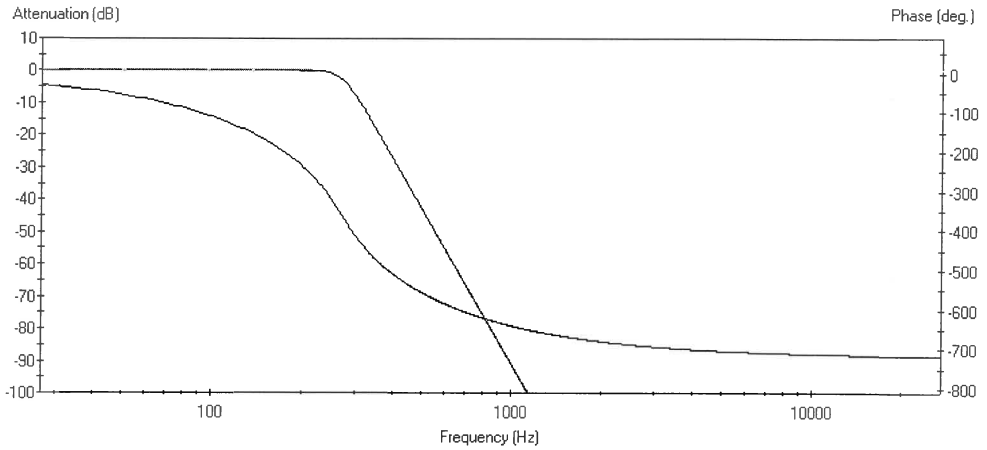

Figure A.6 Eighth-order Butterworth filter frequency response function

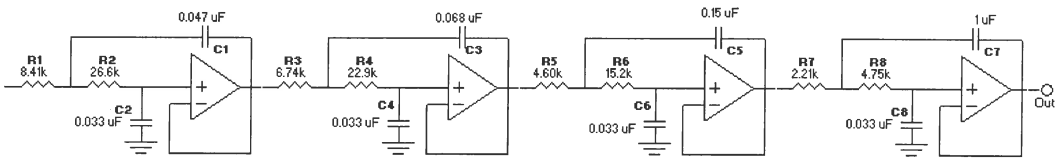

Figure A.7 Eighth-order Butterworth schematic diagram

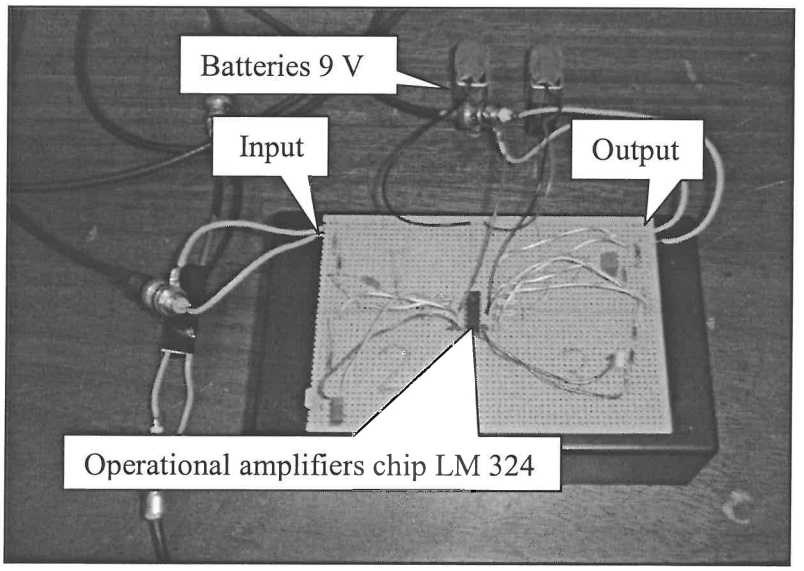

Figure A.8 Hardware implementation of the eighth-order Butterworth filter

The Butterworth filter phase distorts the measured data according to the frequency response function diagram shown in figure A.6. A reverse filtration scheme was developed to rectify the unwanted effect of phase distortion once the signals had been digitised. A random input filter signal was generated with the virtual function generator of the DSP Siglab in order to obtain input-output data from the analogue Butterworth filter, for the estimation of a system identification model. Measurements where taken with the DSP Siglab. An Auto Regressive model with eXternal input (ARX) was fitted on the data. A schematic diagram of the process is shown in figure A.9. The order of the measured data is reversed and re-filtered through the ARX model to remove the phase distortion. Once the data is re-filtered, the order of the data is reversed in order to restore the original sequence of the data. Only the phase of the data is effected by the reverse filtration procedure.

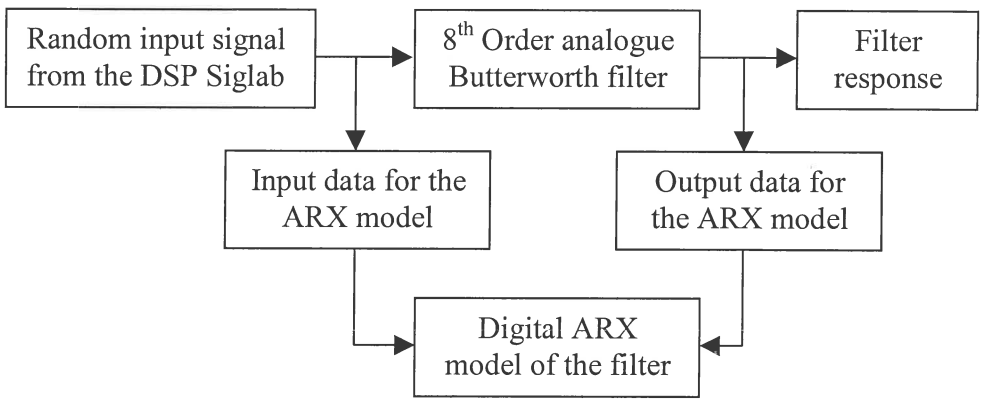

Figure A.9 Phase correction digital filter diagram

A.5 Spur gear test rig

The experimental set-up consisted of a single-stage gearbox, driven by a 5 hp Dodge silicon controlled rectifier motor. Load was applied with the system described in section A.2. The spur gear specifications are tabulated in Table A.2 and the test rig is illustrated in figure A.10.

Table A.2 Spur gear specifications.

Manufacturing standard	DIN3961, Quality 3
Number of teeth on each gear	69
Rated load	20 Nm

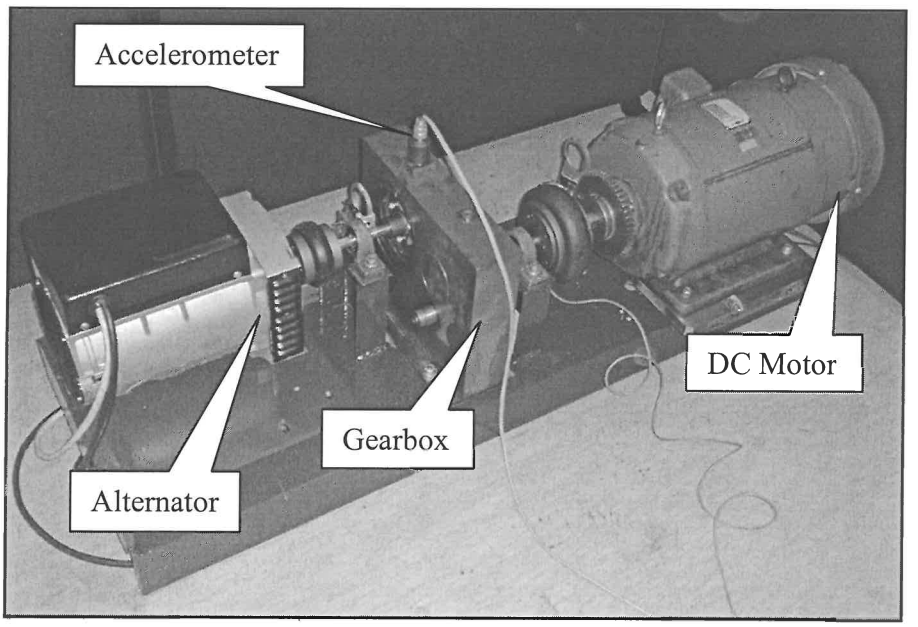

Figure A.10 Experimental set-up of the spur gear test rig

Tyre couplings were fitted between the electrical machines and the gearbox so that the backlash in the system would be restricted to the gears. The rotational speed of the system was measured with a Deuta-Werke magnetic speed sensor, which was set on a gear with 50 teeth as shown in figure A.11. The speed measurement gear was mounted on the output shaft of the electric motor. The magnetic speed sensor was utilised since it present a reliable and robust approach to speed measurement in practice. The average shaft speed during experimentation was 13 Hz.

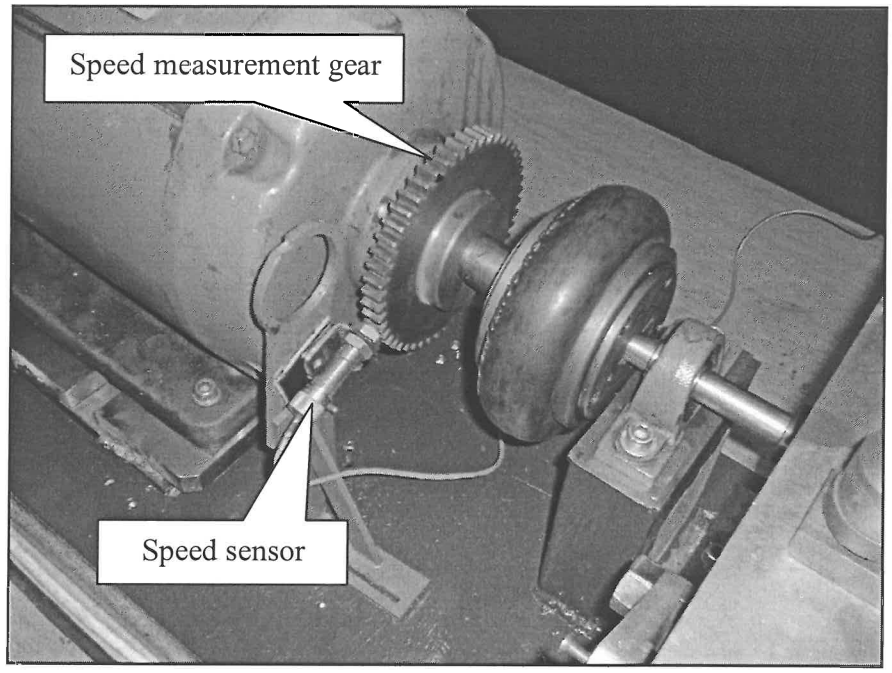

Figure A.11 Gear teeth counter in the spur gear experimental set-up

A synchronising pulse was measured by means of a proximity switch on the key of the shaft. Acceleration measurements were taken in the vertical direction with a 500 mV/g ENTEK ICP industrial accelerometer and the DSP Siglab analyser. Vibration measurements were taken for five different load conditions and three different levels of damage severity in order to evaluate the signal-processing procedures.

Table A.3 lists the specifications for the loading conditions. A sinusoidal load was selected to evaluate a slowly changing load condition, in contrast to the square load condition that creates a rapid change in load. The chirp load condition refers to a sinusoidal load condition where the frequency increases as time progresses. The chirp load condition represents a wider frequency band of the applied load.

The initial vibration measurements were taken without any induced damage. Then face wear was induced on one of the gear teeth by artificially removing material from the gear face. In addition, a crack was induced on the opposite side of the gear. Table A.4 presents the damage details and the induced damage is shown in figures A.12 and A.13.

The fault severity conditions are expressed as the fraction of the root crack length over the 4 mm tooth thickness.

Table A.3 Load case specifications

Load Case	Load Function	Frequency	Minimum Load	Maximum Load
1	Constant	0 Hz	14.4 Nm	14.4 Nm
2	Constant	0 Hz	15.9 Nm	15.9 Nm
3	Sine	0.5 Hz	6.6 Nm	18.6 Nm
4	Square	0.5 Hz	6.8 Nm	20.1 Nm
5	Chirp	0.1- 2 Hz	10.3 Nm	17.3 Nm

Table A.4 Induced damage specifications

	Fault severity 25%	Fault severity 50%
Material removed from face	0.15 mm Nominally	0.3 mm Nominally
Crack length	1 mm	2 mm

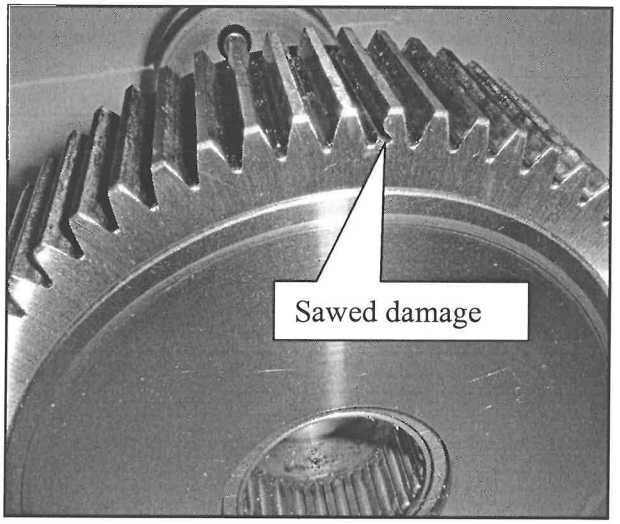

Figure A.12 Sawed crack

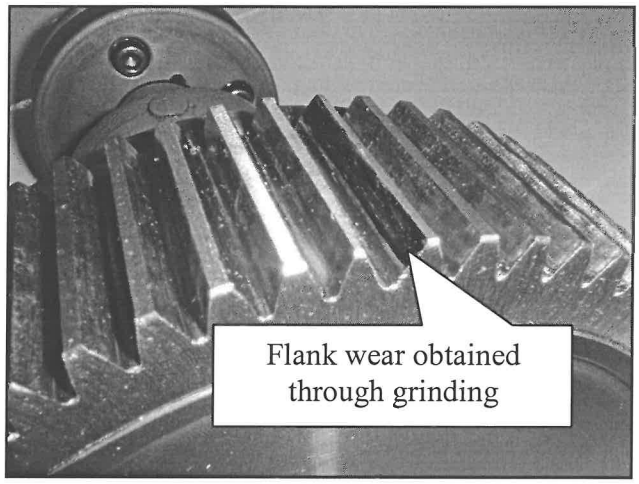

Figure A.13 Flank wear obtained through grinding

A.6 Helical gear test rig

The experimental set-up consisted of three Flender Himmel Motox helical gearboxes, driven by a 5.5 kW three phase four-pole Weg squirrel cage electrical motor. Load was applied with the system described in section A.2. Figures A.14 and A.15 illustrate the test rig. The gearbox test rig was designed to conduct accelerated gear life tests on the Flender E20A gearbox under varying load conditions. Two additional Flender E60A gearboxes were incorporated into the design in order to increase the torque that is applied to the small Flender E20A gearbox. The rated load of the gears in the Flender E20A gearbox was 20 Nm.

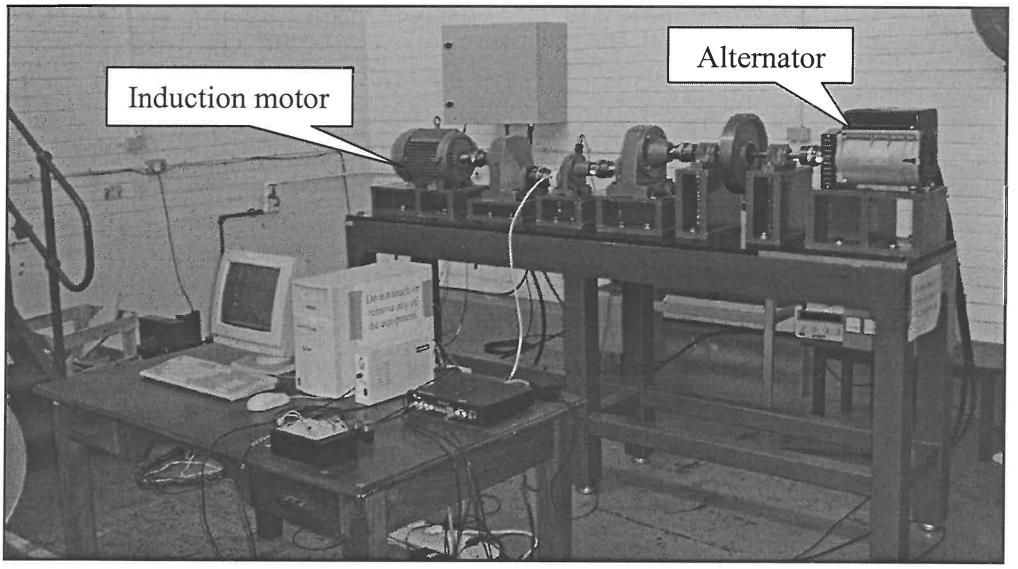

Figure A.14. Experimental set-up of the helical gear test rig

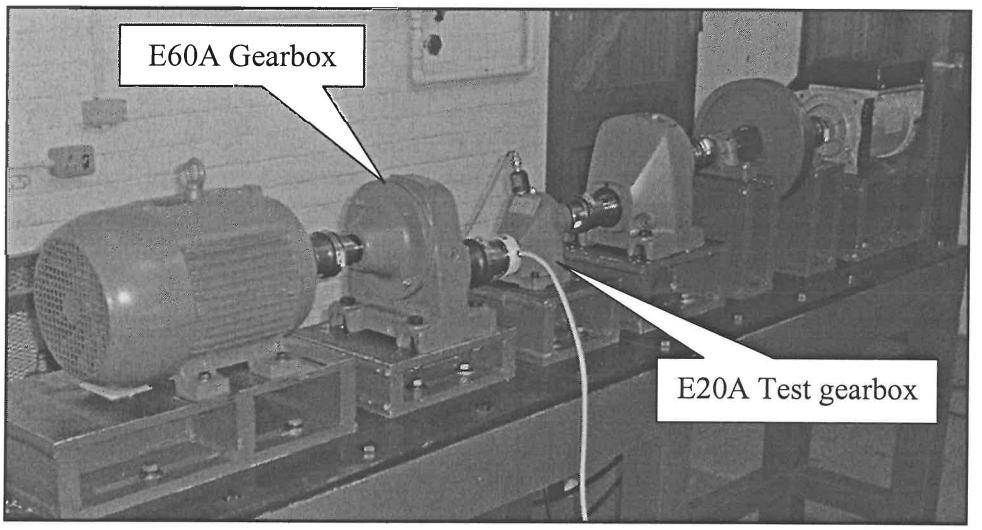

Figure A.15 Experimental set-up of the helical gear test rig

A Hengstler R176T01 1024ED 4A20KF shaft encoder, which produces 1024 pulses per revolution in the form of an analogue push-pull signal was used to measure the IAS for order tracking and condition monitoring purposes. The reference point for the synchronous averaging is measured as a single pulse from the shaft encoder.

Acceleration was measured in the vertical direction on the gear casing with a 10 V/g PCB ICP industrial accelerometer. The instrumentation is shown in figure A.16.

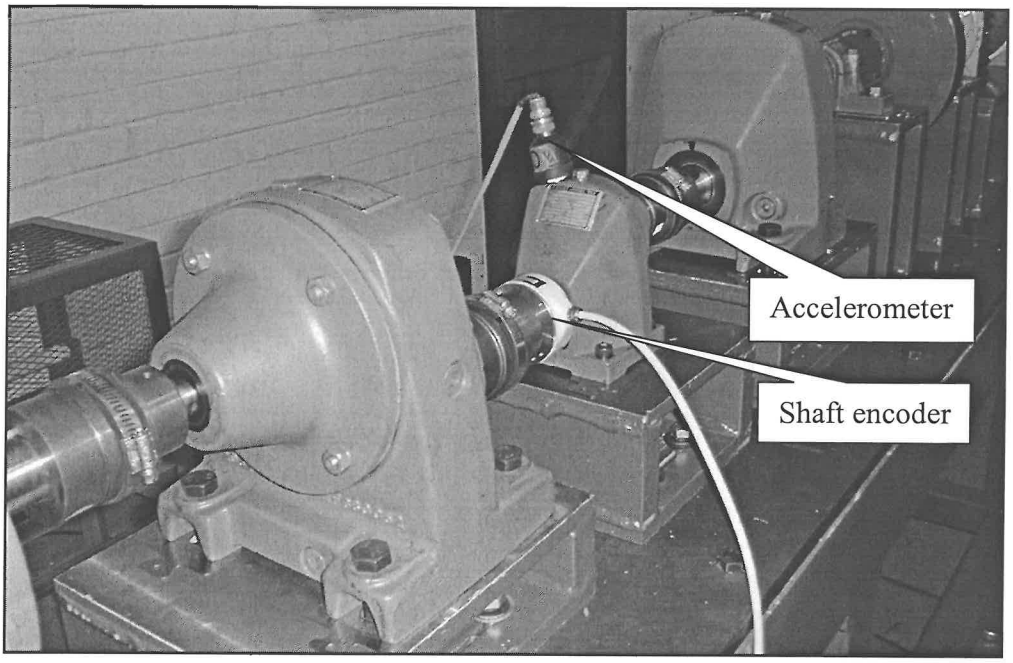

Figure A.16 Accelerometer and shaft encoder mounting positions

Reinforced concrete was cast into the base of the test rig in order to increase the damping levels in the supporting structure. This feature attenuated the response amplitude due to the transmission of reaction forces from the various rotating components. Concrete was cast into the supporting upright pillars in order to increase their stiffness as well as the damping levels. The mounting plate of the test rig was bolted on to the concrete in order to improve the damping effect. A base view of the test rig is shown in figure A.17.

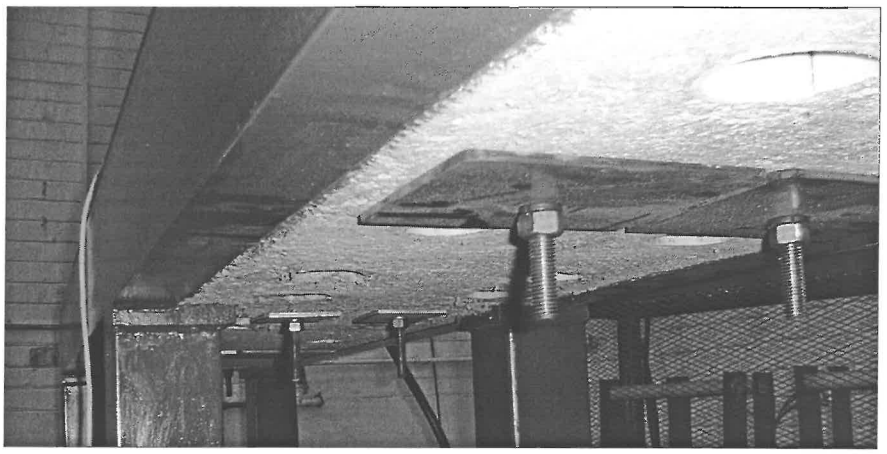

Figure A.17 Concrete reinforcing of the test bench

A variable speed frequency drive shown in figure A.18 was incorporated to control the speed of the induction motor during start up since the initial start up torque produced by the motor will damage the gearwheel in the test gearbox. The rotational speed of the motor is increased from 0 to 25 Hz over a period of 30 s during start up.

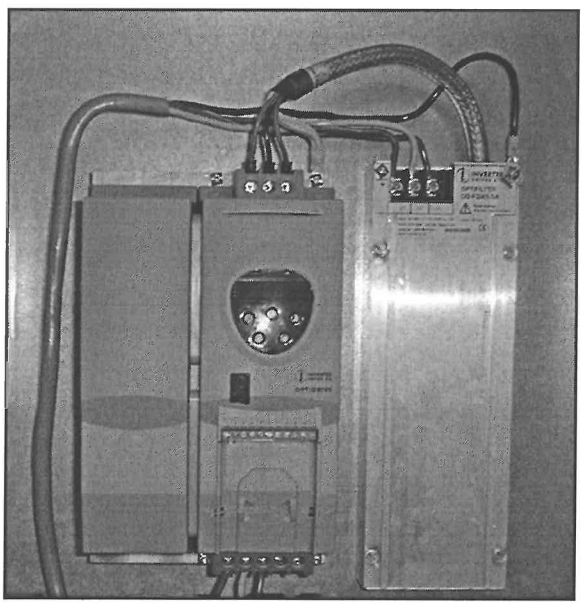

Figure A.18 Variable frequency speed control drive

The specifications for the loading conditions are tabulated in Table A.5. Flank wear was progressively induced on to one of the gear teeth on the gear wheel of the gearbox during experimentation. Details on the amount of wear are presented in Table A.6. The gearwheel of the test gearbox is shown in figure A.19.

Table A.5 Load case specifications

Load Case	Load Function	Frequency	Minimum Load	Maximum Load
1	Constant	0 Hz	10.7 Nm	10.7 Nm
2	Sine	1 Hz	7.4 Nm	14.7 Nm
3	Square	0.3 Hz	7.4 Nm	14.7 Nm
4	Chirp	0.1- 2 Hz	7.4 Nm	14.7 Nm
5	Random	0.1- 2 Hz	7.4 Nm	14.7 Nm

Table A.6 Induced damage specifications

Fault condition	Fault severity
1	100 μm Tooth face removal
2	200 μm Tooth face removal
3	300 μm Tooth face removal

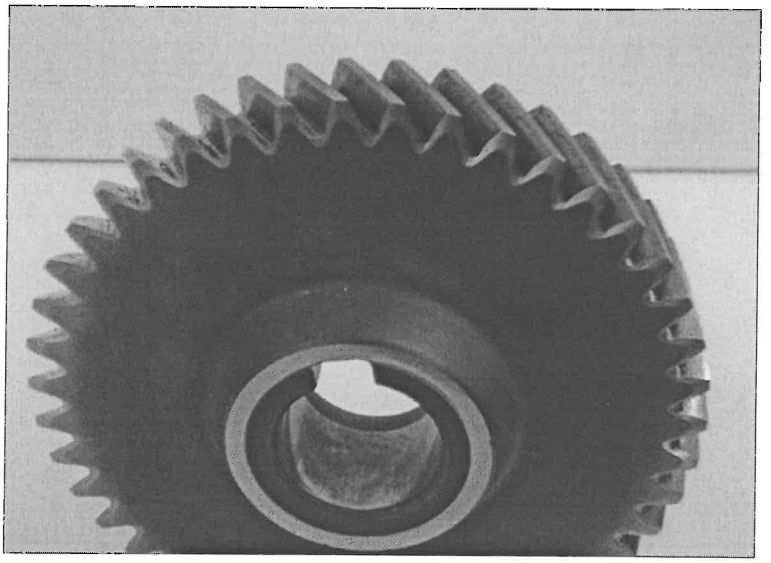

Figure A.19 Gearwheel of the E20A gearbox